Pontifícia Universidade Católica
do Rio de Janeiro

Wendy Johana Sandoval Rojano

Determination of Rare Earth Elements in Geological Samples by Inductively Coupled Plasma Mass Spectrometry

Tese de Doutorado

Thesis presented to the Programa de Pós-graduação em Química of PUC-Rio in partial fullfilment of the requirements for the degree of Doutor(a) em Química.

Advisor: Prof. Tatiana Dillenburg Saint'Pierre

Co-Advisor: Prof. Christiane B. Duyck Pinto

Rio de Janeiro
March 2020

Pontifícia Universidade Católica
do Rio de Janeiro

Wendy Johana Sandoval Rojano

Determination of Rare Earth Elements in Geological Samples by Inductively Coupled Plasma Mass Spectrometry

Thesis presented to the Programa de Pós-graduação em Química of PUC-Rio in partial fulfillment of the requirements for the degree of Doutor em Química. Approved by the Examination Committee.

Prof. Tatiana Dillenburg Saint'Pierre
Advisor
Departamento de Química - PUC-Rio

Prof. Christiane Béatrice Duyck Pinto
Co-Advisor
UFF

Prof. Maria Tereza Weitzel Dias Carneiro Lima
UFES

Prof. Rafaella Regina Alves Peixoto
UFF

Prof. Anderson Araújo Rocha
UFF

PhD. Jefferson Rodrigues de Souza
UFES

Prof. Jose Marcus de Oliveira Godoy
Departamento de Química - PUC-Rio

Rio de Janeiro, March 23rd 2020

Wendy Johana Sandoval Rojano

Graduated in Chemistry at the University of Atlantic (Barranquilla, Colombia) in 2013 and obtained her M.Sc. Degree in Chemistry from the Pontifical Catholic University of Rio de Janeiro in 2016.

Bibliographic data

Sandoval Rojano, Wendy Johana

Determination of rare earth elements in geological samples by inductively coupled plasma mass spectrometry / Wendy Johana Sandoval Rojano ; advisor: Tatiana Dillenburg Saint'Pierre ; co-advisor: Christiane B. Duyck Pinto. – 2020.

99 f. : il. color. ; 30 cm

Tese (doutorado)–Pontifícia Universidade Católica do Rio de Janeiro, Departamento de Química, 2020.

Inclui bibliografia

1. Química – Teses. 2. Elementos terras raras. 3. ICP-MS. 4. ICP OES. 5. Amostras geológicas. I. Saint'Pierre, Tatiana Dillenburg. II. Pinto, Christiane Béatrice Duyck. III. Pontifícia Universidade Católica do Rio de Janeiro. Departamento de Química. IV. Título.

CDD: 540

I would like to dedicate this work to my loving parents, Luisa and Edwin, to my loved sisters, Jennifer, Cindy, Stefania and to my little twins Hansel and Edwin, for their support and care.

Thank you

Acknowledgments

I am so thankful to God for the strength of culminating this dream.

I would like to thank my advisor, Prof. Tatiana Dillenburg Saint'Pierre, for providing me with the research support, flexibility, and research coaching.

I would like to thank Prof. Christiane B. Duyck Pinto, for dedicated help, contribution to work and friendship.

I would like to thank Prof. José Marcus Godoy, for dedicated help and contribution to work.

I would like to thank the jury for their flexibility and valuable contributions to this work.

I would like to thank the PUC-Rio, Brazilian Agencies CNPq and CAPES, for grants and doctoral scholarship and encouraging research.

I would like to thank the Department of Chemistry at PUC-Rio for the opportunity and the support of the research; and of course, to the professors of the department, whose teachings gave me great academic growth, and especially to Fatima Almeida, who has always demonstrated personal and professional availability during this work.

I would like to thank the friends and staff of the LABSPECTRO: Jefferson, Rodrigo, Lais, Rafael, Vitor, Adriana, Alvaro and Mauricio, who were always willing to help me in the laboratory.

I would like to thank my parents and my brothers, for their unconditional love and their support to fulfill this goal.

I would like to thank Alexander, for the companionship, support, encouragement, trust, help and for show me the way of the clarity, peace and serenity.

I would to thank all my friends specially Jesica, Marlin, Stephanie, Jarol, Carlos and Luis Miguel for friendship and support along of these six years.

Finally, I thank all the people who have passed through my life and influenced me in some way, but, eventually, were not mentioned in here.

This study was financed in part by the Coordenação de Aperfeiçoamento de Pessoal de Nível Superior - Brasil (CAPES) - Finance Code 001.

Abstract

Rojano, Wendy Johana Sandoval; Saint'Pierre, Tatiana Dillenburg (Advisor); Pinto, Christiane B. Duyck (Co-advisor). **Determination of Rare Earth Elements in Geological Samples by Inductively Coupled Plasma Mass Spectrometry.** Rio de Janeiro, 2020. 99p. Tese de doutorado - Departamento de Química, Pontifícia Universidade Católica do Rio de Janeiro.

The distribution of rare earth elements (REE) is representative of the rocks and soils that originally contain them and it is often used as a geochemical or an environmental parameter for source identification. This thesis proposes a new method for the determination of rare earth elements (REE), by inductively coupled plasma mass spectrometry (ICP-MS), in challenging environmental samples with high Ba concentrations. The method consists in diluting the wet sample digests, obtained after acid decomposition in an open system, with 10 % (v/v) sulfuric acid for the separation of Ba^{2+} as $BaSO_4$. The interference removal on both Eu isotopes (^{151}Eu and ^{153}Eu) was efficient for Ba concentrations higher than 0.1 mg L^{-1}. Accuracy and precision were verified by analysis of two certified materials, NIST 688 Standard Reference Material of basalt rock, Geological Survey G-2 granite and marine sediment reference material (MESS-3) provided by the National Research Council in Canada (NRC) was used to evaluate the accuracy of the REE determination in marine sediments. The proposed methodology was applied to asphalt pavement and crushed stone. Additionally, for comparison, all samples were decomposed by fusion and major elements and Eu concentrations were determined by inductively coupled plasma optical emission spectrometry (ICP OES). The Eu results were in agreement with the proposed methodology, and limits of detection (LOD) for REE varied from 0.003 mg L^{-1} (Lu) to 0.010 mg L^{-1} (Gd). The distribution of REE was also measured in surface sediments and sediment core collected in Sepetiba Bay, between June and September of 2016. The range of ΣREE concentrations was established between 25-496 mg kg^{-1}. This monitoring is important to evaluate the impact of the fast and unplanned urbanization and development of anthropogenic activities, common to many tropical coastal areas in Brazil.

Keywords

Rare earth elements; ICP-MS; ICP OES; geological samples.

Resumo

Rojano, Wendy Johana Sandoval; Saint'Pierre, Tatiana Dillenburg; Pinto, Christiane B. Duyck. **Determinação de elementos terras raras em amostras geológicas por espectrometria de massa com plasma indutivamente acoplado.** Rio de Janeiro, 2020. 99p. Tese de doutorado - Departamento de Química, Pontifícia Universidade Católica do Rio de Janeiro.

A distribuição de elementos de terras raras (REE) é representativa das rochas e solos que originalmente os contêm e é frequentemente usada como parâmetro geoquímico ou ambiental para identificação de fontes. Este trabalho propõe um novo método de preparo de amostras para a determinação de elementos de terras raras (REE) por espectrometria de massa de plasma acoplada indutivamente (ICP-MS) em amostras ambientais com altas concentrações de Ba. O método consiste na diluição das amostras, obtidas após decomposição ácida em sistema aberto, com ácido sulfúrico 10% (v/v) para a separação de Ba2+ como BaSO4. A remoção da interferência sobre os isótopos de Eu (151Eu and 153Eu) foi eficiente para concentrações de Ba superiores a 0,1 mg L-1. A exatidão e a precisão foram verificadas pela análise de tres materiais certificados, rocha basáltica (NIST 688), Geological Survey (Granite G-2) e sedimento marinho (MESS-3). A metodologia proposta foi aplicada ao pavimento asfáltico, à brita e ao material de referencia certificado. Adicionalmente, todas as amostras foram decompostas por fusão alcalina e as concentrações de elementos majoritários e Eu foram determinadas por espectrometria de emissão ótica de plasma acoplada indutivamente (ICP OES). Os resultados da Eu estavam de acordo com a metodologia proposta, e os limites de detecção (LOD) para REE variaram de 0,003 mg L-1 (Lu) a 0,010 mg L-1 (Gd). A distribuição de REE foi medida em sedimentos superficiais e amostras de testemunhos coletados na Baía de Sepetiba, entre junho e setembro de 2016. A faixa de concentração de ΣREE foi entre 25-496 mg kg-1. Esse monitoramento é importante para avaliar o impacto da urbanização e desenvolvimento rápido e não planejado de atividades antropogênicas, comuns em muitas áreas costeiras tropicais do Brasil.

Palavras-chave

Elementos terras raras; ICP-MS; ICP OES; amostras geológica

Table of contents

List of Figures

List of Tables

List of abbreviations

LOD – limit of detection

LOQ – limit of quantification

RSD- relative standard deviation

SPE- solid phase extraction

CAP - from Portuguese: *cimento asfáltico de petróleo*

XRF - X-ray Fluorescence Spectrometry

CRM - Certified Reference Material

ETV - Electrothermal Vaporization

F AAS - Flame Atomic Absorption Spectrometry

FCC - Fluid catalytic cracking

GF AAS - Graphite Furnace Atomic Absorption Spectrometry

HREE- Heavy rare earth elements

ICP OES - Inductively Coupled Plasma Optical Emission Spectrometry

ICP-MS - Inductively Coupled Plasma Mass Spectrometry

IUPAC - International Union of Pure and Applied Chemistry

LA-ICP-MS - Laser Ablation Inductively Coupled Plasma Mass Spectrometry

Ln - Lanthanides

LREE - Light rare earth elements

MS - Mass Spectrometry

NAA - Neutron Activation Analysis

NASC - North American Shale Composite

PAAS - Post-Archean Australian Shale

REE - Rare earth elements

WC AES - Tungsten Coil Atomic Emission Spectrometry

XRD - X-ray Diffraction Spectrometry

MRI - Magnetic Resonance Imaging

1
Introduction

Despite the difficulties encountered in their extraction from nature and separation by metallurgical processes, rare earth elements (REE: Lanthanides, Sc, and Y) are classified as “strategic critical metals” due to the growing demand for their use in electronic devices, industry and medicine [1,2]. The wide use of REE also raises environmental concerns due to their potential as emerging contaminants [3].

In geological deposits, REE occur mostly in the +3 state, being important geochemical indicators, because of regularities in their distribution patterns regarding the mineral phase, which constitutes a fingerprint of the hosted rock [4]. In particular, fractionation can occur during mineral phase formation, between the Light (LREE: La-Eu) and Heavy (HREE: Gd-Lu) REE, according to the atomic number groups.

These effects can be observed in plots of REE concentrations, after normalization by a representative original rock, generally the Post-Archean Australian Shale (PAAS) or the North American Shale Composite (NASC) [5]. REE patterns can significantly change in the hydrosphere, due to the contact of soils, rocks and sediments with fluids and the dissolution of enriched minerals, such as phosphates [6].

The determination of total concentrations of REE in geological sample often requires decomposition in closed vessels employing concentrated nitric, hydrofluoric and perchloric acids and the rise of the temperature [7,8]. In the case of acidic rocks, such as granite, which are not completely dissolved after wet digestion, authors have proposed a final step using fusion with lithium metaborate, obtaining good agreement with certified values [9].

Inductively coupled plasma mass spectrometry (ICP-MS) is commonly used for the determination of REE in rocks and sediments [10]. In the case of quadrupole-based spectrometers, the oxides of lighter REE and Ba are the most important interfering species among the heavier ones (e.g. BaO^+ in Eu^+ isotopes at m/z: 151 and 153), affecting the concentration in a significant level, even in cases when a careful instrument optimization is carried out. Mathematical corrections have been first proposed for rock analysis [11], however the relative

standard deviations associated to high Ba concentrations limit their precision. More elaborated models based on matrix approaches can improve them, but are more complicated for routine analysis [12].

For this reason, we propose a simple method capable of correcting the spectral interferences. This method is based on wet digestion in an open system, followed by dilution with sulfuric acid solution, for the determination of REE by ICP-MS after the removal of barium by precipitation and separation as $BaSO_4$. The methodology was applied to asphalt pavement and its related crushed stone, which are challenging samples due to the high Ba concentration that limits most methods proposed in literature [13,14]. The accuracy of REE determination was evaluated by the analysis of basalt and granite certified materials. The interference correction over Eu was additionally verified through an independent method, which employs sample fusion and determination by ICP OES. The characterization of asphalt pavement and crushed stone samples was assessed using the geological profiles obtained by the REE chondrite-normalized patterns.

Studies in the literature suggest that the rare earth elements (REE) are contaminants of emerging concern. The main sources of anthropogenic REE include medical facilities, petroleum refining, mining and technology industries, fertilizers, food for animals, electronic wastes and recycling plants [15]. The presence of REE in important fields has attracted increasing attention of scientists to determine and understand the toxicity and the environmental impact, which is still an open challenge. Due to the growing rate of urbanization and a rapid and unplanned development in many tropical coastal areas, there is an increasing concern in relation to the impact of anthropogenic activities on the environment [16]. Many places around the world have been monitored for determination of rare earth elements concentrations, to assess the impact and possible correlation with respiratory and heart diseases [17].

This thesis is structured in six chapters, chapter 1 and 2 are the introduction and objectives of this work, in the chapter 3 a bibliographic review is made to present the theoretical basis on determination of rare earth elements in environmental samples, focusing about the sample preparation and interference correction, besides indicating other relevant information about their potential environmental impact. Chapter 4 contains detailed information on instrumentation, materials and procedures used in this work. The results are presented in chapter 5, referenced to a paper that was published in the *Microchemical Journal*, concerning to the determination of rare earth elements in environmental samples with high concentration of Ba and the results of the determination of rare earth

elements, which are described and discussed. Finally, in chapter 6, the overall conclusion of the thesis is made along with directions for future work.

2
Objectives

2.1
General Objective

Development of spectrometric methods for the determination of rare earth elements in environmental samples by Inductively Coupled Plasma Spectrometric Techniques.

2.2
Specific objectives

- ✓ To determine rare earth elements geological samples with high Ba concentration by ICP-MS employing sulfuric acid for the removal of barium interference.
- ✓ To adjust the conditions for the preparation of geological samples by combining wet digestion and fusion to complete the total decomposition.
- ✓ To remove of barium oxide interference over Eu by dilution in sulfuric acid solution after the precipitation and separation as $BaSO_4$.
- ✓ To apply the proposed approaches approaches in the analysis of asphalt and crushed stone.
- ✓ To characterize the distribution and concentration of REE in sediments of Sepetiba Bay and to identify the main sources and sinks of these elements.
- ✓ To determine the relationship of REE to the various zones and bottom types of Sepetiba Bay.

3
Theoretical fundaments

3.1
Rare Earth Elements

Rare earth elements (REE) were first isolated in the 18th and 19th centuries, as mineral oxides considered rare ones. The term "rare earths" is misused because these elements are much more abundant than many precious metals. These elements are not rare, but rather found in low concentrations throughout the earth's crust. These elements share many properties in common, which make them difficult to separate and distinguish one from the other. REE are usually silver-plated or grey, malleable and ductile and have high electrical conductivity and reactivity at elevated temperatures. They have similar ionic radius and their oxidation state is generally 3+ [18].

Rare earth elements include both the lanthanides (elements from lanthanum (La) to lutetium (Lu) with atomic numbers 57–71 in the periodic table), plus scandium (21) and yttrium (39). They are typically divided in two groups, the light rare elements (LREE), from La to Eu, and the heavy rare earth elements (HREE), from Gd to Lu, this classification is based on their atomic mass and effective ion radius [19,20]. Yttrium and Scandium are also included in the heavy element group and Pm does not exist in nature. LREE (light rare earth elements) include those with a lower atomic mass (weight) than ca. 153 and effective radius larger than 95 pm. HREE (heavy rare earth elements) correspond to those with a higher mean atomic mass than ca. 153 and a lower effective ion radius than 95 pm. Due to its low ion radius, Y is often included in this subgroup as well, in spite of its low atomic mass. MREE is sometimes used in the literature to designate REE of intermediate mean atomic mass and ion radius. This subgroup being rarely well defined [6].

The great difficulty of separating the lanthanides to obtain the individual elements is due to the high similarity of their physical and chemical properties, with very small differences between them in relation to the solubility of their compounds or the formation of complexes. Since they are present, with few exceptions, in the 3+ oxidation state and that they have fairly close ionic rays, the substitution of one

REE by another is free of impediments in several crystalline reticles. Thus, such ease of substitution results in the simultaneous occurrence of several REE in a single mineral, as well as a considerable distribution of such elements in the Earth's crust [2].

Rare earth elements presents the phenomenon of "lanthanide contraction", which consists in a significant decrease in size of atoms and ions with the increase of atomic number. Thus La^{3+}, with the lowest atomic mass (138.9 g mol^{-1}), has the largest ionic radius (1,061 Å), while Lu^{3+} (174.96 g mol^{-1}) has the lowest ionic radius (0.848 Å). The variation between the radium of two neighboring ions is, on average, 0.0152 Å. When we run through the series, from La to Lu, both the nuclear charge and the number of electrons 4f increase step by step. The shielding of one 4f electron by another is imperfect due to the shapes of the orbitals, thus causing the reduction of volume reduction of the entire 4f configuration. The progressive filling of the 4f orbitals from La to Lu, which results in the lanthanide contraction, also induces an increase in electronegativity and variation in the coordination numbers through the La-Lu series. Their coordination numbers vary from 6 to 12, both in the solid state and in solution, with 8 and 9 being the most common coordination numbers [19,21]. In the compounds with trivalent REE ions, the 4f orbitals are located in the inner part of the atom being fully protected by the electrons of the 5s and 5p orbitals. They have limited radial extension and do not participate in the bonds, only a very small involvement occurring with the orbital of the binders. As consequence, the lanthanide ions form complexes with high ionic character [22].

3.2
Occurrence of rare earths in the Earth's crust

The upper continental crust, being the most accessible part of our planet, has been subject of geochemical investigations to establish its composition. However, initially, most researches do not include the rare earth elements. Taylor [23] used for the first time the different abundances of the REE in granitic and basaltic rocks as a basis for estimating the composition of the continental crust, showing that a mixture of 1:1 mafic to silicic igneous rock would produce the observed REE distribution in “average sediment”. This igneous rock mixture was considered, therefore, to represent the composition of average continental crust.

Cerium is the most abundant rare earth element and represent $6.6x10^{-3}$ wt. % in the earth's crust. It is the 25^{th} most abundant element, similar to Cu and it is about four times more abundant than Pb, whereas thulium and lutetium are about

200 times more abundant (0.5 mg kg^{-1}) than gold. In rare earth exploration, the real problem is not their absolute concentration in the crust, but rather, their relative concentration: it is very difficult to find economically exploitable deposits and simple methods of extraction and separation because of their very similar properties [24].

The rare earth elements are associated in different proportions with various minerals, but only a limited number that includes gadolinite, allanite, lopatite, euxenite, apatite, monazite, batsnezite and Xenotime [25,26] have commercial interest. The Monazite is essentially a lanthanide orthophosphate [$Ln(PO_4)$], in which the light elements (La, Ce, Nd, Pr and Sm) predominate. The Batnezite is a fluorocarbon [$LnFCO_3$], containing light elements (La, Ce, Nd and Pr) and Xenotime is a phosphate of Y, with heavy elements (Er, Dy, Gd and Yb) [27].

3.3
Presentation of the rare earth elements profiles

The chemical elements are distributed in the different layers of the earth, lithosphere, hydrosphere, biosphere and atmosphere, and the composition of these layers is determined by the geological history of each one, due to the geochemical and biochemical changes in the environment and also by the properties of the elements found in it. In 1914, Giuseppe Oddo realized that elements with in even atomic number are more abundant than their odd neighbors in the periodic table. Oddo's statement was later reinforced by Willian Draper Harkins, who confirmed this hypothesis, finding elements with even atomic numbers in a proportion of 98 % in meteorite samples [28]. This effect became known as the “Oddo-Harkins” rule, producing a zigzag pattern in a composition-abundance diagram.

The distributions of elements in samples of geological origin are usually normalized by means of recognized standards, such as chondritic values, which are basically the elementary concentrations in chondrite meteorites, which were chosen because they are considered relatively unfractionated materials in the solar system, belonging to the original nucleosynthesis. The concentrations of lanthanides in the solar system are variable due to the different stabilities of atomic nucleus [29].

The REE concentrations are generally plotted as a function of their increasing atomic numbers. The REE with even atomic numbers have generally higher concentrations than their neighbors with odd atomic numbers. The “Oddo-

Harkins effect" normalization is an alternative to eliminate this effect. To get rid of this phenomenon and interpret REE distributions, their concentrations are commonly normalized. The values for normalization are chosen according to the system under investigation [20].

The normalized REE patterns evidence ,for instance, enrichment or depletion of a group or of an individual REE relative to the others. These relative differences are called anomalous fractionation, whose intensities are further quantified by ratios. The fractionation between LREE and HREE is commonly quantified by two distinct ratios, La/Lu and La/Yb, depending on the Lu contents, which are sometimes very small to be accurately measured or by ΣLREE/ΣHREE. In all cases, fractionations are calculated using the normalized concentrations. A REE anomaly is quantified by the ratio of its normalized concentration to the half of the sum of the normalized concentrations of its two neighbors. Different calculations are proposed in the literature for these anomalies. We see here that the choice of the reference is crucial for the subsequent interpretation of the fractionations and anomalies [19]. The commonly employed classical normalization values NASC (North American Shale Composite) and PASS (Post-Archean Australian Shale) are presented in Table 1.

Table 1. REE concentrations (mg kg^{-1}) in some classical references used for normalization [30].

Element	NASC	PAAS
La	32	273,6
Ce	73	570,9
Pr	7,9	63,2
Nd	33	221,9
Sm	5,7	35,2
Eu	1,2	7,2
Gd	5,2	29,9
Tb	0,85	4,5
Dy	5,8	27,1
Ho	1	6,1
Er	3,4	17,3
Tm	0,5	2,4
Yb	3,1	15,4
Lu	0,48	0,032

3.4
Application, economic interest and global rare earth elements distribution

The dominant uses for rare earth elements in the world are for automobile catalysts and petroleum refining catalysts. The most common application of phosphors compounds (that contains Y, Eu, Ce, and Tb) include color television and flat panel displays to cell phones, portable DVDs, laptops, rechargeable batteries for hybrid and electric vehicles, permanent magnets and numerous medical devices [31]. Permanent magnets containing neodymium, gadolinium, dysprosium, and terbium are used in numerous electrical and electronic components and new-generation generators for wind turbines [32]. In medicine, gadolinium is used as ingredient in several compounds for treatments, being commonly used as a contrast agent in magnetic resonance imaging (MRI) [33–35]. The rare earth also exhibit antibacterial, antifungal and nematicidal activities at levels comparable to copper ions, which are widely used as antibacterial metal [36–39]. In agriculture, REE are used in fertilizers. China has widely spread the use of REE based fertilizer since 1990 [40,41]. The area of croplands that have applied REE-based fertilizers has reached about 4 million hectares.

An important consideration are the environmental risks associated to these REE. Their increasing industrial usage can lead to a growing release points into the environment and raising the prospect of REE as significant environmental pollutants [42,43]. The countless applications of rare earth elements have aroused the interest in exploiting these resources, considered by the European Commission as one of the 14 raw materials as metal or group of metals, that are critical for many important emerging technologies [44].

The REE are distributed among many mineral deposits, but only those quite abundant deposits can be called rare earth reserves, what makes them economically viable [45]. Reserves of REE are not equally distributed around the world, the natural reserves of REE are concentrated in few countries, mainly in China, Russia, USA, India, Australia, Brazil, and Malaysia. The whole world REE reserves were about 110 million tons. China ranks the first position, with more than 60 % (55 million tons); Russia, the second one, with about 17 % (19 million tons); United States are the third, with about 12 % (13 million tons), then followed by India (3.1 million tons), Australia (1.6 million tons), Brazil (0.48 million tons), Malaysia (0.3 million tons) and other countries (22 million tons, 20% of total) [45,46].

Unlike other metal recycling industry, the one for rare earth is evolving rapidly. The need for recycling is in part driven by a rapid increase in demand and

scarcity of materials. The recycling option offers several advantages including lower environmental impact and less dependency on countries that control the market for these metals [47]. Raw materials with great potential for recycling rare earths are used in magnets, batteries, lighting and spent catalysts. The materials could be sourced from post- production wastes and postconsumer disposed goods. Clearly, the latter option is expected to be more complex, requiring more extensive physical and chemical treatments and higher energy requirement [48].

3.5
Rare earth elements toxicity

Recent technological advances in medicine, mobile communication and energy have resulted in an increase of the extraction and subsequent use of REE. The growth in industrial applications could be accompanied by their rise in the environment, posing public and ecological health risks. In the context of contaminants of emerging concern, the current studies is limited to the lanthanides (La-Lu), yttrium, and scandium [17].

Several adverse effects in human health associated with REE exposure have been reported such as occupational lung disease associated with the exposure to numerous inorganic elements, such as La, Ce, Nd, Sm, Eu, Tb, Lu [49] and cardio-respiratory diseases associated to atmospheric pollutants [50,51]. Other research has shown some effects associated with the presence of REE with the degradation of different ecosystems.

Saiki *et al*. [50] found a relation between the lanthanum concentrations through the biomonitoring of lichen samples and their mortality rates. This correlation is the indication of possible causes of the mortality due to cardio-respiratory diseases. These findings suggest the application of air pollution biomonitoring as a method to assess risk and adverse health effect of REE, especially in atmospheric samples, such as dust and particulate matter (P.M.).

Rogowska *et al*. [42] analyzed the anthropogenic Gd used as a contrasting agent in magnetic resonance imaging (MRI), after the excretion from the human body (urine) and the influence in the living organisms and on human health.

Gadolinium compound showed potential to migrate across the blood-brain-barrier and accumulate in the brain where they may cause severe damage on the neurological system [15]. Other potential human health effects of REE include; dysfunctional neurological disorders such as reduced intelligence quotient (IQ) in children, associated with La, Ce-pnemoconiosis, (3) bone alteration, genotoxicity

and fibrotic tissue injury, associated with several REE and (4) anti-testicular effects and male sterility. However, epidemiological data in this field are limited and only a small number of investigations on the toxic properties of Gd have been conducted. Therefore, there is need for further research on toxicodynamics and toxicokinetics, and short and long-term exposure effects of REE in humans.

3.6
Spectrometric techniques for the determination of REE

The main techniques used for the determination of lanthanides are inductively coupled plasma optical emission spectrometry (ICP OES) [52,53] and inductively coupled plasma mass spectrometry (ICP-MS) [54], which can be coupled to laser ablation (LA-ICP-MS) [55] for the introduction of the samples. Plasma techniques are the most commonly used in the determination of rare earth elements, since they are multi-elementary, give good precision, accuracy and rapidity of analysis. Determination of lanthanides by Electrothermal Vaporization for aample introduction in plasma source spectrometry (ETV-ICP-MS) is difficult, since these elements are refractory and form carbides with the atomizer's constituent material (graphite tube), which results in reduced sensitivity and pronounced memory effect.

Other techniques also used for the determination of REE are X-ray diffraction spectrometry (XRD), used for qualitative analysis [56], X-ray fluorescence spectrometry (XRF) [57], neutron activation analysis (NAA) [58], capillary electrophoresis (CE) [59] and tungsten coil atomic emission spectrometry (WC AES) [60]. On the other hand, atomic absorption spectrometry with graphite furnace (GF AAS) and flame atomic absorption spectrometry (F AAS), widely used for the determination of several elements, are not recommended for the determination of lanthanides; GF AAS due to the formation of carbides and F AAS due to the formation of flame refractory oxides and the low sensitivity.

3.7
Inductively Coupled Plasma Spectrometric Techniques (ICP-MS and ICP OES)

The definition of plasma is an electrically neutral gas constituted by positive ions and free electrons. Plasmas have sufficiently high energy to virtually atomize, ionize, and excite all elements in the periodic table. For this reason, inductively coupled plasma spectrometric techniques are a powerful tool for the determination

of several elements in a variety of different sample matrices. In this techniques, normally liquid samples are introduced into a radiofrequency (RF) induced argon plasma using nebulizers or sample introduction systems.

The inductively coupled plasma optical emission spectrometry (ICP OES) is based on the measurement of the spontaneous emission of photons from atoms and ions that have been excited in a plasma. In the case of the inductively coupled plasma mass spectrometry (ICP-MS), the ions are separate according to their mass-charge ratio (m/z) and are measured at the detector. The Figure 1 show the processes taking place when a sample droplet is introduced into an inductively coupled plasma spectrometer (ICP).

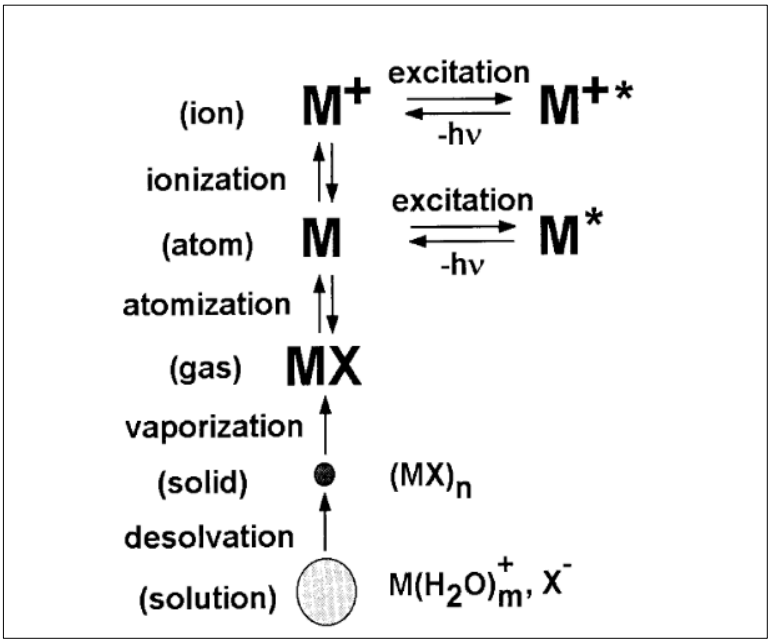

Figure 1. Processes taking place when a sample droplet is introduced into an ICP [61].

3.7.1
Inductively Coupled Plasma Mass Spectrometry (ICP-MS)

Inductively coupled plasma mass spectrometry (ICP-MS) is an analytical technique for the determination of elements through the mass/charge ratio of their isotopes, to provide a qualitative and/or quantitative analysis of a sample. One of its main advantages is the high sensitivity, which can detect species in concentrations up to pg/g.

The fundamental compartments of a single quadrupole ICP-MS are: sample introduction system, inductively coupled plasma (ICP), interface, ion optics, mass analyzer and detector [62]. A short scheme is presented in **¡Error! No se e ncuentra el origen de la referencia.** to describe the most relevant components

of an ICP Mass spectrometer where: 1 Sample; 2 Nebulizer; 3 Spray chamber; 4 Torch; 5 Load coil and plasma; 6 Interface; 7 Lens; 8 Quadrupole; 9 Ion detector; 10 Computer; 11 Mechanical pump and 12 Turbo-molecular pump.

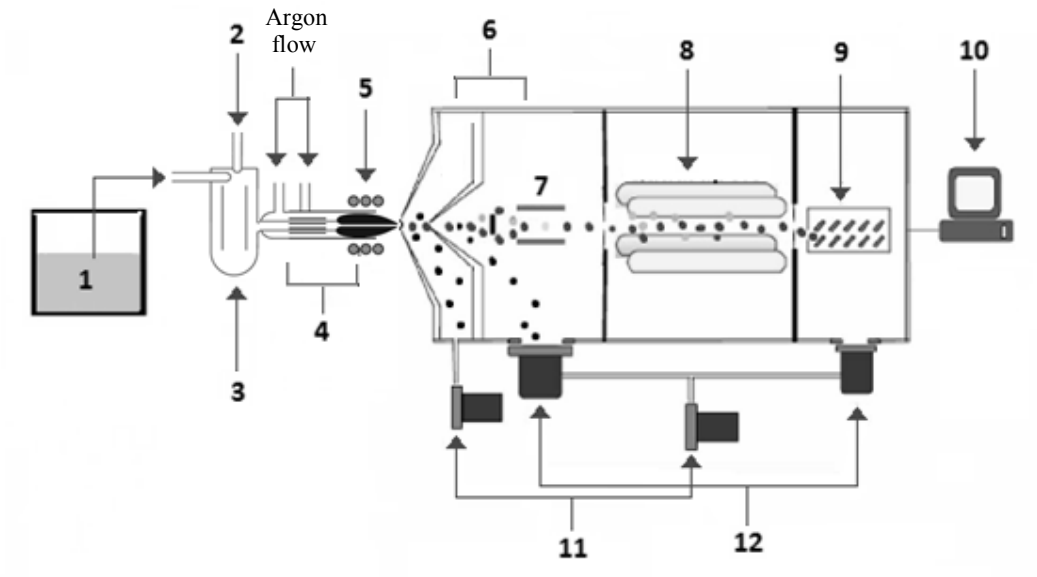

Figure 2. Parts of ICP Mass spectrometer.

The initial step in the use of ICP-MS is the introduction of the sample, usually in aqueous medium (1). The liquid sample is pumped from a vial via peristaltic pump into the nebulizer (2), which sprays the solution into an aerosol that is then carried by the nebulizer gas (also called aerosol carrier gas) through a spray chamber (3), in which the larger droplets are condensed and discarded. More than 95 % of the sample is thus discarded and only the smaller droplets, forming a more homogeneous cloud of aerosol, are carried to the plasma.

The plasma torch (4) normally consists of three concentric tubes, which are usually made from quartz, one outer tube, middle tube, and sample injector. The torch can either be one piece with all three tubes connected, or it can be demountable, in which the tubes and the sample injector are separated. The gas (Ar in most times) used to form the plasma (plasma gas) is passed between the outer and middle tubes at a flow rate of 12–17 L min^{-1}. A second gas flow, the auxiliary gas, passes between the middle tube and the sample injector at ;1 L min^{-1} and it is used to change the position of the base of the plasma relative to the tube and the injector. A third gas flow, the nebulizer gas, also flowing at ;1 L min^{-1} carries the sample, in the form of a fine-droplet aerosol, from the sample introduction

system [63]. The plasma is formed by a high intensity electric discharge at the end of the quartz torch, centered inside an electromagnetic induction coil (5) fed by a radiofrequency source [64].

The ion sampling and extraction interface consists of metal cones (sampling and skimmer cone) with a small circular orifice (<1 mm), through which the ions are extracted from the plasma to the mass spectrometer. The role of the interface region (6) is to transport the ions efficiently and with electrical integrity from the plasma which is at atmospheric pressure (760 Torr) to the mass spectrometer analyzer region at approximately 10^{-6} Torr through the ionic lenses (7), by a turbo molecular pump.

The positive ions beam is focalized by a magnetic field generated through a series of energized plates called ionic lenses (7), toward the quadrupole analyzer, whereas neutral and negative charged species are eliminated by the vacuum pumps. This way, the focusing in a collimated beam of the ions with similar energy distribution takes place. The path of the ions through the ionic lenses depends on their kinetic energy and the applied voltages [64].

The separation of these ions occurs through the application of oscillating electromagnetic fields with different potentials to each pair of rods of the quadrupole (8). The different field configurations applied to the quadrupole electrode pairs are adjusted so that the ion trajectories are separated according to the mass/charge ratios, allowing the ions to reach the detector separated by a unit of atomic mass. The final process is to convert the ions into an electrical signal with an ion detector (9) [64]. The most common design used today is called a discrete dynode detector, which contains a series of metal dynodes along the length of the detector. In this design, when the ions emerge from the mass filter, they impinge on the first dynode and are converted into electrons. As the electrons are attracted to the next dynode, electron multiplication takes place, which results in a very high stream of electrons emerging from the final dynode, amplifying the signal. This electronic signal is then processed by the data handling system (10) and converted into analyte concentration using ICP-MS calibration standards [62,65].

The types of pumps employed in mass spectrometers are mechanical (11) and turbomolecular (12) rotators (60,000 to 90,000 rpm). One of the advantages of turbomolecular pumps in relation to mechanical rotators is the fact that oil is not used for its operation, which reduces the risk of contamination.

3.7.1.1
Mass spectrometry interferences

Inductively coupled plasma mass spectrometry has been widely used for element determination in several samples. However, this technique has spectral and non-spectral interferences, disadvantages that are briefly explained below.

Non-spectral interferences occur in general due to factors that affect the sample transport process, the efficiency of ion production in the plasma or after the extraction and conduction of the ions to the mass analyzer [66]. These interferences are the most easily resolved by the classic methods of internal standardization, standard addition, or the more complex isotopic dilution.

The spectral interferences are the most difficult to circumvent and are usually divided into 4 types: isobaric, double charge, polyatomic and oxide ions. Isobaric interference occurs when isotopes of different elements have the same mass and the same mass/charge ratio, generating overlapping signals. Double charge ion interference occurs mostly due to the presence of elements with low ionization energy and mass 2 times greater than that of the analyte, resulting in similar m/z ratio. The formation of polyatomic ions occurs mainly with elements in high concentrations in the plasma, such as Ar itself and elements of the sample or solvent matrix, such as C, S, N, etc. Although oxide ions are also polyatomic, they receive special attention, as it occurs either with the analyte itself or with an element's isotope with a mass of 16 u less than that of the analyte. The formation of oxides occurs in the coldest regions of the plasma or close to the surface of the sampling cone. Its formation is favored by the introduction of a high rate of the solvated sample, due to the cooling caused in the central channel of the plasma [64].

The main spectral interferences are usually informed by the equipment's software and can be circumvented by choosing an alternative isotope, by applying correction equations or by alternative ways of introducing the sample (when these allow the separation of the analyte from the matrix, eliminating the interfering species). In turn, the interferences caused by oxides and double charge ions are normally controlled by the optimization of the plasma operating conditions, such as the power of the radio frequency and the flow of the nebulization gas, which define the temperature and the sampling position in the plasma [67].

For the determination of REE, the use of ICP-MS presents some important spectral interferences, such as $^{135}BaO^{+}$ over $^{151}Eu^{+}$, $^{144}NdO^{+}$ over $^{160}Gd^{+}$ and $^{143}NdO^{+}$ over $^{160}Tb^{+}$ [68]. There are two ways to resolve such interference:

- The first is the prior physical separation of REE from other elements. Although this method is very reliable because it eliminates the interference almost completely, it represents another complex step in the preparation of the samples and, when working with very low concentrations, the inevitable loss of analyte in the separation can impair the reliability of the results.
- The second path becomes more promising: the use of correction equations for interferences. The disadvantage of this method is the loss of sensitivity, since sometimes, as in the case of BaO in Eu interference, the interference represents up to 70 % of the spectral peak measured in the equipment [69]. Table 2 shows the main interferences in the determination of lanthanides by ICP-MS.

In general, the ICP-MS technique, due to its sensitivity combined with a relatively simple spectrum and multi-element capacity, has been considered the most promising technique for determining REE. The main drawbacks associated with the use of this analytical technique are the presence of interferences such as spectral overlap of oxides MO^+ and hydroxides MOH^+ of light REE (LREE) on heavy REE (HREE). These species occur with 16 u or 16 + 1 u above the metal and present a potential problem for the determination of rare earths [70]. In samples with high levels of Ba, the formation of polyatomic ions, such as BaO^+ and $BaOH^+$, can result in significant interference with both ^{151}Eu and ^{153}Eu isotopes, being significant for the Ba/Eu ratio greater than 200/1 [70].

Table 2. Most common interferences in the determination of lanthanides by ICP-MS [71].

Element	m/z	Interference	Element	m/z	Interference
La	139		**Gb**	158	$^{142}Ce^{16}O^+$
Ce	140		**Tb**	159	$^{143}Nd^{16}O^+$
Pr	141		**Dy**	164	$^{148}Sm^{16}O^+$
Nd	142	$^{142}Ce^+$	**Dy**	162	$^{146}Nd^{16}O^+$
Nd	144	$^{144}Sm^+$	**Dy**	163	$^{147}Sm^{16}O^+$
Nd	146	$^{130}Ba^{16}O^+$	**Ho**	165	$^{149}Sm^{16}O^+$
Sm	152	$^{136}Ba^{16}O^+$	**Er**	166	$^{151}Eu^{16}O^+$
Sm	154	$^{138}Ba^{16}O^+$	**Er**	167	$^{150}Nd^{16}O^+$
Eu	153	$^{137}Ba^{16}O^+$	**Tm**	169	$^{153}Eu^{16}O^+$
Eu	151	$^{135}Ba^{16}O^+$	**Yb**	174	$^{158}Gd^{16}O^+$
Gd	155	$^{139}La^{16}O^+$	**Yb**	172	$^{156}Gd^{16}O^+$
Gd	156	$^{140}Ce^{16}O^+$	**Lu**	175	$^{159}Tb^{16}O^+$

More recently, instrumental developments have promised to correct interferences, but in samples with high Ba concentrations, additional approaches were necessary to lower the BaO^+ levels in the plasma. Bayon *et al.* have proposed the co-precipitation of REE with iron hydroxide after sample digestion using alkaline fusion, prior to the analysis by sector field-inductively coupled plasma-mass spectrometry (SF-ICP-MS) [13]. Nikolaeva *et al.* proposed ultrasonic nebulization, which reduces oxide formation at the sample introduction system into a high-resolution ICP mass spectrometer [14]. Both studies showed limitations in the case of samples with Ba/Eu >1000. Spectrometers equipped with a collision/reaction cell can be strategical for partial or total elimination of the polyatomic interferences (e.g. oxides) by introducing a specific gas or mixture into the cell [68,72–75]. The main drawback is the lowering of the analyte signal, which compromises the limits of quantification, and the incomplete elimination of the interference. Electrothermal vaporization (ETV) could be an alternative for eliminating the sample matrix, but it is not suitable due to the formation of carbides with REE, being an expensive accessory, and thus, not always commercially available [67,76]. In the case of complex matrices, separation methods are recommended [77]. Recently, solid phase extraction (SPE) has been used for matrix removal and pre-concentration of REE in water [78–80]. Despite its broad application for trace element preconcentration, its major drawback is the limited range of pH that can be used, due to solid phase stability and, in the case of geological samples with high Fe and Al concentrations, losses by hydrolysis can occur. Also, the overall procedure is time consuming and prone to contamination.

3.7.2
Inductively Coupled Plasma Optical Emission Spectrometry (ICP OES)

As indicated by its name, Inductively Coupled Plasma Optical Emission Spectroscopy (ICP OES) is a technique that uses a plasma as an ionization source (as well as ICP-MS) and relies on optical emission for analysis. Optical Emission Spectrometry employs the measurement of the intensity of the light emitted by atoms and ions when their electrons decay from excited states. A dispersive system is required to separate the wavelengths emitted. After separation of emitted radiation in different wavelengths, a detector is used to quantify their intensities of the emitted radiation. Different detectors, such as, solid-state or photomultiplier tubes can be used, according to the application and the required performance [61].

The steps of sample introduction and ionization in plasma are similar to those described for ICP-MS. Then, the radiation emitted by the population of atoms and ions is measured in the plasma region called normal region, which has temperatures between 6500 and 6800 K. This radiation enters into a polychromator, through an entrance slot capable of selecting a thin spectral band with the same dimensions of the slit and aligned to the region of the plasma, where the analytes present the maximum ratio between intensity of emission and background intensity. The polychromator is, in general, formed by the entrance slot, mirrors, diffraction grids and an exit window, however, different forms of organization of this optical system can be used for the detection of different regions of the spectrum [81].

Non-spectral interferences are associated with the same causes as those in ICP-MS, being resolved in the same ways. The relevance of interferences is related to the ratio between the concentrations of the interfering species and the analyte [82]. The main spectral interference associated with ICP OES is due to the overlapping of the spectral lines of different elements. There may be a coincidence of lines (total or partial). Three different tactics can be used if spectral overlap occurs. First, the operator can choose interference-free lines for a particular sample. Alternatively, the source of the spectral interference can be identified and its magnitude determined and subtracted from the measured signal. Finally, a multi-line detection scheme can be used with factorial analysis [83].

The determination of REE by ICP OES has the advantages of a fast, sensitive and multi-elemental technique, sufficient for many applications. However, the complexity of the spectrum of many REE and the existence of interference in some of them makes this type of analysis difficult, which often requires techniques for their elimination [68]. In addition, ICP OES requires samples with concentrations many times higher than those presented by rare earth elements in nature. A good alternative, however, for the use of this technique is the combination of it with an ion exchange separation technique, since this last can eliminate interferences and pre-concentrate the analytes at the same time, giving greater sensitivity to the method [84].

3.8
Samples

In general, due of their wide variety of applications, rare earth elements have been determined in different types of samples. The presence of rare earth elements (REE) in geological materials provides important information about the formation and the geochemical processes that rocks undergo. In environmental monitoring, REE have been used as geochemical fingerprints, giving information on rock formation and geochemical processes occurring in the Earth's crust [85], as well as indicator of anthropogenic sources, giving information about origin of archeological samples [12].

From the perspective of environmental monitoring, the biological tissues can be used to identify the REE accumulation in the environment, associated with the anthropogenic impact [86]. In fact, it is known that mollusks incorporate nutrient particles solids filtering water through their siphons. Further, living near the seabed, mollusks are exposed and accumulate REE of sediment particles [87–89].

The REE are determined in environmental samples, such as particulate material (PM2.5) [90], soil [91] and urban river sediments near an industrial effluent source [92]. They are now recognized as emergent pollutants in river systems impacted by anthropogenic activity [93]. Over the past 20 years, significant anthropogenic contributions were reported for Gd, La and Sm, and it is expected that REE contamination in environment is to further increase in a near future.

Other commonly studied samples are urban and industrial residues, such as electric and electronic equipments and fluorescent lamps. The interest in the metals recovery has grown rapidly due to its economic value and the environmental impact they may present for different ecosystems, due to the increasing use of rare earth elements in new technology development.

3.8.1
Sample preparation

The determination of REE in geological samples is generally preceded by decomposition procedures involving acids and mixtures of acids, as well as open or closed decomposition systems. The preparation and complete dissolution of the sample can be the biggest problem for the determination of REE in geological samples. Most procedures employ hydrofluoric acid (for decomposition of refractory silicates) and a mixture of oxidizing acids, such as nitric and perchloric acids. Some of the acids or acid mixtures involved in the decomposition procedures

are: HNO_3 [94], $HF/HNO_3/HClO_4$ [52], $HF/HNO_3/H_3BO_3$ [95] and $HF/HNO_3/HCl/H_3BO_3$ [96].

The complete dissolution of rock samples is difficult due to the presence of resistant minerals, such as garnets, spinel and zircon, which requires the use of hydrofluoric acid. Thus, the choice of the decomposition method depends on the mineral composition of the rock. The alkaline fusion with lithium metaborate is an alternative to the use of HF to promote the complete dissolution of these refractory minerals [84].

However, in some samples, the REE concentration levels are so low that the decomposition/dilution of the samples results in low concentration. For these samples, separation/concentration methods, direct analysis of solids by LA-ICP-MS [55] and suspensions by ETV-ICP-MS [76,97] were proposed, as alternatives to the methods mentioned above.

Other methods can be used, such as acidic leaching assisted by ultrasound, which is considered an alternative for the pretreatment of a solid sample, as this energy facilitates and accelerates some steps, such as dissolution, fusion and extraction, among other effects. Ultrasound assisted extraction has been explored for sample preparation in agricultural, biological and environmental applications [98,99]. The chemical effects of ultrasound have been attributed to cavitation, generating high local temperatures and the mechanical action between the solid and liquid interfaces [100]. Thus, the efficiency of extraction of the analyte depends on the variables that influence the cavitation process, such as temperature, viscosity, presence of solid particles, height of the water column, frequency, and the position of the containers used for the extraction, among others. However, as long as the experimental conditions are constant, the ultrasound device is an excellent way to perform solid-liquid extraction [101].

Alkaline fusion with lithium metaborate can be also used as a method to promote complete dissolution of refractory minerals. However, in some samples, the concentration levels of REEs are so low that the dissolution procedure results in a too excessive dilution of the sample to allow the accurate determination [13].

3.9
Asphalt pavement and crushed stone

Asphalt pavements are made up of a superficial layer of mineral aggregate coated and cemented by asphalt on a support layer that can be asphalt based, crushed stone, slag and gravel or on Portland cement concrete, bricks and blocks. The asphalt mixture used in paving is generally made up of three main

components: aggregate; filler and asphalt cement used as a binder for mineral aggregates [102]. Asphalt petroleum cement (CAP), also called asphalt binder, is a very viscous, semi-solid or solid liquid at room temperature, which shows a thermoplastic behavior, that is, it becomes liquid when heated and returns to its original state after cooling. It is very soluble in benzene, trichloroethylene and carbon disulfide. CAP is the asphalt obtained especially for presenting the qualities and consistencies suitable for direct use in the construction of asphalt layers of pavements. Under extreme conditions, the CAP behaves as elastic solid or as viscous liquid. Thus, the susceptibility to temperature and loading time of a CAP are important variables in the performance of pavements, and should be quantified by rheological tests that determine the fundamental properties of these materials [103]. One of the complexities of studying the asphalt pavement is the variety of its components. The chemical composition can vary due to several factors, such as: the oil source, the type of fractionation, the changes induced in the refining processes and during the aging process [104]. The factors that can be considered for the wear of asphalt cement are the effects of light, water, chemical reactions with the aggregates, microbiological deterioration and absorption of heavy components of the asphalt cement on the surface of the aggregates.

Du *et al*. [105,106] studied the leaching effects of acid rain on the hydraulic properties of the pavement and soil pollution using laboratory tests, such as infiltration and immersion. It was found that the hydraulic conductivity of the soil decreases and there is an increase in the pore, thus causing an increase in the volume of liquid permeated in the soil. The results showed that the concentrations of calcium and lead leachate in the infiltration test were much higher than those in the immersion test, indicating that the infiltration test can be used as a suitable process to investigate the impact of acid rain for the characteristic leaching of metals in solidified cement, causing soil contamination with potentially toxic metals.

Due to the components of geological origin that make up the asphalt pavement, it is possible to find rare earth elements in it and, because of the effects of physical wear, it is possible that these metals are released into waters bodies and soils, which makes the asphalt pavement a relevant matrix for the determination of REE.

3.10
Rare earth element in marine sediment in Sepetiba Bay

Sepetiba Bay is located in the southeastern of Brazil, approximately at latitude 23°S and longitude 44°W about 60 km south of the Rio de Janeiro city. The Bay is separated from the Atlantic Ocean by a sand bar (Restinga de Marambaia), which connects the mainland in the east to an island in the west (Ilha de Marambaia). The Bay is a classic estuarine ecosystem, which consists in a partially enclosed coastal body of water, where the fresh water from rivers and streams is mixed with the salt water from the ocean. The estuaries and their surrounding terrain are places considered transient from land to sea, occur in sheltered coastal regions and present favorable conditions for feeding, protection and reproduction of many animal species, being important transformers of nutrients in organic matter. Besides, the mangrove ecosystem plays an important role in hydrodynamic stability of the marine coast of tropical countries.

During the last decades, several studies have been carried out in the Sepetiba Bay mangrove area due to the development of the region with the process of industrialization. This region became a source of income, generating migratory cycles and risks of contamination due to industrial activities, which have been pointedout as the main responsible for the release of potentially toxic waste in the bay [107,108]. Near to 400 industries including metallurgical, petrochemical and pyrometallurgical smelters, which emitted pollutants to air, soil and water, were established in Sepetiba Basin during the past 30 years [109]. These studies have discussed the anthropogenic influence related to the livestock and agricultural activities and ore transportation to the port in the east of the Bay associated with waste production from the nuclear power plants located in west of Angra dos Reis district [110]. Gonçalves *et al*. [111] evaluated the temporal and spatial mercury trends based on superficial sediment samples and ^{210}Pb-dated sediment profiles. According to their results, Hg distribution in Sepetiba Bay surface sediments shows a concentration gradient, with the highest values in the region close to its main fresh water contributors, São Francisco Channel and Guandu River, a pattern that has not changed during the last twenty years. Based on ^{210}Pb-dated sediment, it is possible to conclude that, in the region under direct influence from the land-based sources, Hg concentrations in surface sediments have increased steadily during the last years and confirm the concentration differences of maximum values observed, when comparing to the literature. Sepetiba Bay suffers environmental impacts caused by several river waters from adjacent basins, with some 30 % of the total Hg flow to Sepetiba Bay and a 10-fold increase in water and sediment

fluxes resulting from this. The decrease of environmental quality compromises both the large biodiversity and the potential economic uses of Sepetiba Bay, including fisheries and tourism.

In other study, the distribution of rare earth elements in surface sediments was measured on samples collected from 40 stations in Florida Bay. This bay receives fresh water from some rivers and several canals from the Everglades, which contribute for the supply of rare earth elements and other metals to the bay [112]. This cited work was the first extensive study of REE determination in Florida Bay, in which the concentrations of Y, La, Ce, Pr, Nd, Sm, Eu, Gd, Tb, Dy, Ho, Er, Tm, Yb and Lu were determined by ICP-MS. The interest in monitoring these elements on this type of ecosystems have grown [113], probably due to the increasing emissions from sources associated with population growth in the region.

4
Experimental

4.1
Apparatus

An inductively coupled plasma mass spectrometer (NexIon™300X, PerkinElmer, USA) was used for the determination of rare earth elements. The sample introduction system was composed of a Meinhard® concentric nebulizer and a cyclonic spray chamber (both Glass Expansion, USA). High purity argon (>99.99 %; Linde, Brazil) was employed for plasma operation. The operational conditions (

Table 3) were optimized for maximum signal intensity, limiting in 3 % the oxides and double charged species. Whenever possible, a non-interfered isotope was monitored. In addition, ^{151}Eu, ^{153}Eu and ^{147}Sm, ^{154}Sm were also monitored for the study of Ba oxides interference correction.

In order to evaluate the decomposition efficiency, major elements (Al, Ba, Ca, Fe, Mg, Mn, Na) were determined by ICP OES, employing an Optima 7300 DV spectrometer (PerkinElmer), the sample introduction system was composed of a seaspray concentric nebulizer and a Twinnabar cyclonic chamber (both Glass Expansion, USA), the operational conditions are also presented in Table 3.

Table 3. Operational conditions used for REE determination.

Parameter	ICP-MS	ICP OES
RF power	1100 W	1400 W
Plasma gas	15 L min^{-1}	15 L min^{-1}
Auxiliary gas	1 L min^{-1}	1 L min^{-1}
Nebulizer gas	0.92 L min^{-1}	0.55 L min^{-1}
Sample uptake rate	1.5 mL min^{-1}	1.5 mL min^{-1}
Replicates	3	3
Dwell time	50 ms	-
Plasma view mode	-	Axial (Al, Fe, Mn,) Radial (Ba, Ca, Mg, Na)
Monitored isotopes	^{137}Ba, ^{139}La, ^{140}Ce, ^{141}Pr, ^{143}Nd, ^{147}Sm, ^{154}Sm, ^{151}Eu, ^{153}Eu ^{157}Gd, ^{159}Tb, ^{163}Dy, ^{163}Ho, ^{166}Er, ^{169}Tm, ^{174}Yb and ^{175}Lu.	-
Emission lines (nm)	-	Al (I)396.153, Ba (II)455.403, Ca (I)422.673, Fe (II) 259.939, Mg (I)285.213, Mn (II)257.610, Na (I)589.592, Eu (I)381.967.

(I) atomic emission and (II) ionic emission

4.2
Reagents and materials

All solutions were prepared using ultrapure water obtained with a MilliQ system (18.2 MΩ cm, Millipore, Bedford, USA). Nitric (65 %), hydrofluoric (40 %), perchloric (70 %) and sulfuric (98 %) acids of analytical grade (all: VETEC, Brazil), were used for sample decomposition. Nitric acid was purified by sub-boiling bi-distillation in quartz still (Duo-PUR, Milestone, USA).

REE multielemental standard of 10 mg L^{-1}, Ba monoelemental standard of 1000 mg L^{-1} (both: PerkinElmer, USA), and Eu monoelemental standard (1000 mg L^{-1}, Merck, Germany) were used to prepare analytical solutions in 10 % (v/v) HNO_3 (1.4 mol L^{-1}) or in 10 % (v/v) H_2SO_4 (1.8 mol L^{-1}). The REE analytical calibration curves were constructed with calibration solutions prepared in the same acid medium as the samples, in the range of 2 to 30 µg L^{-1} of each analyte. In order to correct for non-spectral interferences, a 30 µg L^{-1} Rh solution, diluted from the 1000 mg L^{-1} Rh monoelemental standard (PerkinElmer) was added online by a t-piece and was used as internal standard.

Geological certified reference materials were used for accuracy evaluation of the REE determination in asphalt and crushed stone: G2 (granite), from the US Geological Survey, and Standard Reference Material (SRM) 688 of powdered Cenozoic basalt rock, from the National Institute of Standard Technology (NIST, USA). The sample of asphalt pavement was collected during its maintenance, in Rio de Janeiro (Brazil), and a sample of crushed stone, employed in the city street pavement, was obtained by the Brazilian oil industry, Petrobras. This road pavement is composed of about 90 % crushed stone and 10 % asphalt cement (AC), a viscous mixture of hydrocarbons and residual fuel oil [114].

Marine sediment reference material (MESS-3) provided by the National Research Council in Canada (NRC) was used to evaluate the accuracy of the REE determination in marine sediments. A total of 38 bottom sediments and 3 sediment cores were collected in different sites at the Sepetiba Bay and provided by LABAGUAS (PUC-Rio).

4.3
Procedures

4.3.1
Decomposition procedures applied to reference materials

The reference materials (G2 and SRM 688) were decomposed in an open system, using a method adapted from Ardini *et al.* [115]. Triplicate of 250.0 mg of each sample were weighted to Teflon vessels at 0.1 mg precision and 5 mL of concentrated HNO_3/HF (1:1 v/v) was added. The vessels were left overnight, and then they were heated at boiling temperature for 2 h on a hot plate, adding more acid mixture when necessary. The solutions were evaporated and added with a 1:1 (v:v) concentrated HNO_3/H_3BO_3 mixture, in order to remove the excess of HF. Finally, $HClO_4$ was added and the solutions were evaporated to dryness. The second and third steps were repeated three times. The volumes employed and the general scheme is represented in Figure 3. The residue was added with 10 mL of 10 % (v/v) HNO_3 or 10 % (v/v) H_2SO_4 and quantitatively transferred to a polypropylene flask. The samples solutions were 2000-fold diluted. After wet digestion of these reference materials, a solid residue was still present, then each flask was centrifuged and the supernatant was separated. The residue was submitted to fusion with $LiBO_2$ and dissolution in 10 % (v/v) HNO_3. The REE total concentrations in the supernatant plus dissolved residue were determined.

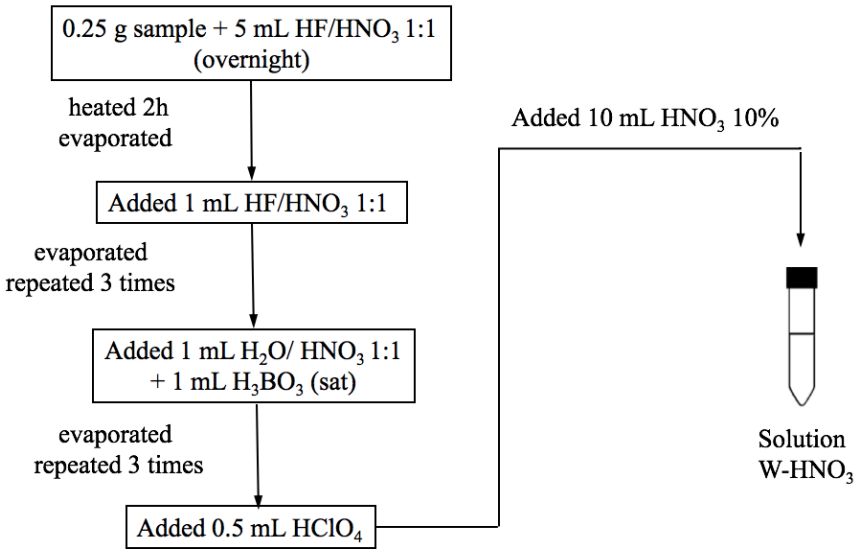

Figure 3. Decomposition procedure applied to G2, SRM 688, asphalt pavement and crushed stone.

The Marine sediment reference material (MESS-3) was decomposed using digester block with an acid mixture, followed by alkali fusion of insoluble residues, the scheme of this sample preparation is shown in Figure 4. The material was submitted to total decomposition in a digester block (DAH-904, Berghof, Germany), adapted from Begum [116]. Triplicate of 250.0 mg of each sample were weighed, at a 0.1 mg precision, to the Teflon vessels (DAB-3) and a mixture of 3 mL HNO_3, 3 mL HF and 3 mL $HClO_4$ was added. The vessels were submitted to a decomposition program, consisting of a 2 h temperature ramp from 25 °C to 200 °C with a 4 h standing at this temperature and then, the system was left to cool down overnight. After the decomposition procedure, the solutions were evaporated in a hot plate to almost dryness and the residues were solubilized with 3 mL of concentrated HNO_3. This step was repeated, in order to remove the excess HF, then the solutions were quantitatively transferred to polypropylene flasks with 10 % (v/v) HNO_3 to a 10 mL final volume. However, the solutions had a small amount of solid residue and the samples were centrifuged for 5 minutes at 4000 rpm, the solid was separated from the supernatant. The residue was submitted to fusion with $LiBO_2$ and REE total concentrations of the supernatant plus residue were determined.

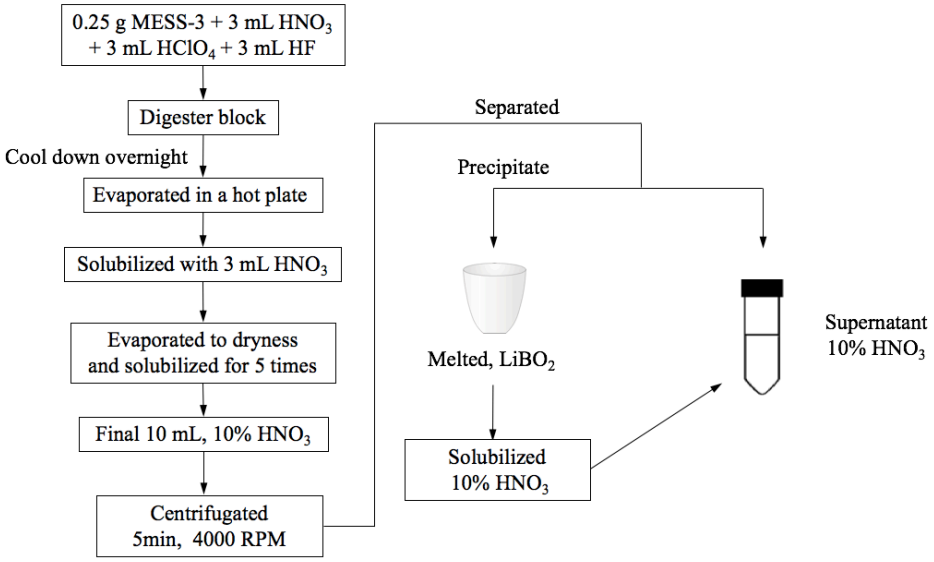

Figure 4. Decomposition procedure applied to MESS-3.

4.3.2
Acid extraction of asphalt pavement and crushes stone

Approximately 50 g of each sample were ground in a porcelain mortar and sifted in a 0.18 mm sieve, after this the samples were submitted to wet digestion in the same way to the reference materials (SRM 688 and G2).

Additionally to wet digestion, an extraction with 10 % (v/v) H_2SO_4 and 10 % (v/v) HNO_3 was conducted, in order to evaluate the mobility of the REE from the samples. The SRM, the asphaltic pavement and the crushed stone were submitted to acid extraction. The acid concentration employed (10 %, v/v) was similar to other works that used sequential extraction procedures [117,118]. However in the case of H_2SO_4, the solution is slightly more acidic (1.8 mol L^{-1}) than HNO_3 solutions (1.4 mol L^{-1}). Triplicate of 250.0 mg of the sample were accurately weighted in polypropylene flasks and 20 mL of 10 % (v/v) HNO_3 or 20 mL of a mixture of H_2SO_4 (10 % v/v each one) was added. The solutions were heated at 80 °C during 1 h and sonicated during 15 min in an ultrasonic bath of 40 kHz and 200 W (T50, Thorton, Brazil). The heating and sonication were repeated two more times. Then, the samples were centrifuged, transferred to polypropylene flasks and stored in refrigerator 4 °C.

4.3.3
Alkaline fusion

The reference materials (SRM 688, MESS-3 and G-2) and the samples (asphalt pavement and crushed stone) presented remaining residue after wet decomposition, this solid residue was treated by fusion using $LiBO_2$. This solid residue was treated as follows: The solid was transferred with ultrapure water to a platinum crucible, then it was dried in a hot plate. The $LiBO_2$ was added and carefully homogenized in the crucible, with the amount of lithium metaborate depending on the amount of residues. The mixture was melted and the obtained product was recovered dissolving it with 10 mL HNO_3 10 % (v/v) in polypropylene flasks. The solution was mixed with the wet decomposition product to a known volume and analyzed by ICP-MS and by ICP OES to determine the REE and major elements.

The total fusion of asphalt pavement and crushed stone were also employed for determination of major elements by ICP OES. In this case, triplicate of 50.0 mg of each sample were weighted, with 0.1 mg precision, to the platinum crucible and 500.0 mg of $LiBO_2$ were added, homogenized and submitted to fusion in a butane torch. The residue was dissolved with HNO_3 10 % (v/v) to a 50 mL final volume. The REE could not be determined by this method, due to the high dilution factor required.

4.3.4
Separation of barium by precipitation with H_2SO_4

In order to evaluate the efficiency of separating Ba^{2+} as $BaSO_4$, a first study was conducted with analytical solutions containing increasing concentration of Ba^{2+} in 10 % (v/v) nitric or sulfuric acids. The separation step consisted in heating the solutions at 80 ºC in a water bath for 1 h, then left to cool overnight, in order to reach equilibrium. After centrifugation at 4000 rpm for 5 min and filtration with 0.22 µm syringe filters (Millipore, Merck, SP, Brazil), the supernatants were separated and stored in refrigerator before analysis by ICP-MS.

The asphalt pavement, crushed stone, Granite G2 and SRM 688 were decomposed by wet digestion in the same way as described in Figure 3 and then analized by ICP-MS. In the case of samples with high barium concentration such as asphalt pavement, crushed stone and Granite G-2, these samples solutions obtained after wet digestion were added with H_2SO_4 10 % (v/v) and submitted to the $BaSO_4$ separation step described above. Additional experiments of sample

extraction with 10 % (v/v) HNO_3 or 10 % (v/v) H_2SO_4 were conducted, in order to compare with total decomposition.

4.3.5
Acid extraction of marine sediment from Sepetiba Bay.

The methodology used to determine rare earth elements in sediment was adapted from US EPA 3050B (1996) [119]. The bottom sediments were dried, homogenized and pulverized in agate mill, for the determination of the rare earth element in the sediment samples, which had been placed in 50 mL polypropylene flasks (Sarstedt AG & Co, Germany). Then, triplicate of 200.0 mg of each sample were weighted, with a precision of 0.1 mg, to polypropylene flasks and 10 mL of ultrapure HNO_3 (Merck, Germany) were added. After 12 hours in rest, the samples were heated until 80 °C in a Digester Block model DigiPrep (SCP Science, Canada), keeping at this temperature for 5 hours. After cooling, 1 mL of hydrogen peroxide 30 % (v/v) (Merck, Germany) was added and the samples were left at rest for more 1 hour. Afterwards, the samples were sonicated (ultrasonic bath Ultra Cleaner USC-3300 (Unique, Brazil) for 1 hour and heated again at 80 °C for the same time. Subsequently, the samples were left at rest for 12 hours. The samples were centrifuged at 4000 rpm for 5 minutes and the first supernatant was separated to another 50 mL polypropylene flasks. Ultrapure water (10 mL) was added to the residue and the mixture was homogenized and centrifuged, under the same conditions. The supernatant was separated and added to the first supernatant in a polypropylene flask with ultrapure water to a final volume of 20 mL, for REE determination by ICP-MS. Both the volumes employed and the general scheme are represented in Figure 5. The preparation of the extracts and the instrumental determinations were accompanied by blank solutions containing all reagents. The certified reference material MESS-3 was extracted in the same way to the sediment samples to establish a fraction to correct the marine sediment samples.

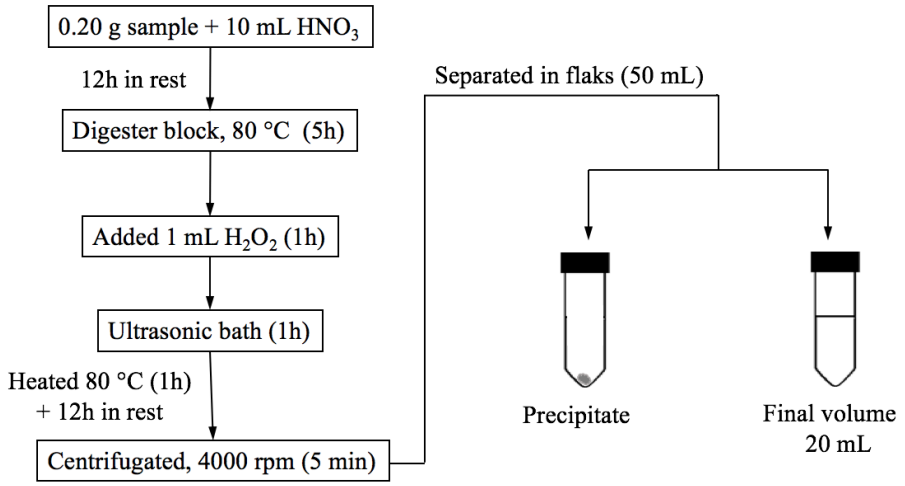

Figure 5. Decomposition of marine sediment.

4.3.6
Surface sediments and core sediments sampling

The samples of marine sediments were provided by LABAGUAS (PUC-Rio). The sediments were collected at different sites at Sepetiba Bay, 38 surface botton samples and 3 samples from the core extracted at 90 cm. The samples were collected between July and October 2016, and the criteria adopted to select these points was a study conducted by INEA in the 1990s as part of a technical cooperation project with FEEMA-Rio de Janeiro State Environmental (FEEMA), 2006), in which the same stations were sampled. Sampling stations are shown in Figure 6. The geographical coordinates are presented in Table 23 and Table 24, at the annex. Distribution plots were drawn using Ocean Data View version 4.

All samples of marine sediment analyzed for the determination of rare earth elements in Sepetiba bay were collected by Gonçalves *et al*., as described in previous work [111].The bottom sediments were collected using a Petersen grab, the samples were stored in plastic recipients, kept in a cooler with ice for transport to laboratory, where samples were preserved in a refrigerator. Sepetiba Bay cores were hand-collected and taken with a gravity corer with PVC tubes of 120 cm and 6 cm of diameter, supplied by the company UWITEC and also immediately sliced into 2.0 cm layers. The samples were weighted and preserved. Sediment dating was carried out on three sediments profiles (T-8, T-18 and T-28, shown in Figure 6.

The sediment cores were sampled by applying a 6.0 cm diameter UWITEC gravity sediment corer and two-centimeter high slicing was applied. ^{210}Pb was determined as described by Godoy *et al*. (1998) [121].

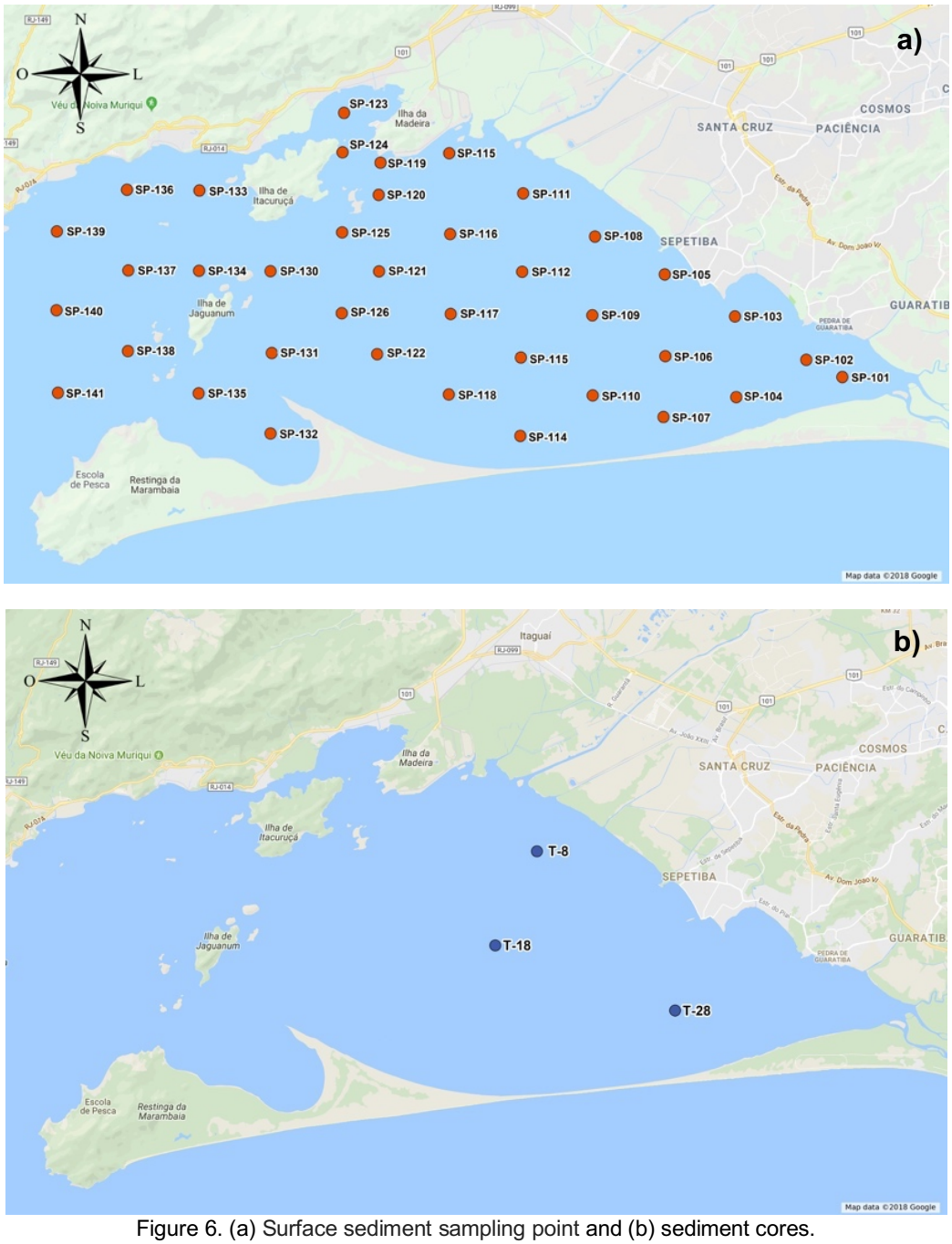

Figure 6. (a) Surface sediment sampling point and (b) sediment cores.

5
Results and Discussion

5.1
Sample analysis with high barium concentration

5.1.1
Accuracy assessment with SRM 688 and G2 certified materials

Accuracy and precision were verified by analysis of the reference materials Basalt Rock (SRM 688) and Granite (G2). Results obtained for these standard reference materials, presented in Table 4 and Table 5, were mostly in agreement with the certified values. The instrumental detection limits (LOD, $3\sigma/s$, n=10, μg L^{-1}) are also reported in Table 4.

The REE in the solutions and supernatants after wet digestion with dilution in 10 % HNO_3 and after wet digestion plus fusion of the certified materials, were determined by ICP-MS. The results of SRM 688 (W-HNO_3 and W/F, Table 4) were compared to those informed in the certificate and to the values obtained from an international proficiency test [122]. The Ba concentration at the employed 2000-fold dilution factor (0.1 mg L^{-1}) did not interfere significantly in the Eu concentration for the SRM 688, then, the addition of sulfuric acid was not necessary. As well, the interferences by LREE oxides on HREE were not significant and results were from 86 % to 107 % of the values reported from the international proficiency test, for the samples decomposed by wet digestion (W-HNO_3), and from 81 % to 112 %, for the wet decomposition plus fusion (W/F). The results obtained by the two sample preparation methods were also in agreement with the informed values international proficiency test, the *t-Student* test was applied in the reference materials. These results are reported in Table 4.

Table 4. REE concentrations (mg kg^{-1}, n=3) in the certified material (SRM 688) after wet digestion and dilution in 10 % (v/v) HNO_3 (W-HNO_3) and wet digestion plus fusion (W/F), LOQ, 10σ/s, n=3, mg kg^{-1}, ($t_{95\%,\ n=3}$=4.303).

				NIST SRM 688					
	Informed	**LOQ**	**GeoPT16****	**W-HNO_3**	***t***	**%**	**W/F**	***t***	**%**
^{139}La	-	0.2	5.2±0.32	5.2±0.2	0.12	100	4.9±0.1	4.30	94
^{140}Ce	13.3*	0.3	12±0.7	12±1	0.43	100	12±1	0.60	100
^{141}Pr	-	0.02	1.69±0.13	1.7±0.1	0.68	101	1.7±0.1	0.07	101
^{143}Nd	-	0.3	8.40±0.49	8.2±0.3	1.51	98	8.3±0.4	0.33	99
^{147}Sm	2.79*	0.03	2.36±0.17	2.02±0.44	1.32	86	2.5±0.2	1.08	106
^{151}Eu	1.07*	0.03	0.98±0.08	0.98±0.16	0.96	100	1.1±0.1	0.71	112
^{153}Eu	1.07*	0.03	0.98±0.08	0.97±0.03	0.75	99	0.98±0.10	0.03	100
^{157}Gd	-	0.05	2.87±0.20	2.9±0.1	1.23	101	2.9±0.3	0.10	101
^{159}Tb	0.448*	0.01	0.51±0.05	0.50±0.04	0.57	98	0.48±0.05	0.99	94
^{163}Dy	-	0.06	3.30±0.22	3.3±0.1	1.21	100	3.2±0.2	0.81	97
^{165}Ho	-	0.01	0.72±0.06	0.62±0.07	2.54	86	0.70±0.03	1.04	97
^{166}Er	-	0.02	2.10±0.15	2.2±0.1	1.71	105	2.1±0.1	0.85	100
^{169}Tm	-	0.02	0.31±0.03	0.29±0.01	2.38	94	0.26±0.01	4.11	84
^{174}Yb	2.09*	0.05	2.06±0.15	2.2±0.2	1.23	107	2.10±0.13	0.57	102
^{175}Lu	0.34*	0.02	0.32±0.03	0.32±0.05	0.04	100	0.26±0.02	4.14	81

*Informed values.
**Values reported from the international proficiency test [122].
(*t*) *t-Student*
(%) Percentage of recovery

The certified reference material (Granite-G2) was dissolved in nitric acid media (W-HNO_3) and sulfuric acid media (W-H_2SO_4), to evaluate the reduction of interference by BaO over Eu. The results obtained for G2 (W-HNO_3 and W-H_2SO_4), presented in Table 5, were mostly in agreement with the certified values, except for Tm, Yb and Lu (below 70 %). It is possible that losses occurred during the wet digestion process, though, a conclusion could not be raised, since some values are informed and these elements are in low concentrations. Concerning the Ba interference, a recovery of 114 % of the certified value was obtained for Eu in 10 % HNO_3 solutions, due to the high Ba concentration (0.8 mg L^{-1}), which corresponds to a Eu equivalent concentration of about 0.3 μg L^{-1} (see 5.1.2). On the other hand, the supernatant obtained from 10 % H_2SO_4 solutions resulted in good agreement (96 % of the certified value). Additionally, the removal of BaO^+ interference could be evidenced with another interfered isotope, the ^{154}Sm, although the choice of a non-interfered isotope, ^{147}Sm, is recommended. For this purpose, the ratio of the intensities of the interfered/non-interfered Sm isotopes (^{154}Sm/^{147}Sm) in the G2 was calculated. The solution in 10 % HNO_3 presented

$^{154}Sm/^{147}Sm$ intensities ratio equal to 2.57, whereas the intensities ratio (1.57) in the supernatant obtained after treatment with H_2SO_4, was similar to the isotopic ratio of 1.51.

Table 5. REE concentrations (mg kg^{-1}, n=3) in the certified material (Granite-G2) after wet digestion and dilution in 10 % (v/v) HNO_3 (W-HNO3), or in dilution in 10 % (v/v) H2SO4 (W-H2SO4 and wet digestion plus fusion (W/F), ($t_{95\%,\ n=3}$=4.303).

	Granite-G2							
	Certified	**W-HNO_3**	**%**	**W/F**	**%**	**W-H_2SO_4**	***t***	**%**
^{139}La	89±8	87±1	98	84±1	94	90±1.48	0.87	101
^{140}Ce	160±10	161±3	101	150±3	94	153±10	1.18	96
^{141}Pr	18*	18±1	100	16.4±0.3	91	17.7±0.75	0.63	100
^{143}Nd	55±6	55±4	100	51±1	93	54.2±0.3	4.13	99
^{147}Sm	7.2±0.7	7.4±0.5	103	7.2±0.4	100	7.36±0.1	2.70	102
^{151}Eu	1.4±0.12	1.6±0.1	114	1.59±0.04	114	1.34±0.06	2.08	96
^{153}Eu	1.4±0.12	1.7±0.1	121	1.72±0.03	123	1.32±0.08	1.64	94
^{157}Gd	4.3*	4.7±0.5	109	5.2±0.4	121	4.3±0.14	0.15	100
^{159}Tb	0.48*	0.500±0.01	104	0.49±0.01	102	0.54±0.03	3.75	113
^{163}Dy	2.4±0.3	2.02±0.17	84	2.02±0.10	84	2.41±0.01	2.31	100
^{165}Ho	0.4*	0.32±0.03	80	0.32±0.04	80	0.38±0.01	4.24	95
^{166}Er	0.92*	0.94±0.02	102	0.91±0.09	99	0.92±0.04	0.12	100
^{169}Tm	0.18*	0.080±0.001	44	0.08±0.01	44	0.09±0.01	-	50
^{174}Yb	0.8±0.2	0.41±0.02	51	0.62±0.07	78	0.50±0.01	-	63
^{175}Lu	0.11*	0.06±0.01	55	0.07±0.01	64	0.06±0.01	-	55

*Informed values
(*t*) *t-Student*
(%) Percentage of recovery
(-) values significantly different

The major elements (Al, Ca, Fe, Mg, Mn, Na, Ba) were also determined to evaluated the accuracy with the certified values (Table 6 and

Table 7), demonstrating that the acid decomposition and the conditions of sample preparation were efficient for determination of both, rare earth elements and major elements, in this type of samples.

Table 6. Certified and determined concentrations of major elements (Wt %) in the NIST SRM 688, (n=3), after wet digestion (W) and wet digestion plus fusion (W/F) by ICP OES.

	Basalt Rock		
	Cert.	**W**	**W/F**
Al_2O_3	17.36±0.09	16.01±0.30	17.53±0.12
CaO	12.17	11.41±0.22	12.19±0.15
Fe_2O_3	10.35±0.04	9.74±0.20	10.40±0.12
MgO	8.4	8.2±0.18	8.5±0.10
MnO	0.167±0.002	0.155±0.001	0.161±0.001
Na_2O	2.15±0.03	2.10±0.03	2.04±0.02
Ba	173	160±4	173±1

Table 7. Certified and determined concentrations of major elements (Wt %) in the G2, (n=3), after wet digestion (W) and wet digestion plus fusion (W/F) by ICP OES.

	G2		
	Cert.	**W**	**W/F**
Al_2O_3	15.39±0.3	13.39±0.29	15.59±0.91
CaO	1.96±0.08	1.50±0.03	1.91±0.17
Fe_2O_3	2.66±0.17	2.37±0.06	2.65±0.14
MgO	0.75±0.03	0.67±0.03	0.74±0.02
MnO	0.03±0.01	0.029±0.001	0.032±0.002
Na_2O	4.08±0.13	3.79±0.04	3.97±0.09
Ba	1880±23	1624±63	1854±45

The concentration of rare earth elements obtained after both methods of sample preparation (wet digestion and digestion plus fusion) were in agreement with the certified values, which demonstrates that these elements are not lost in the solid residue that remains after wet digestion. In the case of the major elements, a loss in the concentration of Al and Ca can be observed in the samples treated by wet decomposition when compared with the values obtained by wet digestion plus fusion. This is probably due to the formation of insoluble fluorides ($NaAlF_4$, $MgAlF_5$, CaF_2) that will remain in the solid residue resulting from decomposition [123].

5.1.2
Removal of barium interference by precipitation with H_2SO_4

The barium solutions prepared in 10 % (v/v) nitric acid and the supernatants obtained after adding 10 % (v/v) sulfuric acid to these solutions (see 4.3.4), were correlated against monoelemental Eu analytical calibration curves. These were

prepared in the same medium, due to the signal suppression observed in 10 % (v/v) sulfuric acid Figure 7. The obtained signal intensities of $^{137}Ba^{16}O+$ and $^{138}Ba^{16}O+$ species were measured at m/z 151 and 153, respectively, to calculate the Eu equivalent concentrations.

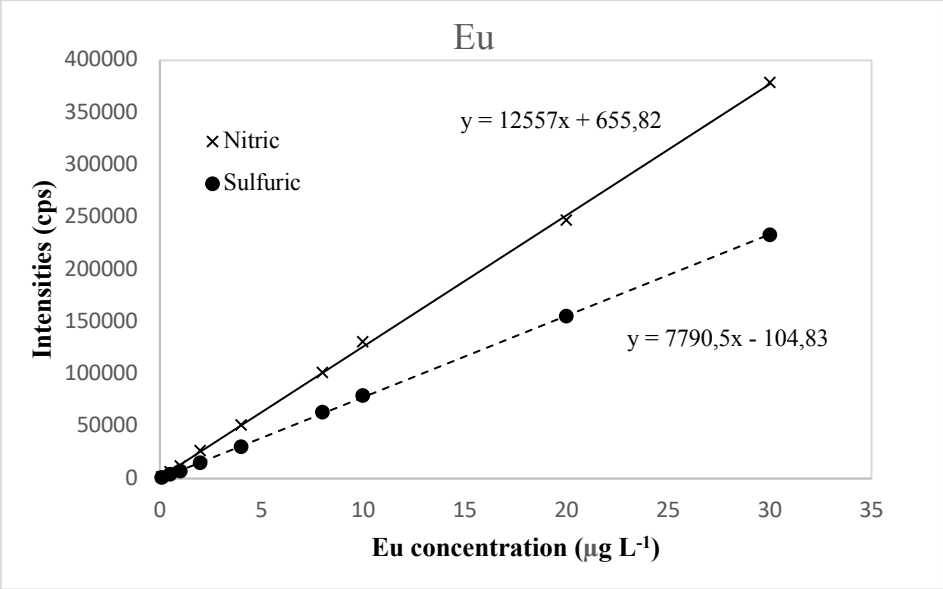

Figure 7. Analytical calibration curves for Eu in 10 % HNO_3 (straight line) and 10 % H_2SO_4 (dashed line).

The correlations between BaO signal and Eu equivalent concentration are shown in Figure 8 for a maximum Ba concentration of 0.7 mg L^{-1}. In both acidic medium, the Eu equivalent concentration has increased linearly up to approximately 0.1 mg L^{-1} of Ba, which corresponds to an Eu equivalent concentration of about 0.04 µg L^{-1}, above which $BaSO_4$ precipitate in sulfuric acid. This Ba concentration corresponds to a solubility of about 0.2 mg L^{-1} $BaSO_4$ in the 1.8 mol L^{-1} H_2SO_4 solution, which is lower than the one reported in pure water (2.5 mg L^{-1}) [124], due to the effects of common ion and ionic strength on equilibrium [125]. At higher Ba concentrations, the Eu equivalent concentration decreases in the sulfuric solutions, for the same reasons.

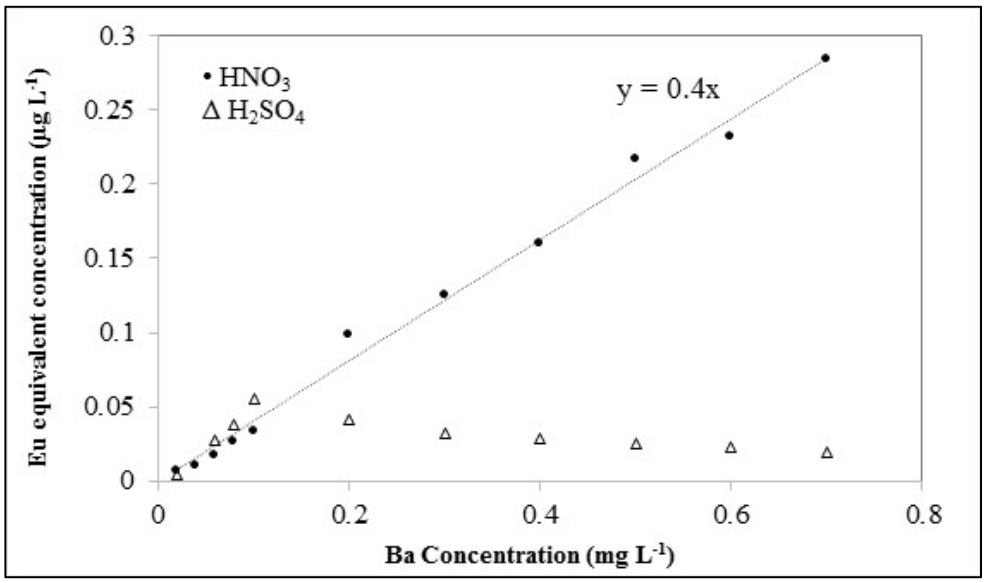

Figure 8. Equivalent concentration of Eu against an analytical calibration curve of Ba in 10 % (v/v) HNO_3 or H_2SO_4.

5.1.3
Asphalt pavement and crushed stone composition

The asphalt and crushed stone samples were submitted to the wet digestion with or without adding sulfuric acid and the results are presented in Table 8. A good agreement was obtained for the REE concentrations in the solutions (W-HNO_3) and supernatants (W-H_2SO_4), indicating that these elements do not co-precipitate with $BaSO_4$, possibly due to their complexation with sulfate [126,127]. In the case of Eu, the concentrations obtained from the nitric solutions were about 6 % higher than the ones from the supernatants of the sulfuric acid solutions. A mathematical correction based on the equation proposed by Bacon [11] was applied to the results from nitric solutions, in order to compare the proposed method for Ba interference correction with a simple approach. However, in the case of crushed stone, the result (9.0 $\pm$ 0.3 mg L^{-1}) was not in agreement with the measured value (W-H_2SO_4, Table 8). Then, Eu present in the wet digests of the samples was determined by ICP OES. Their concentrations (7.4 $\pm$ 0.5 mg L^{-1}) were in agreement with the ones obtained by the proposed method (W-H_2SO_4, Table 8).

The asphaltic pavement and crushed stone were decomposed combining the wet digestion and alkaline fusion, the last being applied over the reminiscent residues to guarantee the total decomposition of the sample. The results are reported in the Table 8 as wet digestion plus fusion (W/F). Additionally, the elemental composition of the samples were determined by the fusion method (Table 9), with a predominance of Al and Fe, as in lateritic soils [128]. The excess

of Al possibly forms insoluble fluorides during the wet digestion procedure [123], without compromising the REE concentrations in solution, which was evidenced by the good agreement between results from wet digestion and wet digestion followed by fusion of the residue (Table 9).

Table 8. Concentrations of REE (mg kg^{-1}) in the asphalt pavement and crushed stone samples (n=3), after wet digestion and dilution in 10 % (v/v) HNO_3 (W-HNO_3), treatment with 10 % (v/v) H_2SO_4 (W-H_2SO_4) and wet digestion plus fusion (W/F).

	Asphaltic pavement			**Crushed stone**		
	W-HNO_3	**W-H_2SO_4**	**W/F**	**W-HNO_3**	**W-H_2SO_4**	**W/F**
^{139}La	46±2	49±3	49±5	30±3	27±3	30±2
^{140}Ce	99±6	103±8	102±9	72±7	70±5	71±4
^{141}Pr	12±1	11±1	12±1	9.8±0.8	10±1	10±1
^{143}Nd	45±2	45±4	44±4	46±3	49±3	42±2
^{147}Sm	9.2±1.1	9.8±0.8	9.6±1.1	7.7±0.8	8.4±0.4	7.6±0.3
^{151}Eu	2.2±0.1	1.98±0.11	2.2±0.2	8.2±0.8	7.7±0.3	8.3±0.2
^{153}Eu	2.1±0.1	1.91±0.04	2.4±0.1	8.7±0.7	7.6±0.4	8.6±0.3
^{157}Gd	9.9±0.7	9.04±1.10	9.5±1.4	6.9±0.7	7.2±0.4	6.7±0.4
^{159}Tb	1.6±0.3	1.5±0.2	1.6±0.3	0.88±0.10	0.93±0.03	0.83±0.01
^{163}Dy	8.8±1.2	8.9±1.3	9.1±1.9	4.6±0.3	4.7±0.4	4.3±0.2
^{165}Ho	1.9±0.3	1.9±0.3	1.8±0.3	0.90±0.06	0.88±0.05	0.78±0.06
^{166}Er	5.3±0.8	5.2±0.6	5.5±0.5	2.5±0.2	2.5±0.1	2.2±0.2
^{169}Tm	0.7±0.1	0.74±0.09	0.79±0.06	0.33±0.03	0.34±0.03	0.32±0.04
^{174}Yb	4.8±0.7	4.8±0.5	4.7±0.1	2.1±0.2	2.2±0.2	1.9±0.1
^{175}Lu	0.67±0.10	0.67±0.07	0.67±0.04	0.34±0.05	0.36±0.02	0.32±0.02

Table 9. Measured concentrations of major elements (Wt %) in crushed stone and asphalt pavement (n=3), after wet digestion (W), fusion (F) and wet digestion plus fusion (W/F), by ICP OES.

	Crushed stone			**Asphaltic pavement**		
	W	**F**	**W/F**	**W**	**F**	**W/F**
Al	8.07±0.56	8.94±0.11	9.10±0.27	6.13±0.26	7.06±0.01	6.67±0.14
Ca	2.72±0.36	2.96±0.09	2.96±0.10	1.03±0.05	1.21±0.05	1.25±0.01
Fe	4.99±0.23	5.29±0.23	4.93±0.19	2.09±0.10	1.97±0.01	2.12±0.03
Mg	0.57±0.09	0.62±0.02	0.59±0.02	0.28±0.01	0.26±0.01	0.28±0.01
Mn	0.13±0.01	0.14±0.01	0.13±0.01	0.046±0.003	0.045±0.001	0.045±0.001
Na	2.16±0.14	2.15±0.12	2.12±0.05	2.15±0.09	2.37±0.01	2.11±0.03
Ba	3654±201	3953±31	3807±128	1316±55	1520±10	1393±35

5.1.4
Geological profiles

Alternatively, SRM 688 and crushed stone were submitted to direct extraction with 10 % H_2SO_4 (Table 10). This procedure resulted in low recoveries for the SRM 688 (from 40 % for Yb to 69 % for Ce) and it is not recommended for REE characterization of an unknown sample. However, although the concentrations in solution were lower than those obtained for wet digestion, they can be employed for evaluating the REE profile, since they were similar by both methods, as shown in Figure 9 and Figure 10.

Table 10. Concentrations of REE (mg kg^{-1}, n=3) and extraction percentage (%) in NIST SRM 688, crushed stone, after extraction with 10 % (v/v) H_2SO_4.

	GeoPT16**	SRM 688	%	Crushed stone	%
^{139}La	5.2±0.32	3.71±0.08	61	12.19±0.79	41
^{140}Ce	12±0.7	8.23±0.11	69	30.95±1.57	43
^{141}Pr	1.69±0.13	1.13±0.02	67	4.47±0.14	46
^{143}Nd	8.40±0.49	5.28±0.23	63	21.19±0.25	46
^{147}Sm	2.36±0.17	1.25±0.04	53	3.77±0.11	49
^{151}Eu	0.98±0.08	0.42±0.03	43	1.76±0.02	21
^{153}Eu	0.98±0.08	0.42±0.01	43	1.76±0.02	20
^{157}Gd	2.87±0.20	1.39±0.01	48	3.13±0.08	45
^{159}Tb	0.51±0.05	0.23±0.01	45	0.39±0.02	44
^{163}Dy	3.30±0.22	1.47±0.06	45	1.85±0.04	40
^{165}Ho	0.72±0.06	0.31±0.01	43	0.34±0.01	38
^{166}Er	2.10±0.15	0.96±0.02	46	0.96±0.02	38
^{169}Tm	0.31±0.03	0.13±0.01	42	0.124±0.004	38
^{174}Yb	2.06±0.15	0.83±0.03	40	0.729±0.001	35
^{175}Lu	0.32±0.03	0.13±0.01	41	0.114±0.007	34

*Values reported from the international proficiency test [122].

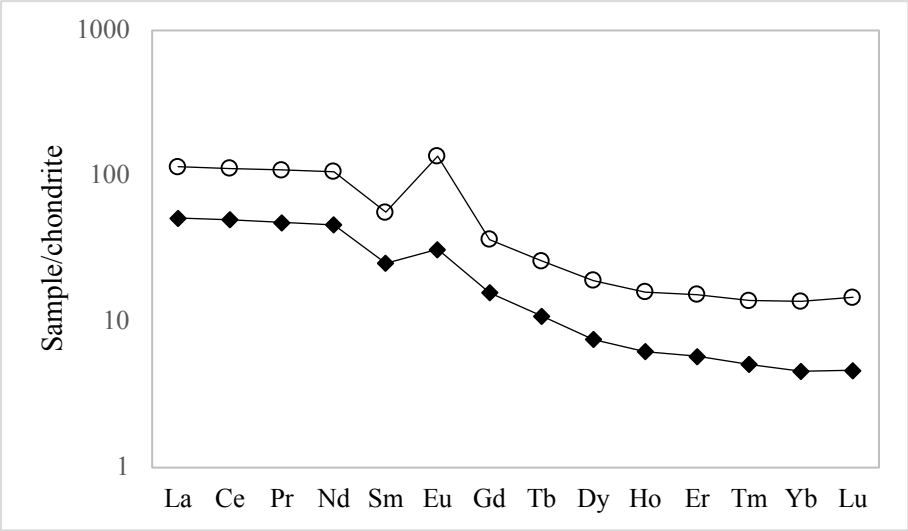

Figure 9. REE patterns of the crushed stone, normalized to NASC, after wet digestion and dilution in 10 % H_2SO_4 (○) and after extraction with 10 % (v/v) H_2SO_4 (♦).

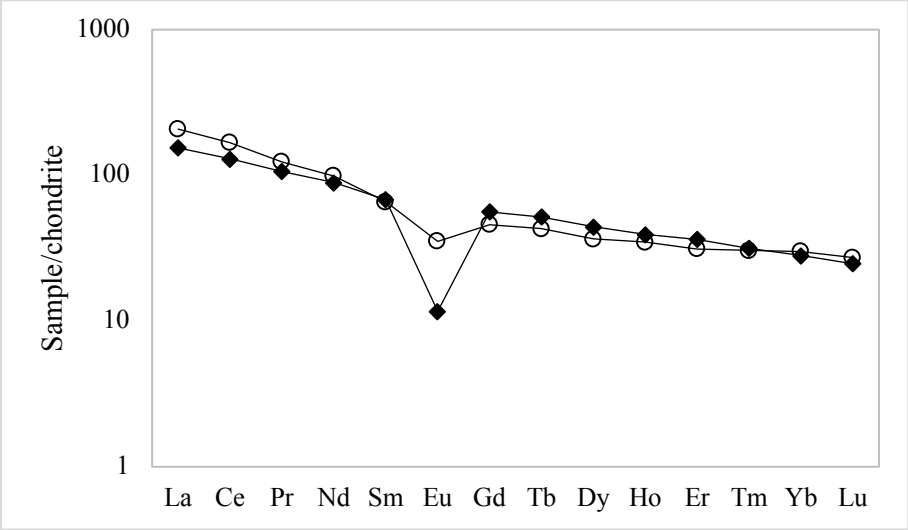

Figure 10. REE patterns of the asphalt pavement, normalized to NASC, after wet digestion and dilution in 10 % H_2SO_4 (○) and after extraction with 10 % (v/v) H_2SO_4 (♦).

The REE distribution or geological profile is based on the normalization of the REE concentrations in the sample, to the ones in a reference chondrite, as recommended by the North American Shale Composite (NASC) [129]. This profile attests for the original mineral and it is usually employed in environmental studies in order to observe modifications due to mineral formation or dissolution. In the case of the certified materials, the geological profiles obtained by the different methodologies are in agreement with those constructed with the certified values, for SRM 688 (Figure 11) and mostly for G2 (Figure 12). It can be observed that in this granite (G2), light and medium REE are enriched relatively to HREE, due to phase separation during their formation.

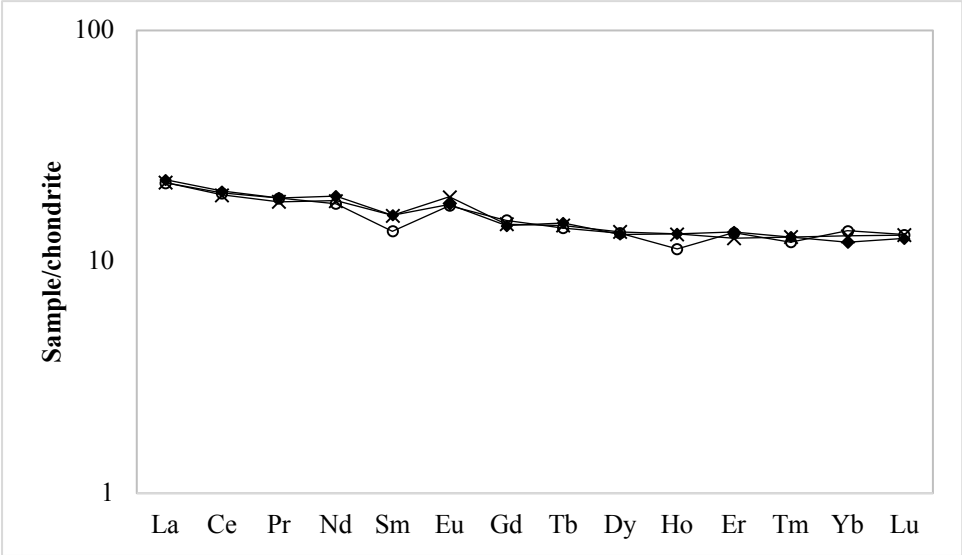

Figure 11. REE patterns normalized to NASC for SRM 688 after total decomposition and dilution in (○) 10 % (v/v) HNO_3 or (♦) 10 % (v/v) H_2SO_4 and (×) from reference [130].

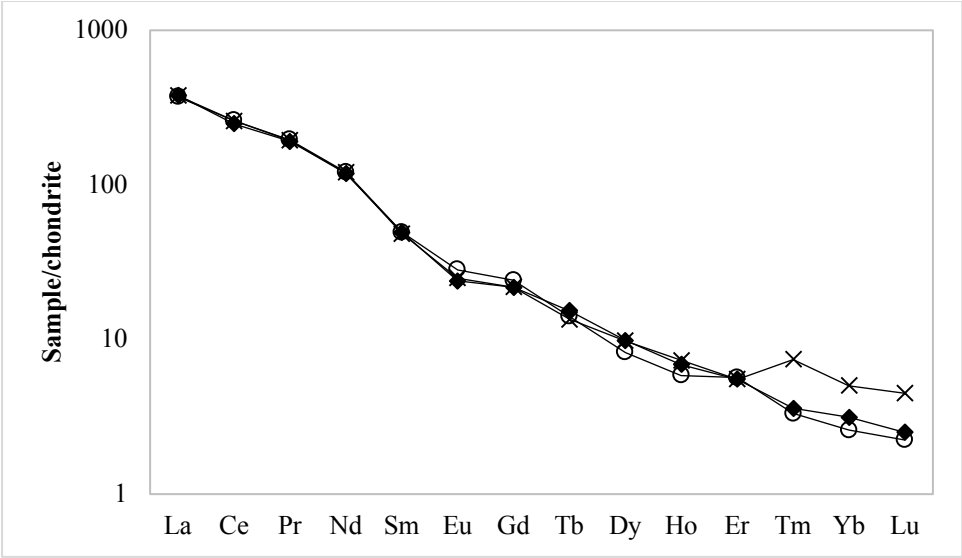

Figure 12. REE patterns normalized to NASC for G2 after wet digestion and dilution in (○) 10 % (v/v) HNO_3 or (♦) 10 % (v/v) H_2SO_4, (×) certified value and (+) wet digestion plus fusion.

The geological profiles of the asphalt pavement and the original crushed stone that composes about 90 % of it were established in Figure 13. In both samples, enrichment of light and medium REE is observed, as expected for sediments and sandy soils from Rio de Janeiro, which are composed mainly of alterites [128]. A positive Eu anomaly was observed in the crushed stone. Even if the origin of such materials unknown, a possible explanation is the presence of minerals such as carbonatites, which would explain the high percentage of Ca (15 %) relatively to other major elements, and the high Ba concentrations. The REE associated to these minerals are more readily soluble than those in granite, such as G2, and it corroborates to the good recovery of REE after the wet digestion of these samples. On the other hand, the presence of such minerals results in REE

more easily mobilized to the environment by weathering, in particular LREE, which are more soluble than HREE.

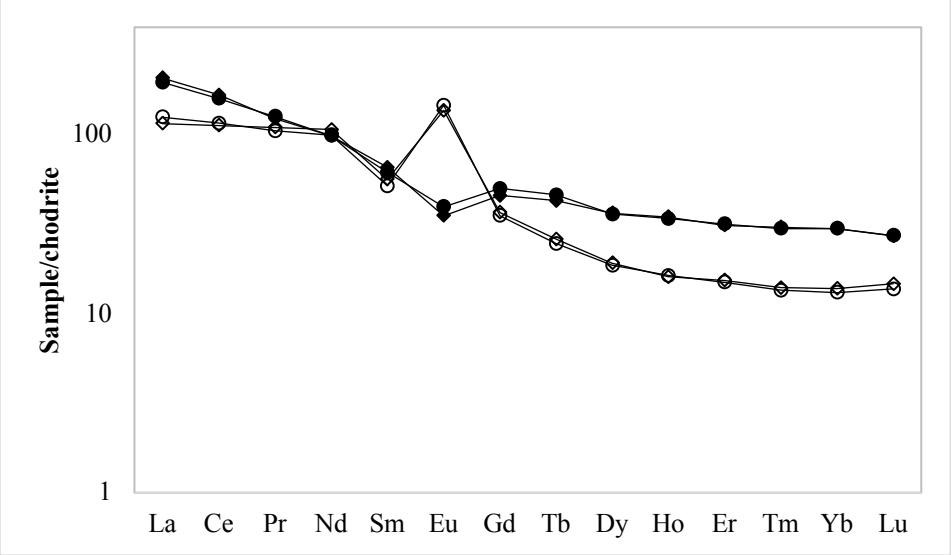

Figure 13. REE patterns normalized to NASC for crushed stone after wet digestion and dilution in (○) 10 % (v/v) HNO_3 or (◊) 10 % (v/v) H_2SO_4, and for asphalt pavement after wet digestion and dilution in (●) 10 % (v/v) HNO_3 or (♦) 10 % (v/v) H_2SO_4.

5.2
Sample analysis of surface marine sediment and sediment core

5.2.1
Precision and accuracy of the method

Accuracy and precision were verified by analysis of the reference material MESS-3 (Marine Sediment by National Research Council, Canada). Results obtained for this standard reference material, as well as certified and determined values, and detection limits are reported in Table 11. Reproducibility and precision were tested by means of three replicate analyses of the sample, showing a standard deviation of less than 8 % in the results of wet digestion and less than 20 % in the case of fusion. Results obtained for MESS-3 were mostly in agreement with the certified values, ranged between 84 % to 109 %, the *t-Student* test was applied in this reference material.

The sediment samples were analyzed following the procedure used for sample preparation showen in 4.3.5. The conditions of analysis of the sample solutions by quadrupole ICP-MS are presented in

Table 3. The reference material was extracted in the same way as sediment samples to establish a correction factor. This factor was subsequently applied to

the samples to estimate their real concentration. Both concentration values determined in the extracts of the reference material and the correction factor are reported in Table 12.

Table 11. REE concentrations (mg kg^{-1}) in the certified material MESS-3 (marine sediment) after wet digestion plus fusion (W/F). Limits of quantification, LOQ, 10σ/s, n=3, mg kg^{-1}, ($t_{95\%,\ n=3}$=4.303).

	LOQ	Reference*	W/F	Recovery (%)	*t-Student*
^{139}**La**	0.2	40.5±0.01	35.2±2.2	87	4.17
^{140}**Ce**	0.3	77.96±0.03	68.6±3.8	88	4.27
^{141}**Pr**	0.02	8.23±0.02	8.01±0.40	97	0.95
^{143}**Nd**	0.3	33.3±0.01	30.5±1.2	92	4.04
^{147}**Sm**	0.03	6.7±0.02	5.63±0.45	84	4.12
^{151}**Eu**	0.03	1.55±0.02	1.45±0.06	94	2.89
^{157}**Gd**	0.05	5.11±0.04	5.55±0.29	109	2.63
^{159}**Tb**	0.01	0.800±0.01	0.679±0.05	85	4.19
^{163}**Dy**	0.06	4.8±0.01	5.08±0.11	106	4.41
^{165}**Ho**	0.01	0.96±0.01	0.976±0.036	102	0.77
^{166}**Er**	0.02	3.010±0.01	2.97±0.07	99	0.99
^{169}**Tm**	0.02	0.400±0.04	0.386±0.007	96	3.46
^{174}**Yb**	0.05	2.60±0.01	2.61±0.07	100	0.25
^{175}**Lu**	0.02	0.430±0.04	0.423±0.011	98	1.10

*Values reported from the international proficiency test [116].

Rare earth elements do not have certified values in the MESS-3 material, however, Begun *et al.* have reported the concentration values of these elements after validation for the determination of trace and rare earth elements in marine sediment reference materials by ICP-MS, comparing the acid digestion methods in open and closed system. This study is reported in “Reference for Trace Metals and other Constituents” [116]. Certified trace and major elements were determined in this marine sediment (MESS-3) by ICP OES and ICP-MS, to verify both precision and accuracy. Also, in this case a satisfactory agreement between the determined values and the certified ones was generally observed, within 85 % (Na, Co) and 104 % (V). The results obtained after this analysis are reported in Table 13 and Table 14.

Table 12. REE concentrations (mg kg^{-1}, n=3) in the certified materials (MESS-3) after leaching and the correction factor.

	MESS-3	Correction factor
^{139}La	18,4±0,6	0,53
^{140}Ce	38,7±2,9	0,56
^{141}Pr	4,88±0,371	0,61
^{143}Nd	20,7±2,0	0,68
^{147}Sm	4,56±0,40	0,81
^{151}Eu	1,04±0,05	0,75
^{157}Gd	4,44±0,50	0,80
^{159}Tb	0,584±0,051	0,86
^{163}Dy	2,72±0,148	0,56
^{165}Ho	0,477±0,0311	0,49
^{166}Er	1,27±0,07	0,43
^{169}Tm	0,144±0,012	0,36
^{174}Yb	0,841±0,046	0,32
^{175}Lu	0,115±0,007	0,28

Table 13. Results obtained for the certified reference materials MESS-3 for major and trace elements by ICP OES, after wet digestion plus fusion. Limits of quantification LOQ, 10σ/s, n=3, mg kg^{-1}.

	Emission line	LOQ	Certificate	Measured	%
Ba	455.403	0.8	926±1	919±11	99
Sr	421.552	0.8	129±11	125±2	97
V	311.071	0.4	243±10	253±7	104
Zn	206.200	4.0	159±8	152±5	96
Al	396 axial	4.0	8.59±0.23	7.63±0,67	89
Ca	317.933	40	1.47±0.06	1.39±0.01	94
Fe	259.939	4.0	4.34±0.11	4.11±0.06	95
K	766.490	200	2.6*	2.40±0.09	92
Mg	285.213	40	1.6*	1.42±0.09	88
Na	589.592	40	1.6*	1.36±0.03	85

*information value only
Ba, Sr, V, Zn in mg kg^{-1}
Al, Ca, Fe, K, Mg, Na in Wt%
(%) Percentage of recovery

Table 14. Results obtained for the certified reference materials MESS-3 for trace elements (mg kg^{-1}) by ICP-MS, after wet digestion plus fusion. Limits of quanification (LOQ, 10σ/s, n=3, μg kg^{-1}).

	LOQ	Certificate	Measured	%
^{75}As	0.005	21.2±1.1	21.4±4.1	101
^{138}Ba	0.009	926.3±1	907±13	98
^{9}Be	0.001	2.3±0.12	2.05±0.14	89
^{59}Co	0.002	14.4±2.0	12.2±0.3	85
^{53}Cr	0.03	105±4	94.1±2.9	90
^{65}Cu	0.009	33.9±1.6	34.1±0.5	101
^{55}Mn	0.07	324±12	304±8	94
^{60}Ni	0.008	46.9±2.2	40.3±1.6	86
^{208}Pb	0.006	21.1±0.7	18.2±0.3	86
^{88}Sr	0.5	129±11	134±2	104

(%) Percentage of recovery

5.3
Marine sediment sample analysis

As mentioned above, sediment samples were supplied by LABAGUAS and both, the particle size and humidity percentage of surface sediments were determined in a previous work, as well as the dating by ^{210}Pd of sediment cores [111,131].

5.3.1
Grain-size distribution

Rare earth elements distribution in Sepetiba Bay bottom sediments depends on the locations of river mouths and the patterns of tidal currents, as shown in Figure 14. Particle size distribution has been shown to be a major factor controlling metal concentrations [132], the accumulation of metals occurring mainly in the fine grained portion of the sediments. This is the fraction smaller than 63 μm, which comprises clay and silt, and the fraction larger than 63 μm is attributed to sand and gravel. The percentage of fine-grained sediments in the samples analyzed did show a significant variation, ranging from 0.1 to 100 %. Hence, variations in concentration in the studied samples should probably be due to these parameters. There are significant correlations between rare earth elements concentrations and fine granulometry of sediments. This relationship can be seen in the bar graph of Figure 15. The rare earth elements concentrations in Sepetiba bay are attributed to continental input of particulate material and the constant flow of the two major rivers (Sao Francisco and Guandu Rivers, located in north-central

and northeast of the Bay, respectively), which are artificially controlled by a water treatment plant located upstream from the major industrial area [133]. The Sepetiba Bay basin receives a large volume of water through water transposition to these rivers, because these are the primary source of suspended material in this area. Mangrove area generally presents high accumulation of rare earth elements. Moreover, the inner bay area also presents higher concentrations than open bay sediments, due to the accumulation of fine sediments.

The Figure 15 shows the sample points in increasing order of rare earth elements concentration (from left to right) evidence that clay and silt are rich of rare earth elements. Meanwhile, when their concentration decreases, the sediment composition in sand and gravel increases. This is explained since Sepetiba Bay mangrove sediments are dominated by silt and clay, and in the intensive mangrove zone sediments, clay concentration is higher than other fractions. This facilitates filtration and adsorption of the elements along with nutrients in the coastal sediments. Meanwhile, in samples in center of the bay, which have high fractions of silt and clay, the REE concentrations decrease due to the dynamic of tidal movements which does not allow their deposition. The Generalized patterns of tidal currents system at Sepetiba Bay was obteines by the “Sistema de Previsão de Correntes de Maré em Águas Rasas (SISCORAR), versão 2.0”.

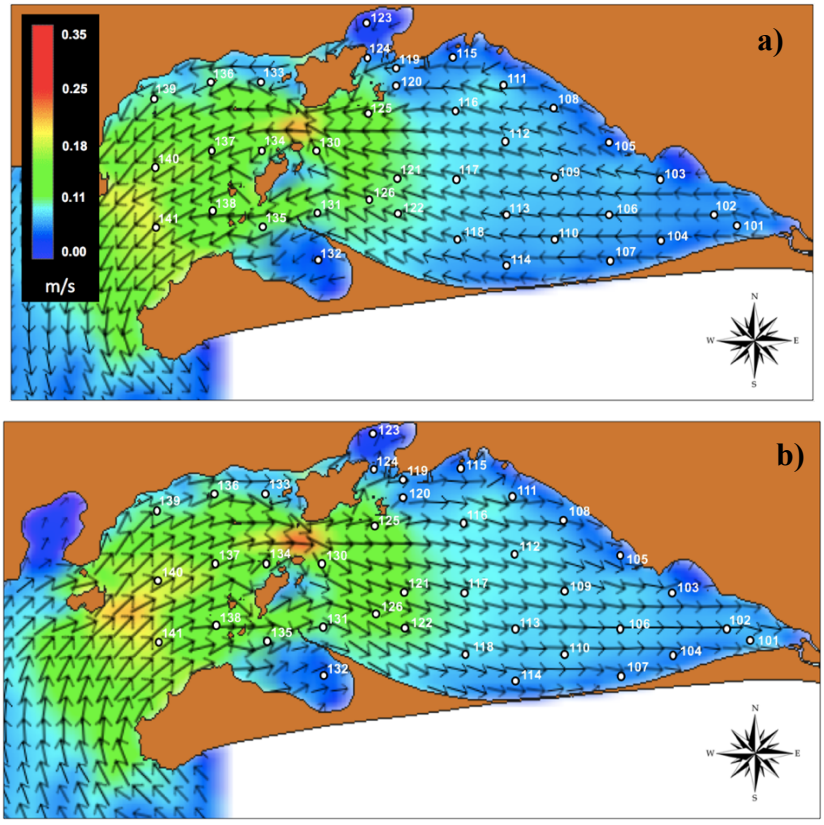

Figure 14. Generalized patterns of tidal currents system at Sepetiba Bay, a) output current tidal and b) input current tidal.

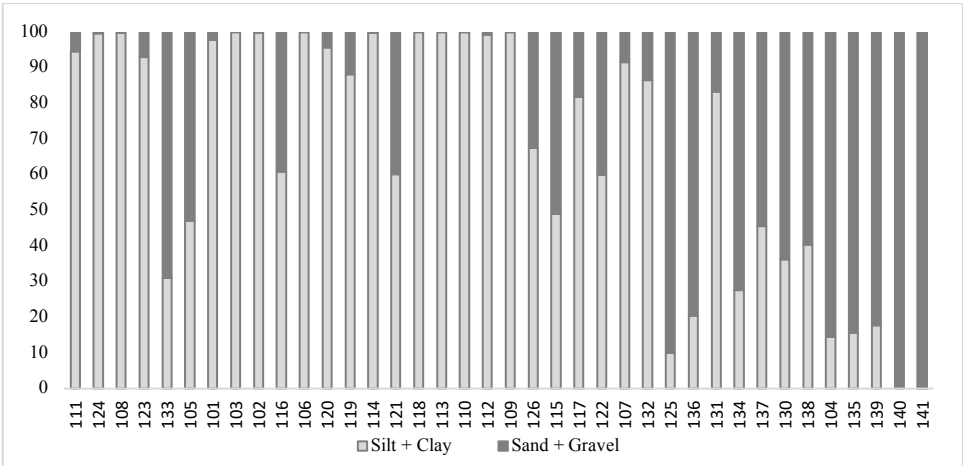

Figure 15. Sample points in increasing order of REE concentrations (from left to right) and its granulometric characteristics.

5.3.2
Humidity determination in surface sediments

Humidity values varied between 15 % and 81 %, with an average value of 62%. The humidity is directly related to the granulometric composition of the samples. For this reason, a large variation in the percentage of humidity is expected. The Figure 16 shows how the points with low percentage of humidity are grouped in the outer zone of the bay, where there is notably lower content of fine grain. These points contain a percentage of humidity lower than 40%, including points 125 and 130. Despite having low humidity, these points are located close to the central flow inlet and outlet channels of the Bay, where the speed and depth are higher and, as a result, causes a large drag of fine material and the percentage of humidity is lower.

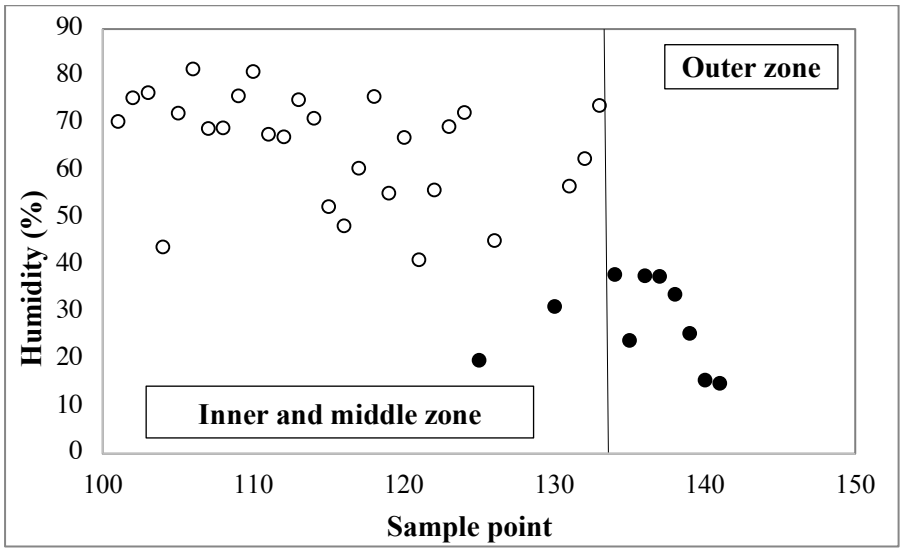

Figure 16. Humidity percent of Sepetiba Bay sediments.

5.3.3
Rare earth elements determination in surface sediment and sediment cores in Sepetiba Bay

The surface sediment sampling points are shown in 4.3.6. The concentrations of REE in suface sediments collected between June and September of 2016 are given in Table 15. Station 141 had the lowest concentration of ΣREE (25 mg kg^{-1}), while station 111 had the highest concentration of ΣREE (496 mg kg^{-1}). The light rare earth elements (LREE) are more abundant than the heavy rare earth elements (HREE). Ca. 93 %-96 % of the REE in Sepetiba Bay sediments are from La to Eu and 4%-7% from Gd to Lu.

Table 15. The concentrations (mg kg^{-1}) of rare earth elements in Sepetiba Bay sediments collected between June and September of 2016. Values with SD of three replicates are showed in annex (Table 16-Table 22) .

	La	Ce	Pr	Nd	Sm	Eu	Gd	Tb	Dy	Ho	Er	Tm	Yb	Lu	LRRE	HREE	Σ REE
101	90	186	19	63	8.4	1.7	7.1	0.84	6.1	1.3	3.9	0.57	3.8	0.64	369	24	393
102	87	177	18	59	8.2	1.7	7.1	0.77	6.1	1.3	3.8	0.55	4.0	0.63	357	17	374
103	87	182	18	60	8.7	1.8	7.0	0.83	6.3	1.3	4.3	0.63	4.5	0.76	363	19	382
104	28	57	5.9	20	2.9	0.45	2.6	0.27	1.9	0.34	1.1	0.14	1.0	0.14	117	4.9	122
105	92	192	18	61	8.7	1.8	7.3	0.88	6.6	1.3	4.2	0.63	4.5	0.69	381	19	400
106	81	166	16	56	8.1	1.7	6.8	0.79	5.7	1.2	3.8	0.57	3.9	0.62	335	17	352
107	60	123	13	41	6.5	1.1	5.3	0.60	4.1	0.85	2.7	0.39	2.7	0.40	250	12	262
108	99	204	20	67	10	1.8	8.3	0.94	7.1	1.4	4.6	0.65	4.4	0.73	410	20	430
109	70	146	14	48	6.8	1.5	6.1	0.69	5.1	1.1	3.4	0.50	3.4	0.52	293	15	307
110	73	149	14	49	7.3	1.5	6.3	0.72	5.1	1.1	3.3	0.50	3.4	0.56	299	15	314
111	112	241	23	75	11	2.0	9.5	1.09	8.0	1.7	5.6	0.78	5.8	0.89	472	24	496
112	70	147	15	50	7.3	1.3	5.9	0.68	4.8	0.92	3.1	0.40	2.8	0.46	296	13	310
113	75	151	15	51	7.6	1.6	6.4	0.76	5.4	1.1	3.5	0.51	3.3	0.53	307	15	322
114	79	160	16	55	7.7	1.5	6.8	0.80	5.4	1.1	3.6	0.51	3.6	0.54	326	16	342
115	67	132	13	45	6.4	1.2	5.6	0.63	4.6	0.94	3.1	0.44	2.9	0.51	271	13	284
116	87	176	18	59	8.3	0.94	7.2	0.74	4.7	0.87	2.5	0.33	2.1	0.32	356	12	367
117	62	137	13	44	6.2	1.2	5.6	0.59	4.2	0.82	2.6	0.37	2.5	0.37	268	11	280
118	77	157	16	53	7.6	1.6	6.8	0.73	5.4	1.1	3.6	0.46	3.7	0.54	319	16	334
119	78	163	17	56	7.8	1.4	6.7	0.72	5.2	1.1	3.2	0.42	3.1	0.47	329	14	344
120	81	164	16	54	8.2	1.5	6.8	0.79	5.6	1.1	3.5	0.49	3.6	0.54	332	16	348
121	80	162	16	57	7.6	0.86	6.8	0.69	4.2	0.76	2.2	0.26	1.7	0.26	331	10	341
122	63	128	13	44	6.2	1.0	5.4	0.59	4.1	0.78	2.5	0.33	2.3	0.31	260	11	271
123	97	199	20	67	10	1.8	8.7	0.94	6.8	1.4	4.4	0.66	4.1	0.64	404	19	423
124	95	212	20	67	10	2.0	8.5	0.93	6.8	1.4	4.5	0.64	4.2	0.68	413	19	433
125	53	108	11	39	5.9	0.33	4.8	0.46	2.6	0.40	1.2	0.10	0.66	0.09	222	5.4	227
126	71	143	15	51	7.8	0.71	6.4	0.63	4.1	0.67	1.9	0.22	1.5	0.21	295	9.2	304
130	39	77	8.2	27	4.0	0.47	3.4	0.36	2.2	0.40	1.2	0.14	1.0	0.16	158	5.5	164
131	45	95	9.3	32	4.6	1.0	4.1	0.46	3.3	0.68	2.2	0.29	2.0	0.31	191	9.2	200
132	55	116	12	40	5.8	1.1	4.9	0.52	3.9	0.79	2.5	0.31	2.3	0.38	234	11	245
133	92	192	19	63	9.3	1.8	8.1	0.91	6.2	1.2	4.3	0.61	4.0	0.63	385	18	403
134	39	95	8.7	30	4.1	0.83	3.8	0.38	2.9	0.56	1.8	0.27	1.8	0.26	182	7.9	190
135	19	39	4.1	14	1.9	0.27	1.7	0.16	1.1	0.21	0.6	0.08	0.54	0.08	79	2.8	82
136	45	121	9.1	33	4.3	0.85	3.6	0.40	2.7	0.53	1.8	0.28	1.7	0.27	217	7.7	224
137	40	79	8.2	28	4.0	0.58	3.7	0.35	2.4	0.44	1.4	0.17	1.3	0.16	163	6.1	169
138	35	70	7.3	25	3.7	0.47	3.1	0.31	1.9	0.33	1.0	0.14	0.84	0.12	145	4.7	150
139	18	37	3.6	12	1.6	0.34	1.5	0.16	1.1	0.21	0.7	0.09	0.71	0.10	74	3.0	77
140	7.9	16	1.7	5.5	0.72	0.05	0.71	0.06	0.3	0.04	0.2	0.01	0.15	0.01	33	0.82	34
141	6.1	12	1.2	4.3	0.56	0.06	0.54	0.04	0.3	0.04	0.1	0.01	0.07	0.01	24	0.57	25

The greatest concentrations of REE in Sepetiba Bay sediments were found in the north-central and northeast zones of the bay near the coast (Inner zone). The points with the highest concentration are represented in the red region shown in the Figure 17, with a concentration between 374 and 496 mg kg^{-1}. This is a large area of mangrove ecosystem, promoting strong sedimentation, which creates extensive mud flats that are natural sinks for metals. This high sedimentation rate is also favored by transport through Sepetiba Bay, determined by rivers mouths and the patterns of tidal currents.

The highest concentrations of rare earth elements were found at points 111, 124, 108, 123, 133, 105, 101, 103 and 102, most of them with a percentage between 93 and 100 % of fine grain. Therefore, these sediments are mostly sand and gravel. On the contrary, points 105 and 133 have a percentage lower than 50 %. In the case of 105, this point is near the Sepetiba beach, which changes the composition of the sediment. These proportions are illustrated in the Figure 17.

The lowest concentrations of rare earth elements were found in the western of the bay (Outer zone) and in a sandbar. They are represented in the blue-violet regions shown in the Figure 17, with a concentration between 25 and 190 mg kg^{-1}, which corresponds to the points 134, 137, 130, 138, 104, 135, 139, 140 and 141 with a percentage between 0.1 and 46 % of fine grain. These sediments are mostly sand and gravel. This region corresponds to that in which the regional winds add seawater from the Atlantic Ocean through the western channel, creating a clockwise current pattern with the highest tidal current velocity. For this reason, a large sediment deposition is not achieved, which explains the low concentrations of rare earth elements. The remaining points are basically in the central area of the bay (Middle zone) represented by the green-yellow region in the Figure 17, which combines intermediate and low tidal speeds with fine-grain sediments, finding concentrations between 367 and 200 mg kg^{-1}. Furthemore, the rare earth elements concentration in bottom sediments decreases as a function of distance from the mouth of the main rivers, responsible for transporting the largest amount of waste that arrives in the bay.

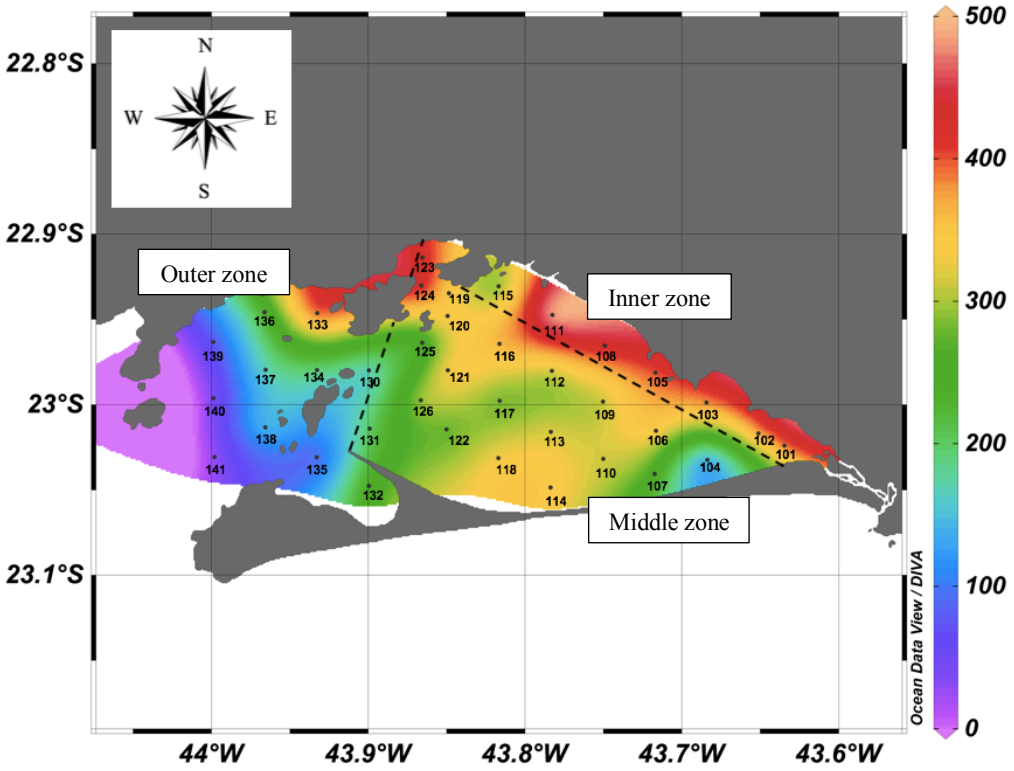

Figure 17. Total REE Sepetiba Bay and the surface sediment sampling points.

5.4
Shale-normalized REE Patterns

The North American Shales Composite (NASC) was used to normalize the REE concentrations in marine sediments. The factor was calculated as the ratio of the REE concentrations in each concentration point divided by the concentration of that element in the NASC. The shale normalization was calculated for 38 sampling stations in the Sepetiba Bay. Four sample points were chosen to compare the normalized profiles, the study area being divided into three zones: inner, middle and outer. A representative point of each zone (chosen taking into account the particle size and concentration), namely, 111 (inner), 122 (middle) and 141 (outer), as well as an additional transition point (130), are presented in Figure 18. The chondrite-normalized REE patterns of the marine sediments were characterized by higher LREE than HREE, as show in Figure 18.

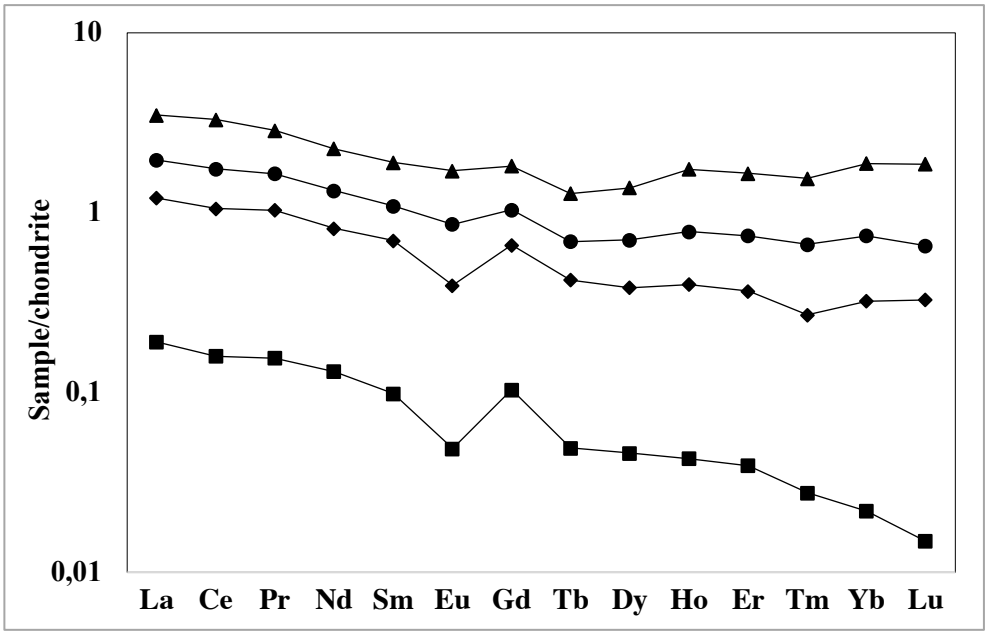

Figure 18. A NASC normalized REE patterns for marine sediments: Point 111 (▲), 122 (●), 130 (◆) and 141 (■) in Sepetiba Bay.

The points 111 and 122, inner and middle respectively, are characterized by a flat HREE pattern. Meanwhile, the point 130 corresponds to a transition zone, presenting a slight depletion in HREE pattern. The point 141, in the outer, shows a strong depletion and, according to the graph, a Eu anomaly is emphasized (Figure 18). This evidences a pattern that relates the composition, concentration and location of the collected samples in the bay. Results of the total concentration were used to establish baseline data and correlations between the Ce, Gd and Eu anomalies and the distribution patterns. In general, the chondrite-normalized ratios of REE show LREE enrichment and HREE depletion. The anomalies were calculated as follows [134,135]:

$$\frac{Ce}{Ce^*} = \frac{3Ce_N}{2La_N + Nd_N}$$

$$\frac{Gd}{Gd^*} = \frac{Gd_N}{0.33Sm_N + 0.67Tb_N}$$

$$\frac{Eu}{Eu^*} = \frac{Eu_N}{\sqrt{(Sm_N)(Gd_N)}}$$

Distribution of Ce, Gd, and Eu anomalies of the marine sediments of Sepetiba Bay is shown in Figure 19. Variations of Ce anomalies are influenced by a number of factors such as terrigenous input, the depositional environment, and

diagenesis. A Ce anomaly of >1 and <1 indicates positive and negative anomalies, respectively. The Ce/Ce* anomaly is between 0.93 and 1.31, with an average of 1.02 (Figure 19).

The Gd anomaly primarily results from the lower solubility and deposition of La and Gd complexes, compared with the other respective neighbors in the REE series. This is an indicator of complex processes that are operating in the system that have made them nonavailable and that are basically controlled by surface adsorption of REE on marine particles that subsequently settle to the bottom [136]. In the Sepetiba Bay sediments, the Gd anomaly ranges from 1.16 to 1.59, with an average of 1.27 (Figure 19). This positive Gd/Gd* anomaly is mainly the result of various human activities, mainly from aquaculture, industrial pollution and changes in land use patterns.

The Eu anomaly in the sediments ranges from 0.28 to 1.06, with an average of 0.84 (Figure 19). The Eu/Eu* ratios vary in the sediments, implying the contribution of other sources, as well as changes in lithology during erosional processes. The most remarkable features are the enrichment of HREE with respect to NASC, a relatively positive anomaly to Gd/Gd*and negative anomaly to Eu/Eu* and Ce/Ce*.

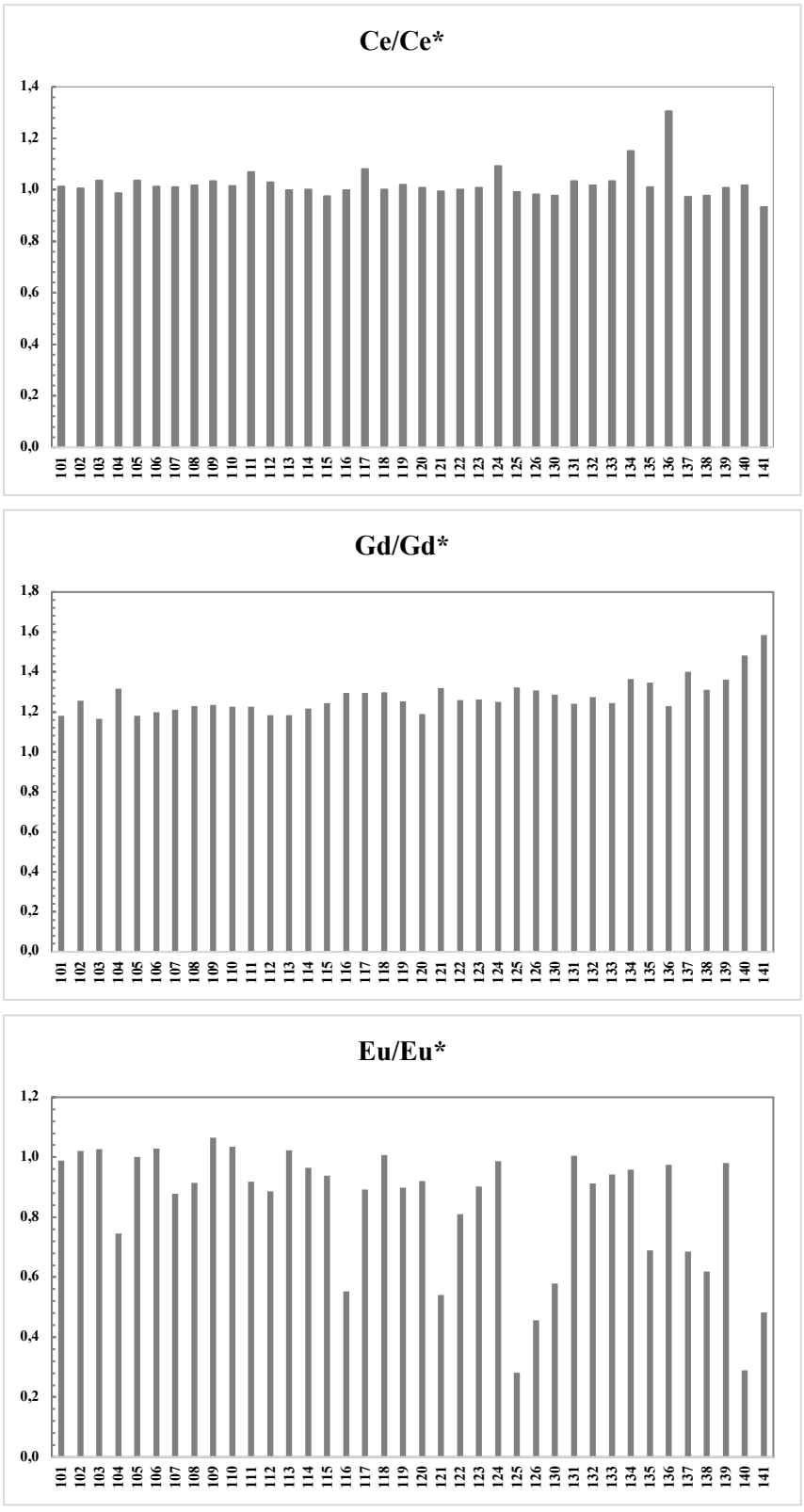

Figure 19. Distribution of Ce, Gd, and Eu anomalies in the sediments of the Sepetiba Bay.

5.5
Rare earth elements concentration in sediment cores

Three sediment cores (T8-T18-T28) of Sepetiba Bay are important witnesses of metal contamination. In this study the rare earth elements distribution in these sediment cores was determined to evaluate temporal evolution of the contamination in the bay. The study reports variations in rare earth elements concentrations majoritary above background levels. Two of these sediments were dated by ^{210}Pb [131].

Sedimentation rates were assessed at three points in the Bay of Sepetiba, in order to calculate the ages of each sectioned layer of the core. The activity of ^{210}Pb was determined after leaching the dried material with HBr and subsequent precipitation as $PbCrO_4$, according to the methodology proposed by Godoy [121]. The ages of each segment were calculated using the CF:CR model (Constant flow: constant speed) [131].

Sediment core (T8) is located approximately 2.7 km from the north coast of Sepetiba Bay, close to the Guandu River. The results of ^{210}Pb activity in this sample were very low or lower than the limits of quantification of the method, preventing the correct dating of the sample. This sediment core is close to the internal coast of the bay, in front of main affluent rivers, where the sedimentation speed is too high. Therefore, the vertical profile shows a big variation.

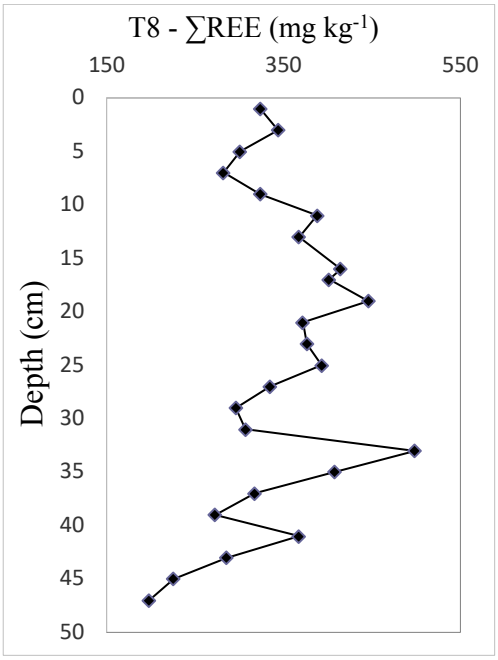

Figure 20. Rare earth elements concentration vertical profile in sediment core T8 (mg kg^{-1} dry bulk sediments).

The variation of the concentration of rare earth elements along the 50 cm depth of the sediment core is presented in Figure 20. Despite it is not dating, it shows significant variations and it could be associated with different events taking place around the Bay of Sepetiba in the last decades.

The sediment core (T-18) was collected in the central region of Sepetiba Bay and it is located in the same transect where point T8 is located, being the distance until the mouth of the main rivers, approximately 7.6 km. In this region, sediments of fine granulometry predominate, in which the content of silt and clay are greater than 90 %.

The sediment core (T-28) was located in the eastern region of the Sepetiba Bay, approximately 5.5 km from the Sepetiba beach and 3.2 km from the Marambaia sandbar. In this region, fine sediments predominate, silt and clay are practically all the material, with contents of approximately 80 % and 20 %, respectively. Sediment dating was carried out on two sediment profiles T-18 and T-28, the variation on these sediment cores are presented in Figure 21.

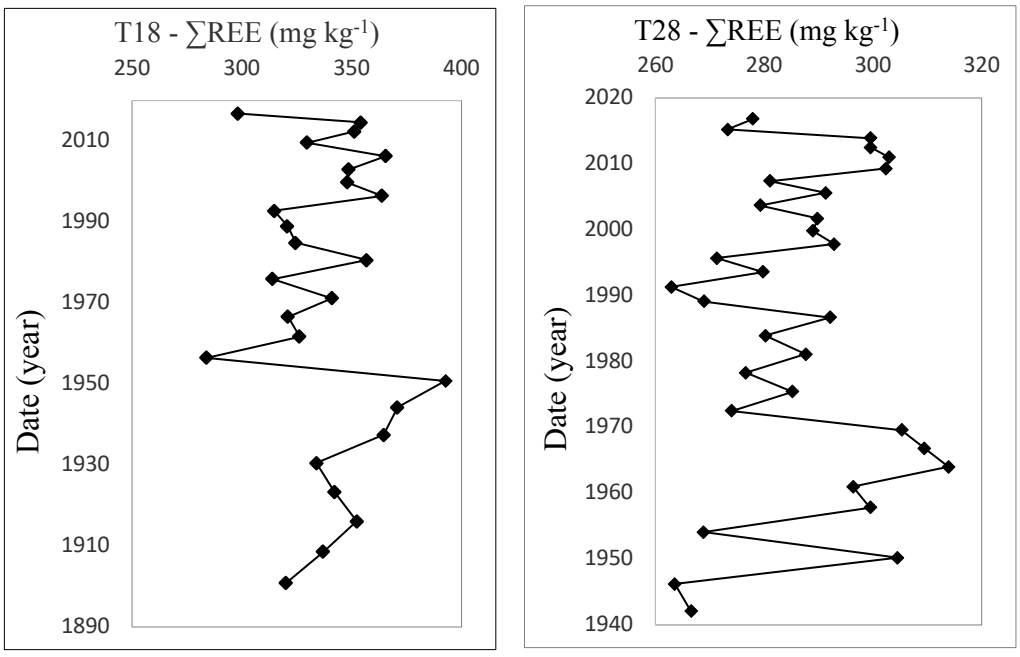

Figure 21. Rare earth elements concentration vertical profile in sediment core T18 and T28 (mg kg^{-1} dry bulk sediments).

The population inhabiting the Sepetiba Bay basin increased from 600,000 in 1978 to 1.2 million in the late 1980s, reaching about 1.7 million in 2000, and the changes that have occurred around the bay can be seen reflected in the variation in the concentration of rare earth elements since the 1980s, as shown in the Figure 21.

Studies of changes in sediment transport and sedimentation rates have proved valuable in understanding changes in aquatic environments because they may cause a large range of transformations in the physical structure of water bodies. For instance, a reduction of sediment transport and corresponding decrease in sedimentation rates may increase erosion in coastal zones. On the other hand, increasing sedimentation rates may silt up protected coastal sites, such as estuaries, seagrass beds and mangroves.

At the beginning of the century, civil works were initiated in the bay's basin, mostly to control malaria, and included digging and straightening of river channels and the building of artificial canals. Although of relatively small scale, these engineering works more than doubled the sediment accumulation rates in the bay. In the 1950s, to supply water for the fast growing population and the development of industrial activities, the Paraiba do Sul River waters were diverged to Sepetiba Bay basin, through the Guandu River, and then distributed among the channels that discharge into Sepetiba Bay.

The results of three sediment cores show the variations in the REEs distribution pattern within the upper 90 cm of the sediment cores studied, these sediment cores are located in the middle zone (with high porcent in fine grain) and may play an important role in the fate of nutrient and pollutants to Sepetiba Bay.

The Figure 21 shows two sediment cores that were dated. It can be seen that, in the 1950s, an increase in the concentration of rare earth elements coincides with change the waters flux of the Paraiba do Sul river to Sepetiba Bay basin.

6
Conclusion

A method was developed for the removal of Ba in solutions obtained after the wet digestion of environmental samples, by addition of sulfuric acid solution addition and separation of the $BaSO_4$ formed. Consequently, spectral interferences from BaO formation on both Eu isotopes were successfully eliminated, and REE in the supernatants were determined by ICP-MS. The method was suitable for samples with Ba concentrations higher than 0.2 mg L^{-1} and was successfully applied to environmental samples of asphalt and crushed stone, being the first REE characterization of these materials. The wet digestion of the samples resulted in a small amount of residue, attributed to insoluble fluorides, such as aluminum fluoride, during the procedure and it was not significant in the recovery of REE. The accuracy of the method was evaluated with the reference materials SRM 688 and G2, resulting in good recoveries for most REE. Besides, the Eu concentrations in the samples determined by ICP-MS were in agreement with the ones obtained by ICP OES. In the case of the crushed stone, the Eu results obtained by mathematical correction were significantly different due to the limitation of the mathematical approach, being the proposed method for this interference correction especially recommended for samples with high Ba concentrations. The major elemental composition of the samples suggested the presence of carbonatites that explains the high Ba concentrations observed. The chondrite-normalized pattern of REE in the asphalt pavement showed a depletion of Eu and enrichment of HREE, in comparison to the crushed stone's one, appointing to the potential potential mobility of REE in this material.

Weathering plays a significant role in REE distribution in the Sepetiba Bay ecosystem. The continental weathering process is the main source for REE in the mangrove sediments; considerable input also comes from anthropogenic activities and the marine environment. The elements are significantly altered in the mangrove region. The bottom sediments are characterized by ΣREE = 25 to 496 mg kg^{-1}. The average values of LREE and HREE are 265 and 17 mg kg^{-1}, respectively. LREE are more enriched in the mangrove sediment than HREE, perhaps because of their high adsorption capacity onto clay matter in the coastal environment.

The most remarkable features are the enrichment of HREE with respect to NASC, a relatively positive Gd/Gd* anomaly, and negative Eu/Eu* and Ce/Ce* anomalies, which are derived from both anthropogenic and natural weathering inputs. Chemical weathering mechanisms in the coastal zone have led to extensive fractionation of REE contributed from various natural processes in the adjoining river streams and estuarine zones. The concentrations of REE existing in Sepetiba Bay and the characteristic of the surface sediments can be useful as sediment tracers of the rivers that feed the bay. Determination and comparation of concentration of rare earth elements and normalized profiles of samples of these rivers will be necessary to compare with the concentrations in the surface sediments in the Sepetiba Bay.

The results of three sediment cores show the variation of REE and an enrichment in one region and at specific depths. These changes coincide with the spatial and temporal water diversion from Paraiba do Sul River, through the Guandu River, and then distributed among the channels that discharge into Sepetiba Bay. The modifications in the REE distribution pattern within the sediment cores suggest that fine-grained sediments discharged by diversions in the water systems, well preserved in the mangrove forest, have affected the rare earth elements composition of Sepetiba Bay.

7
Future work

The increase in applications of rare earth elements (REE) has led to emerge a need of studying their environmental impact. REE are present in products such as electronic devices and lamps [137]. Improper disposal of these materials can represent a releasing of REE, among other elements, to the environment. Acid rain highly impacts the environment and may cause the mobilization of potentially toxic metals into the soil and natural waters.

In this work rare earth elements were determined in different samples as asphalt pavement, crushed stone and marine sediment. Currently we are also working on the determination of rare earth elements and potentially toxic metals in fluorescent lamp powder and simulating the effect of acid rain after leaching.

For now, the preliminary study has demonstrated that leaching the fluorescent lamps powder with simulated acid rain for only 1 h was already enough for extracting REE. Such result contributions confirm that improper disposal of lamps can be a source of environmental contamination.

Due to time constrain it was not possible to exhaust all possibilities related to this research. Therefore, some important points should be addressed as:

- To optimize leaching time.
- To optimize leaching volume and to assess extraction capacity.
- To create a contaminated synthetic soil to leach synthetic acid rain and evaluate the mobility of REE and potentially toxic metals.

8
References

[1] S. Ilyas, M.-S. Kim, J.-C. Lee, A. Jabeen, H. Bhatti, Bio-Reclamation of Strategic and Energy Critical Metals from Secondary Resources, Metals (Basel). 7 (2017) 207. https://doi.org/10.3390/met7060207.

[2] J. Zhang, B. Zhao, B. Schreiner, Rare Earth Elements and Minerals, in: Sep. Hydrometall. Rare Earth Elem., Springer International Publishing, Cham, 2016: pp. 1–17. https://doi.org/10.1007/978-3-319-28235-0_1.

[3] V. Gonzalez, D.A.L. Vignati, C. Leyval, L. Giamberini, Environmental fate and ecotoxicity of lanthanides: Are they a uniform group beyond chemistry?, Environ. Int. 71 (2014) 148–157. https://doi.org/10.1016/j.envint.2014.06.019.

[4] F. Lesnov, Consistent patterns of rare earth element distribution in accessory minerals from rocks of mafic-ultramafic complexes, Open Geosci. 5 (2013). https://doi.org/10.2478/s13533-012-0121-z.

[5] A. Pourmand, N. Dauphas, T.J. Ireland, A novel extraction chromatography and MC-ICP-MS technique for rapid analysis of REE, Sc and Y: Revising CI-chondrite and Post-Archean Australian Shale (PAAS) abundances, Chem. Geol. 291 (2012) 38–54. https://doi.org/10.1016/j.chemgeo.2011.08.011.

[6] G. Tyler, Rare earth elements in soil and plant systems - A review, Plant Soil. 267 (2004) 191–206. https://doi.org/10.1007/s11104-005-4888-2.

[7] M. Pansu, J. Gautheyrou, Handbook of soil analysis: mineralogical, organic and inorganic methods, Springer Science & Business Media, 2007.

[8] K. Nakamura, Q. Chang, Precise Determination of Ultra-Low (sub-ng g -1) Level Rare Earth Elements in Ultramafic Rocks by Quadrupole ICP-MS, Geostand. Geoanalytical Res. 31 (2007) 185–197. https://doi.org/10.1111/j.1751-908X.2007.00859.x.

[9] N.N. Fedyunina, K.B. Ossipov, I.F. Seregina, M.A. Bolshov, M.A. Statkus, G.I. Tsysin, Determination of rare earth elements in rock samples by inductively coupled plasma mass-spectrometry after sorption

preconcentration using Pol-DETATA sorbent, Talanta. 102 (2012) 128–131. https://doi.org/10.1016/j.talanta.2012.07.026.

[10] B. Zawisza, K. Pytlakowska, B. Feist, M. Polowniak, A. Kita, R. Sitko, Determination of rare earth elements by spectroscopic techniques: a review, J. Anal. At. Spectrom. 26 (2011) 2373. https://doi.org/10.1039/c1ja10140d.

[11] J.R. Bacon, A.M. Ure, The correction of interference effects in the determination of the rare earth elements and hafnium by spark-source mass spectrometry, Anal. Chim. Acta. 105 (1979) 163–176. https://doi.org/10.1016/S0003-2670(01)83748-X.

[12] Y. Suzuki, T. Suzuki, N. Furuta, Determination of Rare Earth Elements (REEs) in Airborne Particulate Matter (APM) Collected in Tokyo, Japan, and a Positive Anomaly of Europium and Terbium, Anal. Sci. 26 (2010) 929–935. https://doi.org/10.2116/analsci.26.929.

[13] G. Bayon, J.A. Barrat, J. Etoubleau, M. Benoit, C. Bollinger, S. Révillon, Determination of Rare Earth Elements, Sc, Y, Zr, Ba, Hf and Th in Geological Samples by ICP-MS after Tm Addition and Alkaline Fusion, Geostand. Geoanalytical Res. 33 (2009) 51–62. https://doi.org/10.1111/j.1751-908X.2008.00880.x.

[14] I. V. Nikolaeva, S. V. Palesskii, O.A. Koz'menko, G.N. Anoshin, Analysis of geologic reference materials for REE and HFSE by inductively coupled plasma-mass spectrometry (ICP-MS), Geochemistry Int. 46 (2008) 1016–1022. https://doi.org/10.1134/S0016702908100066.

[15] W. Gwenzi, L. Mangori, C. Danha, N. Chaukura, N. Dunjana, E. Sanganyado, Sources, behaviour, and environmental and human health risks of high-technology rare earth elements as emerging contaminants, Sci. Total Environ. 636 (2018) 299–313. https://doi.org/10.1016/j.scitotenv.2018.04.235.

[16] R. Ramesh, A.L. Ramanathan, R. Arthur James, V. Subramanian, S.B. Jacobsen, H.D. Holland, Rare earth elements and heavy metal distribution in estuarine sediments of east coast of India, Hydrobiologia. 397 (1999) 89–99. https://doi.org/https://doi.org/10.1023/A:1003646631589.

[17] X. Huang, G. Zhang, A. Pan, F. Chen, C. Zheng, Protecting the environment and public health from rare earth mining, Earth's Futur. 4 (2016) 532–535. https://doi.org/10.1002/2016EF000424.

[18] M.A. Alam, L. Zuga, M.G. Pecht, Economics of rare earth elements in ceramic capacitors, Ceram. Int. 38 (2012) 6091–6098. https://doi.org/10.1016/j.ceramint.2012.05.068.

[19] C. Laveuf, S. Cornu, A review on the potentiality of Rare Earth Elements to trace pedogenetic processes, Geoderma. 154 (2009) 1–12. https://doi.org/10.1016/j.geoderma.2009.10.002.

[20] P. Henderson, General geochemical properties and abundances of the rare earth elements., Rare Earth Elem. Geochemistry. (1983) 1–32. https://doi.org/10.1016/b978-0-444-42148-7.50006-x.

[21] A. Abrão, Química e tecnologia das terras-raras, CETEM/CNPq, Rio de Janeiro, 1994.

[22] L. Perrin, L. Maron, O. Eisenstein, Lanthanide Complexes: Electronic Structure and H—H, C—H, and Si—H Bond Activation from a DFT Perspective, in: 2004: pp. 116–133. https://doi.org/10.1021/bk-2004-0885.ch007.

[23] S.R. Taylor, Abundance of chemical elements in the continental crust : a new table, Geochim. Cosmochim. Acta. 28 (1964) 1273–1285.

[24] S.M. Taylor, Stuart Ross and McLennan, The continental crust: its composition and evolution, Blackwell Scientific Pub., Palo Alto, CA, 1985.

[25] M. Engi, Petrochronology Based on REE-Minerals: Monazite, Allanite, Xenotime, Apatite, Rev. Mineral. Geochemistry. 83 (2017) 365–418. https://doi.org/10.2138/rmg.2017.83.12.

[26] A.P. Jones, F. Wall, Williams C. Terry, Rare earth minerals: chemistry, origin and ore deposits, Springer Science & Business Media, 1995.

[27] Pradip, D.W. Fuerstenau, The role of inorganic and organic reagents in the flotation separation of rare-earth ores, Int. J. Miner. Process. 32 (1991) 1–22. https://doi.org/10.1016/0301-7516(91)90016-C.

[28] A.M. Nikanorov, The Oddo-Harkins rule and distribution of chemical elements in freshwater ecosystems, Dokl. Earth Sci. 426 (2009) 600–604. https://doi.org/10.1134/S1028334X09040205.

[29] P. Henderson, General Geochemical Properties and Abundances of the Rare Earth Elements, in: Rare Earth Elem. Geochemistry, 1984: pp. 1–32. https://doi.org/10.1016/B978-0-444-42148-7.50006-X.

[30] F.R.S. Bentlin, Desenvolvimento de métodos analíticos para a

determinação de lantanídeos por técnicas de espectrometria atômica com plasma indutivamente acoplado, Tese Doutorado - Univ. Fed. Do Rio Gd. Do Sul. (2012) 122.

[31] K. Smith Stegen, Heavy rare earths, permanent magnets, and renewable energies: An imminent crisis, Energy Policy. 79 (2015) 1–8. https://doi.org/10.1016/j.enpol.2014.12.015.

[32] O. Gutfleisch, M.A. Willard, E. Brück, C.H. Chen, S.G. Sankar, J.P. Liu, Magnetic materials and devices for the 21st century: Stronger, lighter, and more energy efficient, Adv. Mater. 23 (2011) 821–842. https://doi.org/10.1002/adma.201002180.

[33] J. Lohrke, T. Frenzel, J. Endrikat, F.C. Alves, T.M. Grist, M. Law, J.M. Lee, T. Leiner, K.C. Li, K. Nikolaou, M.R. Prince, H.H. Schild, J.C. Weinreb, K. Yoshikawa, H. Pietsch, 25 Years of Contrast-Enhanced MRI: Developments, Current Challenges and Future Perspectives, Adv. Ther. 33 (2016) 1–28. https://doi.org/10.1007/s12325-015-0275-4.

[34] Y.D. Xiao, R. Paudel, J. Liu, C. Ma, Z.S. Zhang, S.K. Zhou, MRI contrast agents: Classification and application (Review), Int. J. Mol. Med. 38 (2016) 1319–1326. https://doi.org/10.3892/ijmm.2016.2744.

[35] L. Thunus, R. Lejeune, Overview of transition metal and lanthanide complexes as diagnostic tools, Coord. Chem. Rev. 184 (1999) 125–155. https://doi.org/10.1016/S0010-8545(98)00206-9.

[36] T. Wakabayashi, A. Ymamoto, A. Kazaana, Y. Nakano, Y. Nojiri, M. Kashiwazaki, Antibacterial, Antifungal and Nematicidal Activities of Rare Earth Ions, Biol. Trace Elem. Res. 174 (2016) 464–470. https://doi.org/10.1007/s12011-016-0727-y.

[37] Z. Hui, F. Jia, W. He, Bacteriostatic effect of cerium humic acid complex, J. Rare Earths. 17 (1999).

[38] I. Cota, V. Marturano, B. Tylkowski, Ln complexes as double faced agents: Study of antibacterial and antifungal activity, Coord. Chem. Rev. 396 (2019) 49–71. https://doi.org/10.1016/j.ccr.2019.05.019.

[39] G.M. Esteban-Parra, I. Moscoso, J. Cepeda, J.A. García, M. Sánchez-Moreno, A. Rodríguez-Diéguez, M. Quirós, Lanthanide(III) Based Complexes Containing 5,7-Dimethyl-1,2,4-triazolo[1,5-a]pyrimidine as Long-Lived Photoluminescent Antiparasitic Agents, Eur. J. Inorg. Chem.

(2019) 308–317. https://doi.org/10.1002/ejic.201901119.

[40] X. Pang, D. Li, A. Peng, Application of rare-earth elements in the agriculture of China and its environmental behavior in soil, Environ. Sci. Pollut. Res. 9 (2002) 143–148. https://doi.org/10.1007/BF02987462.

[41] S. Zhang, X. quan Shan, Speciation of rare earth elements in soil and accumulation by wheat with rare earth fertilizer application, Environ. Pollut. 112 (2001) 395–405. https://doi.org/10.1016/S0269-7491(00)00143-3.

[42] J. Rogowska, E. Olkowska, W. Ratajczyk, L. Wolska, Gadolinium as a new emerging contaminant of aquatic environments, Environ. Toxicol. Chem. 37 (2018) 1523–1534. https://doi.org/10.1002/etc.4116.

[43] G. Pagano, M. Guida, F. Tommasi, R. Oral, Health effects and toxicity mechanisms of rare earth elements—Knowledge gaps and research prospects, Ecotoxicol. Environ. Saf. 115 (2015) 40–48. https://doi.org/10.1016/j.ecoenv.2015.01.030.

[44] E.U. Commission, Tackling the Challenges in Commodity Markets and on Raw Materials, Brussels Eur. Comm. (2011).

[45] S. Massari, M. Ruberti, Rare earth elements as critical raw materials: Focus on international markets and future strategies, Resour. Policy. 38 (2013) 36–43. https://doi.org/10.1016/j.resourpol.2012.07.001.

[46] Z. Chen, Global rare earth resources and scenarios of future rare earth industry, J. Rare Earths. 29 (2011) 1–6. https://doi.org/10.1016/S1002-0721(10)60401-2.

[47] N. Haque, A. Hughes, S. Lim, C. Vernon, Rare earth elements: Overview of mining, mineralogy, uses, sustainability and environmental impact, Resources. 3 (2014) 614–635. https://doi.org/10.3390/resources3040614.

[48] V. Balaram, Rare earth elements: A review of applications, occurrence, exploration, analysis, recycling, and environmental impact, Geosci. Front. 10 (2019) 1285–1303. https://doi.org/10.1016/j.gsf.2018.12.005.

[49] F. Sampsonas, A. Kaparianos, V. Tzelepi, V. Zolota, K. Karkoulias, M. Tsiamita, N. Mastronikolis, K. Spiropoulos, Miliary pattern due to occupational lung disease in a patient with laryngeal cancer, Eur. Rev. Med. Pharmacol. Sci. 14 (2010) 43–45.

[50] M. Saiki, J.O. Santos, E.R. Alves, F.A. Genezini, M.P. Marcelli, P.H.N. Saldiva, Correlation study of air pollution and cardio-respiratory diseases

through NAA of an atmospheric pollutant biomonitor, J. Radioanal. Nucl. Chem. 299 (2014) 773–779. https://doi.org/10.1007/s10967-013-2698-1.

[51] P.J. Haley, J. Haley, 6 (1991) 809–820.

[52] R. Djingova, J. Ivanova, Determination of rare earth elements in soils and sediments by inductively coupled plasma atomic emission spectrometry after cation-exchange separation, Talanta. 57 (2002) 821–829. https://doi.org/10.1016/S0039-9140(02)00126-1.

[53] M.. Navarro, H.H.G.. Ulbrich, S. Andrade, V.. Janasi, Adaptation of ICP–OES routine determination techniques for the analysis of rare earth elements by chromatographic separation in geologic materials: tests with reference materials and granitic rocks, J. Alloys Compd. 344 (2002) 40–45. https://doi.org/10.1016/S0925-8388(02)00302-X.

[54] S. Wu, M. He, B. Hu, Z. Jiang, Determination of trace rare earth elements in natural water by electrothermal vaporization ICP-MS with pivaloyltrifluoroacetone as chemical modifier, Microchim. Acta. 159 (2007) 269–275. https://doi.org/10.1007/s00604-007-0764-5.

[55] K. Tanaka, Y. Takahashi, H. Shimizu, Determination of rare earth element in carbonate using laser-ablation inductively-coupled plasma mass spectrometry: An examination of the influence of the matrix on laser-ablation inductively-coupled plasma mass spectrometry analysis, Anal. Chim. Acta. 583 (2007) 303–309. https://doi.org/10.1016/j.aca.2006.10.023.

[56] L. Pietrelli, B. Bellomo, D. Fontana, M.. Montereali, Rare earths recovery from NiMH spent batteries, Hydrometallurgy. 66 (2002) 135–139. https://doi.org/10.1016/S0304-386X(02)00107-X.

[57] I.E. De Vito, R.A. Olsina, A.N. Masi, Preconcentration and elimination of matrix effects in XRF determinations of rare earth elements by preparing a thin film through chemofiltration, J. Anal. At. Spectrom. 16 (2001) 275–278. https://doi.org/10.1039/b008165p.

[58] R.S. Dybczyński, E. Czerska, B. Danko, K. Kulisa, Z. Samczyński, Comparison of performance of INAA, RNAA and ion chromatography for the determination of individual lanthanides, Appl. Radiat. Isot. 68 (2010) 23–27. https://doi.org/10.1016/j.apradiso.2009.09.002.

[59] Y. SUN, M. SUN, G. ZHAO, Applicability of Capillary Electrophoresis to the Analysis of Trace Rare Earth Elements in Geological Samples, Anal. Sci. 22

(2006) 551–555. https://doi.org/10.2116/analsci.22.551.

[60] G.L. Donati, J.A. Nóbrega, C.C. Nascentes, B.T. Jones, Indirect determination of iodide by tungsten coil atomic emission spectrometry, Microchem. J. 93 (2009) 242–246. https://doi.org/10.1016/j.microc.2009.07.015.

[61] C.B. Boss, K.J. Fredeen, Concepts, Instrumentation and techniques in ICP-OES, PerkinElmer. (2004) 2–11. http://www.perkinelmer.co.uk/CMSResources/Images/44-159043GDE_Concepts-of-ICP-OES-Booklet.pdf.

[62] S.C. Wilschefski, M.R. Baxter, Inductively Coupled Plasma Mass Spectrometry: Introduction to Analytical Aspects, Clin. Biochem. Rev. 40 (2019) 115.

[63] R. Thomas, A beginner's guide to ICP-MS - Part III: The plasma source, Spectroscopy. 16 (2001) 26-+. https://doi.org/10.1007/978-0-387-93837-0.

[64] M.F. Giné-Rosias, Espectrometria de massas com fonte de plasma. (ICP-MS), Primeira, Piracicaba: CPG-CENA-USP, São Paulo, 1999. https://doi.org/10.1590/S1414-753X2001000800001.

[65] R. Thomas, Practical guide to ICP-MS: a tutorial for beginner, 2013.

[66] E. Evans, J. Giglio, Interferences in inductively coupled plasma mass spectrometry. A review, J. Anal. At. Spectrom. 8 (1993) 1. https://doi.org/10.1039/ja9930800001.

[67] F.G. Pinto, R.E. Escalfoni, T.D. Saint'Pierre, Sample Preparation for Determination of Rare Earth Elements in Geological Samples by ICP-MS: A Critical Review, Anal. Lett. 45 (2012) 1537–1556. https://doi.org/10.1080/00032719.2012.677778.

[68] F. Ardini, F. Soggia, F. Rugi, R. Udisti, M. Grotti, Conversion of rare earth elements to molecular oxide ions in a dynamic reaction cell and consequences on their determination by inductively coupled plasma mass spectrometry, J. Anal. At. Spectrom. 25 (2010) 1588. https://doi.org/10.1039/b927108b.

[69] M. Ulrich, S. Bureau, C. Chauvel, C. Picard, Accurate Measurement of Rare Earth Elements by ICP-MS after Ion-Exchange Separation: Application to Ultra-Depleted Samples, Geostand. Geoanalytical Res. 36 (2012) 7–20. https://doi.org/10.1111/j.1751-908X.2011.00116.x.

[70] K. Jarvis, Determination of rare earth elements in geological samples by inductively coupled plasma mass spectrometry, J. Anal. At. Spectrom. 4 (1989) 563. https://doi.org/10.1039/ja9890400563.

[71] P. Dulski, Interferences of oxide, hydroxide and chloride analyte species in the determination of rare earth elements in geological samples by inductively coupled plasma-mass spectrometry, Fresenius. J. Anal. Chem. 350 (1994) 194–203. https://doi.org/10.1007/BF00322470.

[72] P.B. Armentrout, Fundamentals of ion–molecule chemistry, J. Anal. At. Spectrom. 19 (2004) 571–580. https://doi.org/10.1039/B313133E.

[73] Z. Du, R.S. Houk, Attenuation of metal oxide ions in inductively coupled plasma mass spectrometry with hydrogen in a hexapole collision cell, J. Anal. At. Spectrom. 15 (2000) 383–388. https://doi.org/10.1039/a905046i.

[74] S.D. Tanner, V.I. Baranov, D.R. Bandura, Reaction cells and collision cells for ICP-MS: a tutorial review, Spectrochim. Acta Part B At. Spectrosc. 57 (2002) 1361–1452. https://doi.org/10.1016/S0584-8547(02)00069-1.

[75] F. Guéguen, A. Nonell, M. Granet, G. Favre, H. Isnard, F. Chartier, Eu isotopic measurements with in situEu/Gd/Sm separation using O 2 as a reactant gas in collision/reaction cell based MC-ICP-MS, J. Anal. At. Spectrom. 25 (2010) 201–205. https://doi.org/10.1039/B912605H.

[76] F.G. Pinto, F.G. Lepri, T.D. Saint'Pierre, J.B.B. da Silva, L.M. Costa, A.J. Curtius, Direct Determination of Dy, Sm, Eu, Tm, and Yb in Geological Samples by Slurry Electrothermal Vaporization Inductively Coupled Plasma Mass Spectrometry, Anal. Lett. 43 (2010) 949–959. https://doi.org/10.1080/00032710903491062.

[77] S.P. Verma, E. Santoyo, High-Performance Liquid and Ion Chromatography: Separation and Quantification Analytical Techniques for Rare Earth Elements, Geostand. Geoanalytical Res. 31 (2007) 161–184. https://doi.org/10.1111/j.1751-908X.2007.00842.x.

[78] A. Fisher, D. Kara, Determination of rare earth elements in natural water samples – A review of sample separation, preconcentration and direct methodologies, Anal. Chim. Acta. 935 (2016) 1–29. https://doi.org/10.1016/j.aca.2016.05.052.

[79] T. Watanabe, Y. Saito-Kokubu, H. Murakami, T. Iwatsuki, Onsite chelate resin solid-phase extraction of rare earth elements in natural water samples:

its implication for studying past redox changes by inorganic geochemistry, Limnology. 19 (2018) 21–30. https://doi.org/10.1007/s10201-017-0513-3.

[80] Y. Zhu, A. Itoh, T. Umemura, H. Haraguchi, K. Inagaki, K. Chiba, Determination of REEs in natural water by ICP-MS with the aid of an automatic column changing system, J. Anal. At. Spectrom. 25 (2010) 1253. https://doi.org/10.1039/c003125a.

[81] M.F. Giné, Espectrometria de Emissão Atômica com Plasma Acoplado Indutivamente ICP-AES, J. Chem. Inf. Model. الحا العدد (1998) 43. https://doi.org/10.1017/CBO9781107415324.004.

[82] P.W.J.M. Boumans, J.J.A.M. Vrakking, Spectral interferences in inductively coupled plasma atomic emission spectrometry-I. A theoretical and experimental study of the effect of spectral bandwidth on selectivity, limits of determination, limits of detection and detection power, Spectrochim. Acta Part B At. Spectrosc. 40 (1985) 1085–1105. https://doi.org/10.1016/0584-8547(85)80051-3.

[83] J.W. Olesik, Elemental analysis using ICP-OES and ICP/MS, Anal. Chem. 63 (1991). https://doi.org/10.1021/ac00001a001.

[84] V. Balaram, Recent trends in the instrumental analysis of rare earth elements in geological and industrial materials, TrAC - Trends Anal. Chem. 15 (1996) 475–486. https://doi.org/10.1016/S0165-9936(96)00058-1.

[85] C.Q. Liu, A. Masuda, A. Okada, S. Yabuki, J. Zhang, Z.L. Fan, A geochemical study of loess and desert sand in northern China: Implications for continental crust weathering and composition, Chem. Geol. 106 (1993) 359–374. https://doi.org/10.1016/0009-2541(93)90037-J.

[86] N. Grosjean, M. Le Jean, C. Berthelot, M. Chalot, E.M. Gross, D. Blaudez, Accumulation and fractionation of rare earth elements are conserved traits in the Phytolacca genus, Sci. Rep. 9 (2019) 18458. https://doi.org/10.1038/s41598-019-54238-3.

[87] J. Riondato, F. Vanhaecke, L. Moens, R. Dams, Determination of rare earth elements in environmental matrices by sector-field inductively coupled plasma mass spectrometry, Fresenius. J. Anal. Chem. 370 (2001) 544–552. https://doi.org/10.1007/s002160100801.

[88] Z. Wang, L. Yin, H. Xiang, X. Qin, S. Wang, Accumulation patterns and species-specific characteristics of yttrium and rare earth elements (YREEs)

in biological matrices from Maluan Bay, China: Implications for biomonitoring, Environ. Res. 179 (2019) 108804. https://doi.org/10.1016/j.envres.2019.108804.

[89] E. Bonnail, R. Pérez-López, A.M. Sarmiento, J.M. Nieto, T.Á. DelValls, A novel approach for acid mine drainage pollution biomonitoring using rare earth elements bioaccumulated in the freshwater clam Corbicula fluminea, J. Hazard. Mater. 338 (2017) 466–471. https://doi.org/10.1016/j.jhazmat.2017.05.052.

[90] S. Wang, R. Yu, G. Hu, Q. Hu, Q. Zheng, Distribution and source of rare earth elements in PM2.5 in Xiamen, China, Environ. Toxicol. Chem. 36 (2017) 3217–3222. https://doi.org/10.1002/etc.3902.

[91] L. Tripathee, S. Kang, D. Rupakheti, Q. Zhang, R.M. Bajracharya, C.M. Sharma, J. Huang, A. Gyawali, R. Paudyal, M. Sillanpää, Spatial distribution, sources and risk assessment of potentially toxic trace elements and rare earth elements in soils of the Langtang Himalaya, Nepal, Environ. Earth Sci. 75 (2016). https://doi.org/10.1007/s12665-016-6140-1.

[92] U. Tamim, R. Khan, Y.N. Jolly, K. Fatema, S. Das, K. Naher, M.A. Islam, S.M.A. Islam, S.M. Hossain, Elemental distribution of metals in urban river sediments near an industrial effluent source, Chemosphere. 155 (2016) 509–518. https://doi.org/10.1016/j.chemosphere.2016.04.099.

[93] C. Hissler, R. Hostache, J.F. Iffly, L. Pfister, P. Stille, Anthropogenic rare earth element fluxes into floodplains: Coupling between geochemical monitoring and hydrodynamic sediment transport modelling, Comptes Rendus - Geosci. 347 (2015) 294–303. https://doi.org/10.1016/j.crte.2015.01.003.

[94] Z. Yu, P. Robinson, P. McGoldrick, An Evaluation of Methods for the Chemical Decomposition of Geological Materials for Trace Element Determination using ICP-MS, J. Geostand. Geoanalysis. 25 (2001) 199–217. https://doi.org/10.1111/j.1751-908X.2001.tb00596.x.

[95] J. Ivanova, R. Djingova, S. Korhammer, B. Markert, On the microwave digestion of soils and sediments for determination of lanthanides and some toxic and essential elements by inductively coupled plasma source mass spectrometry, Talanta. 54 (2001) 567–574. https://doi.org/10.1016/S0039-9140(00)00640-8.

[96] R. Prego, M. Caetano, C. Vale, J. Marmolejo-Rodríguez, Rare earth

elements in sediments of the Vigo Ria, NW Iberian Peninsula, Cont. Shelf Res. 29 (2009) 896–902. https://doi.org/10.1016/j.csr.2009.01.009.

[97] M. He, B. Hu, Z. Jiang, Electrothermal vaporization inductively coupled plasma mass spectrometry for the determination of trace amount of lanthanides and yttrium in soil with polytetrafluroethylene emulsion as a chemical modifier, Anal. Chim. Acta. 530 (2005) 105–112. https://doi.org/10.1016/j.aca.2004.08.074.

[98] J. MIERZWA, S.B. ADELOJU, H.S. DHINDSA, Ultrasound Accelerated Solid-Liquid Extraction for the Determination of Selenium in Biological Samples by Electrothermal Atomization Atomic Absorption Spectrometry., Anal. Sci. 13 (1997) 189–193. https://doi.org/10.2116/analsci.13.189.

[99] F. Priego Capote, M.D. Luque de Castro, Ultrasound in analytical chemistry, Anal. Bioanal. Chem. 387 (2006) 249–257. https://doi.org/10.1007/s00216-006-0966-4.

[100] R.F. Contamine, A.M. Wilhelm, J. Berlan, H. Delmas, Power measurement in sonochemistry, Ultrason. - Sonochemistry. 2 (1995). https://doi.org/10.1016/1350-4177(94)00010-P.

[101] C.C. Nascentes, M. Korn, M.A.. Arruda, A fast ultrasound-assisted extraction of Ca, Mg, Mn and Zn from vegetables, Microchem. J. 69 (2001) 37–43. https://doi.org/10.1016/S0026-265X(00)00192-2.

[102] M. de F.A.D.S. Araújo, Efeito da radiação solar no envelhecimento do concreto betuminoso usinado a quente, (2007) 77.

[103] G.F. Manoel, A.P. Louzada, E. V Cardoso, M.E.S.R. Silva, R.F.S. Freitas, Preparação E Caracterização De Asfaltos Modificados Pelo Polímero Estireno-Butadieno- Estireno -Sbs a Partir Do Cimento Asfáltico De Petróleo Cap50/70 Regap, An. Do 10º Congr. Bras. Polímeros. 10 (2009) 8.

[104] J.R.E. Zegarra, Avaliação de misturas produzidas com ligantes asfálticos peruanos convencional pen 60 / 70 e modificados por polímero sbs tipo i 60 / 60 e pg 76 -22., Diss. Mestr. (2007).

[105] Y.-J. Du, N.-J. Jiang, S.-L. Shen, F. Jin, Experimental investigation of influence of acid rain on leaching and hydraulic characteristics of cement-based solidified/stabilized lead contaminated clay, J. Hazard. Mater. 225–226 (2012) 195–201. https://doi.org/10.1016/j.jhazmat.2012.04.072.

[106] Y.-J. Du, M.-L. Wei, K.R. Reddy, Z.-P. Liu, F. Jin, Effect of acid rain pH on

leaching behavior of cement stabilized lead-contaminated soil, J. Hazard. Mater. 271 (2014) 131–140. https://doi.org/10.1016/j.jhazmat.2014.02.002.

[107] Barcellos, L.D. Lacerda, Cadmium and zinc source assessment in the Sepetiba Bay and basin region, Environ. Monit. Assess. 29 (1994) 183–199. https://doi.org/10.1007/BF00546874.

[108] L.D. de Lacerda, W.C. Pfeiffer, M. Fiszman, Heavy metal distribution, availability and fate in Sepetiba Bay, S.E. Brazil, Sci. Total Environ. 65 (1987) 163–173. https://doi.org/10.1016/0048-9697(87)90169-0.

[109] E. V. Silva-Filho, C.J. Sanders, M. Bernat, A.M.G. Figueiredo, S.M. Sella, J. Wasserman, Origin of rare earth element anomalies in mangrove sediments, Sepetiba Bay, SE Brazil: used as geochemical tracers of sediment sources, Environ. Earth Sci. 64 (2011) 1257–1267. https://doi.org/10.1007/s12665-011-0942-y.

[110] M.M. Molisani, R. V. Marins, W. Machado, H.H.M. Paraquetti, E.D. Bidone, L.D. Lacerda, Environmental changes in Sepetiba Bay, SE Brazil, Reg. Environ. Chang. 4 (2004) 17–27. https://doi.org/10.1007/s10113-003-0060-9.

[111] R.A. Gonçalves, D.F. Oliveira, P.H.G. Ferreira, C.E. Rezende, P. Almeida, L.D. de Lacerda, J.M. Godoy, Decadal and spatial variation of Hg concentrations in sediments of a multi-stressor impacted estuary, Mar. Pollut. Bull. 135 (2018) 1158–1163. https://doi.org/10.1016/j.marpolbul.2018.08.053.

[112] V.G. Caccia, F.J. Millero, Distribution of yttrium and rare earths in Florida Bay sediments, Mar. Chem. 104 (2007) 171–185. https://doi.org/10.1016/j.marchem.2006.11.001.

[113] J. Borrego, N. López-González, B. Carro, O. Lozano-Soria, Origin of the anomalies in light and middle REE in sediments of an estuary affected by phosphogypsum wastes (south-western Spain), Mar. Pollut. Bull. 49 (2004) 1045–1053. https://doi.org/10.1016/j.marpolbul.2004.07.009.

[114] E.T. Harrigan, A Manual for Design of Hot-Mix Asphalt with Commentary, National Academies Press, Washington, D.C., 2011. https://doi.org/10.17226/14524.

[115] F. Ardini, F. Soggia, F. Rugi, R. Udisti, M. Grotti, Comparison of inductively coupled plasma spectrometry techniques for the direct determination of rare

earth elements in digests from geological samples, Anal. Chim. Acta. 678 (2010) 18–25. https://doi.org/10.1016/j.aca.2010.07.036.

[116] Z. Begum, V. Balaram, S.M. Ahmad, M. Satyanarayanan, T.G. Rao, Determination of trace and rare earth elements in marine sediment reference materials by ICP-MS: comparison of open and closed acid digestion methods, At. Spectrosc. 28 (2007) 41.

[117] M. Mittermüller, J. Saatz, B. Daus, A sequential extraction procedure to evaluate the mobilization behavior of rare earth elements in soils and tailings materials, Chemosphere. 147 (2016) 155–162. https://doi.org/10.1016/j.chemosphere.2015.12.101.

[118] J.A. Gásquez, E. Delima, R.A. Olsina, L.D. Martinez, M. De La Guardia, A fast method for apatite selective leaching from granitic rocks followed through rare earth elements and phosphorus determination by inductively coupled plasma optical emission spectrometry, Talanta. 67 (2005) 824–828. https://doi.org/10.1016/j.talanta.2005.04.008.

[119] U.S. EPA1996, Method 3050B: Acid digestion of sediments, sludges, and soils, Environ. Prot. Agency Washington, DC, USA. (1996).

[120] F.E. de E. do M.A. (FEEMA), Baía de Sepetiba, Rios da Baixada da Baía de Sepetiba, Diagnóstico de Qualidade de Águas e Sedimentos, Rio de Janeiro, 2006.

[121] J.M. Godoy, I. Moreira, C. Wanderley, F.F. Simões Filho, A.A. Mozeto, An alternative method for the determination of excess 210Pb in sediments, Radiat. Prot. Dosimetry. 75 (1998) 111–115.

[122] S. Potts, PJ and Thompson, M and Webb, PC and Wilson, GEOPT16--An international proficiency test for analytical geochemistry laboratories--report on round 16/February 2005 (Nevada basalt BNV-1, Int. Assoc. Geoanalysts Unpubl. Rep. (2005).

[123] F. Krug, FJ and Rocha, Métodos de preparo de amostras para análise elementar, São Paulo: EditSBQ-Sociedade Brasileira de Química, 2016.

[124] K. Dunn, E. Daniel, P.J. Shuler, H.J. Chen, Y. Tang, T.F. Yen, Mechanisms of Surface Precipitation and Dissolution of Barite: A Morphology Approach, J. Colloid Interface Sci. 214 (1999) 427–437. https://doi.org/10.1006/jcis.1999.6224.

[125] H. Safari, A. Shokrollahi, M. Jamialahmadi, M.H. Ghazanfari, A. Bahadori,

S. Zendehboudi, Prediction of the aqueous solubility of BaSO4 using pitzer ion interaction model and LSSVM algorithm, Fluid Phase Equilib. 374 (2014) 48–62. https://doi.org/10.1016/j.fluid.2014.04.010.

[126] M.E. Åström, M. Nystrand, J.P. Gustafsson, P. Österholm, L. Nordmyr, J.K. Reynolds, P. Peltola, Lanthanoid behaviour in an acidic landscape, Geochim. Cosmochim. Acta. 74 (2010) 829–845. https://doi.org/10.1016/j.gca.2009.10.041.

[127] J.C. Fernández-Caliani, C. Barba-Brioso, J.D. De la Rosa, Mobility and speciation of rare earth elements in acid minesoils and geochemical implications for river waters in the southwestern Iberian margin, Geoderma. 149 (2009) 393–401. https://doi.org/10.1016/j.geoderma.2009.01.004.

[128] D.R. Araripe, A.V.B. Bellido, S.R. Patchineelam, R.M. Latini, L.F. Bellido, D.I.T. Fávaro, Trace and major elements in geological samples from Itingusssú River Basin, Sepetiba Bay—Rio de Janeiro, J. Radioanal. Nucl. Chem. 290 (2011) 381–389. https://doi.org/10.1007/s10967-011-1220-x.

[129] J.T. Wasson, G.W. Kallemeyn, Compositions of Chondrites, Philos. Trans. R. Soc. A Math. Phys. Eng. Sci. 325 (1988) 535–544. https://doi.org/10.1098/rsta.1988.0066.

[130] P.J. Potts, M. Thompson, P.C. Webb, S. Wilson, GEOPT16--An international proficiency test for analytical geochemistry laboratories--report on round 16/February 2005 (Nevada basalt BNV-1), Int. Assoc. Geoanalysts Unpubl. Rep. (2005).

[131] R.A. Gonçalves, Estudo da variação temporal e espacial de metais tóxicos em sedimentos da Baía da Sepetiba , RJ , Brasil, 2018.

[132] U. Forstner, Lecture Notes in Earth Sciences, (1989).

[133] FEEMA, BACIA DA BAÍA DE SEPETIBA, Jackeline, Rio de Janeiro, 2001.

[134] M. Bau, P. Dulski, Anthropogenic origin of positive gadolinium anomalies in river waters, Earth Planet. Sci. Lett. 143 (1996) 245–255. https://doi.org/10.1016/0012-821x(96)00127-6.

[135] S. Gao, K.H. Wedepohl, The negative Eu anomaly in Archean sedimentary rocks: Implications for decomposition, age and importance of their granitic sources, Earth Planet. Sci. Lett. 133 (1995) 81–94. https://doi.org/10.1016/0012-821X(95)00077-P.

[136] M.B.K. Prasad, A. Ramanathan, Distribution of Rare Earth Elements in the

Pichavaram Mangrove Sediments of the Southeast Coast of India, J. Coast. Res. 1 (2008) 126–134. https://doi.org/10.2112/05-0533.1.

[137] S.B. Castor, J.B. Hedrick, Rare earth elements, Ind. Miner. Rocks. (2006) 769–792.

9
Annex

Table 16. Results (mg kg^{-1}) obtained for bottom sediments from Sepetiba Bay (Stations 101-106)

	101	102	103	104	105	106
^{139}La	90.3±3.5	87.3±4.0	86.6±4.2	28.0±0.7	92.4±5.3	80.6±4.3
^{140}Ce	186±12	176±8	182±12	56.6±2.0	192±10	166±11
^{141}Pr	18.5±1.5	17.6±1.2	17.7±1.1	5.86±0.30	18.3±1.6	16.4±1.4
^{143}Nd	63.3±4.6	58.6±4.2	59.7±3.7	20.1±1.2	60.8±5.1	56.0±5.2
^{147}Sm	8.39±0.64	8.21±0.42	8.69±0.55	2.94±0.19	8.68±0.68	8.10±0.29
^{151}Eu	1.68±0.11	1.71±0.12	1.76±0.05	0.454±0.028	1.76±0.09	1.68±0.09
^{157}Gd	7.07±0.68	7.06±0.46	6.99±0.74	2.60±0.28	7.33±0.91	6.80±0.60
^{159}Tb	0.842±0.077	0.766±0.031	0.827±0.058	0.265±0.024	0.876±0.059	0.788±0.036
^{163}Dy	6.08±0.20	6.14±0.28	6.29±0.34	1.95±0.15	6.61±0.40	5.66±0.29
^{165}Ho	1.31±0.12	1.28±0.08	1.32±0.09	0.339±0.018	1.35±0.09	1.18±0.12
^{166}Er	3.95±0.19	3.81±0.19	4.34±0.39	1.08±0.06	4.24±0.51	3.83±0.35
^{169}Tm	0.571±0.066	0.551±0.069	0.631±0.064	0.139±0.030	0.632±0.092	0.570±0.030
^{174}Yb	3.81±0.10	3.95±0.24	4.47±0.44	1.03±0.18	4.53±0.50	3.89±0.53
^{175}Lu	0.635±0.071	0.631±0.035	0.764±0.069	0.141±0.032	0.691±0.063	0.620±0.060

Table 17. Results (mg kg-1) obtained for bottom sediments from Sepetiba Bay (Stations 107-112)

	107	108	109	110	111	112
^{139}La	60.1±2.3	99.3±3.3	69.6±2.7	72.6±3.6	112±5	70.2±2.7
^{140}Ce	123±10	204±11	146±8	148±10	240±10	147±7
^{141}Pr	12.5±1.2	20.2±1.6	14.4±1.0	14.3±1.1	22.6±1.7	14.6±0.6
^{143}Nd	41.2±3.6	67.1±6.9	48.1±4.2	48.8±3.4	74.9±4.4	49.7±3.2
^{147}Sm	6.45±0.66	9.80±0.59	6.84±0.45	7.29±0.40	10.8±0.6	7.27±0.49
^{151}Eu	1.14±0.07	1.82±0.15	1.51±0.13	1.55±0.06	2.05±0.07	1.28±0.03
^{157}Gd	5.33±0.79	8.35±0.87	6.06±0.60	6.29±0.63	9.45±0.60	5.90±0.44
^{159}Tb	0.598±0.064	0.937±0.065	0.694±0.063	0.718±0.045	1.09±0.12	0.681±0.018
^{163}Dy	4.09±0.13	7.07±0.61	5.13±0.29	5.14±0.46	7.97±0.19	4.77±0.22
^{165}Ho	0.847±0.081	1.42±0.11	1.09±0.06	1.08±0.09	1.74±0.05	0.924±0.025
^{166}Er	2.69±0.26	4.64±0.41	3.36±0.36	3.27±0.25	5.62±0.44	3.11±0.12
^{169}Tm	0.394±0.043	0.654±0.082	0.496±0.027	0.505±0.035	0.776±0.041	0.399±0.048
^{174}Yb	2.65±0.20	4.35±0.32	3.42±0.35	3.36±0.34	5.82±0.35	2.82±0.22
^{175}Lu	0.403±0.031	0.730±0.060	0.525±0.060	0.559±0.077	0.894±0.106	0.458±0.027

Table 18. Results (mg kg^{-1}) obtained for bottom sediments from Sepetiba Bay (Stations 113-118)

	113	114	115	116	117	118
^{139}La	74.7±2.0	79.0±1.9	67.5±3.1	87.1±4.2	62.1±1.5	77.3±3.7
^{140}Ce	150±5	160±5	132±6	175±9	137±6	156±8
^{141}Pr	15.0±0.7	16.1±0.8	13.2±0.8	17.7±1.4	12.9±0.9	15.7±1.2
^{143}Nd	50.8±3.5	54.6±3.1	44.9±3.2	58.9±5.4	43.5±3.7	53.1±3.7
^{147}Sm	7.59±0.58	7.72±0.56	6.39±0.22	8.33±0.49	6.20±0.33	7.57±0.79
^{151}Eu	1.57±0.07	1.54±0.08	1.24±0.10	0.940±0.030	1.16±0.13	1.59±0.08
^{157}Gd	6.38±0.45	6.83±0.39	5.62±0.66	7.17±0.82	5.57±0.56	6.84±0.68
^{159}Tb	0.757±0.056	0.800±0.032	0.632±0.035	0.738±0.051	0.593±0.054	0.729±0.076
^{163}Dy	5.37±0.27	5.42±0.39	4.59±0.28	4.71±0.28	4.21±0.37	5.43±0.50
^{165}Ho	1.11±0.08	1.09±0.08	0.937±0.063	0.867±0.084	0.821±0.047	1.14±0.10
^{166}Er	3.48±0.20	3.59±0.21	3.11±0.27	2.52±0.15	2.58±0.30	3.55±0.45
^{169}Tm	0.505±0.043	0.512±0.016	0.444±0.029	0.328±0.047	0.368±0.029	0.461±0.038
^{174}Yb	3.33±0.21	3.60±0.28	2.88±0.15	2.11±0.38	2.49±0.13	3.65±0.27
^{175}Lu	0.535±0.014	0.542±0.048	0.506±0.038	0.317±0.071	0.365±0.055	0.537±0.066

Table 19. Results (mg kg^{-1}) obtained for bottom sediments from Sepetiba Bay (Stations 119-124)

	119	120	121	122	123	124
^{139}La	77.9±5.5	80.8±3.9	79.9±0.8	62.8±2.1	97.1±4.4	95.0±3.9
^{140}Ce	162±5	164±9	162±7	127±4	198±10	211±11
^{141}Pr	16.9±0.8	16.3±1.1	16.4±1.0	13.0±0.7	20.0±1.6	19.8±1.3
^{143}Nd	55.8±3.3	54.5±4.9	56.6±3.6	43.7±3.4	67.3±4.7	66.7±7.0
^{147}Sm	7.79±0.37	8.18±0.98	7.65±0.69	6.20±0.16	9.98±0.71	9.73±1.12
^{151}Eu	1.42±0.10	1.51±1.46	0.856±0.078	1.03±0.07	1.85±0.15	1.97±0.11
^{157}Gd	6.65±0.66	6.76±0.61	6.77±0.61	5.38±0.51	8.66±0.71	8.46±1.06
^{159}Tb	0.724±0.055	0.786±0.080	0.688±0.058	0.588±0.034	0.941±0.053	0.935±0.084
^{163}Dy	5.19±0.34	5.59±0.33	4.19±0.17	4.09±0.07	6.76±0.30	6.82±0.49
^{165}Ho	1.06±0.04	1.11±0.05	0.761±0.062	0.784±0.092	1.40±0.12	1.36±0.09
^{166}Er	3.24±0.30	3.46±0.21	2.18±0.15	2.53±0.06	4.41±0.42	4.52±0.59
^{169}Tm	0.423±0.027	0.485±0.030	0.261±0.019	0.332±0.030	0.660±0.059	0.638±0.064
^{174}Yb	3.12±0.31	3.58±0.43	1.69±0.20	2.31±0.24	4.06±0.14	4.19±0.32
^{175}Lu	0.475±0.089	0.542±0.043	0.264±0.014	0.315±0.031	0.644±0.059	0.679±0.045

Table 20. Results (mg kg^{-1}) obtained for bottom sediments from Sepetiba Bay (Stations 125-133)

	125	126	130	131	132	133
^{139}La	52.5±1.3	70.8±2.3	38.6±2.2	44.9±2.3	55.5±1.4	91.6±5.8
^{140}Ce	108±5	142±6	76.8±5.9	94.8±6.4	116±5	192±14
^{141}Pr	11.3±0.5	15.2±1.1	8.15±0.66	9.35±0.56	11.7±0.5	19.1±1.2
^{143}Nd	39.2±2.4	50.9±3.6	26.9±2.8	32.0±2.9	39.8±3.6	63.3±5.2
^{147}Sm	5.85±0.21	7.76±0.47	3.98±0.48	4.58±0.62	5.77±0.46	9.32±0.58
^{151}Eu	0.329±0.033	0.708±0.068	0.472±0.035	0.956±0.118	1.07±0.04	1.81±0.10
^{157}Gd	4.80±0.42	6.42±0.75	3.44±0.37	4.08±0.42	4.90±0.36	8.12±0.59
^{159}Tb	0.456±0.038	0.629±0.041	0.359±0.028	0.465±0.032	0.515±0.027	0.908±0.080
^{163}Dy	2.56±0.21	4.10±0.38	2.22±0.15	3.28±0.19	3.87±0.18	6.25±0.24
^{165}Ho	0.398±0.026	0.668±0.035	0.398±0.042	0.677±0.055	0.789±0.067	1.20±0.08
^{166}Er	1.19±0.10	1.85±0.21	1.25±0.12	2.23±0.19	2.48±0.19	4.26±0.43
^{169}Tm	0.095±0.016	0.224±0.037	0.135±0.030	0.289±0.038	0.313±0.035	0.614±0.068
^{174}Yb	0.656±0.061	1.49±0.09	0.998±0.148	2.00±0.17	2.31±0.12	3.99±0.25
^{175}Lu	0.092±0.018	0.213±0.038	0.157±0.038	0.307±0.028	0.384±0.053	0.629±0.039

Table 21. Results (mg kg^{-1}) obtained for bottom sediments from Sepetiba Bay (Stations 134-139)

	134	135	136	137	138	139
^{139}La	39.4±1.4	18.5±0.6	45.1±1.7	39.9±2.2	35.2±3.8	17.9±0.9
^{140}Ce	94.6±6.4	38.9±0.9	121±4	78.9±8.0	70.3±9.7	36.6±1.8
^{141}Pr	8.66±0.61	4.12±0.30	9.14±0.28	8.17±0.83	7.33±1.03	3.64±0.24
^{143}Nd	30.3±3.2	14.0±1.0	32.6±2.0	27.5±3.5	24.7±3.2	12.3±1.3
^{147}Sm	4.06±0.21	1.85±0.12	4.30±0.31	3.96±0.43	3.75±0.69	1.63±0.11
^{151}Eu	0.828±0.083	0.266±0.025	0.846±0.039	0.576±0.057	0.469±0.070	0.343±0.037
^{157}Gd	3.79±0.37	1.66±0.16	3.61±0.28	3.67±0.33	3.15±0.76	1.54±0.14
^{159}Tb	0.379±0.033	0.164±0.02	0.401±0.048	0.349±0.033	0.310±0.034	0.156±0.010
^{163}Dy	2.86±0.18	1.14±0.06	2.71±0.08	2.36±0.20	1.91±0.22	1.06±0.15
^{165}Ho	0.562±0.051	0.211±0.030	0.532±0.040	0.444±0.036	0.325±0.034	0.213±0.030
^{166}Er	1.80±0.26	0.618±0.053	1.83±0.15	1.35±0.19	1.05±0.19	0.687±0.122
^{169}Tm	0.275±0.058	0.084±0.005	0.277±0.027	0.171±0.019	0.141±0.030	0.090±0.016
^{174}Yb	1.79±0.15	0.538±0.094	1.69±0.14	1.28±0.13	0.840±0.133	0.708±0.082
^{175}Lu	0.263±0.048	0.077±0.011	0.267±0.018	0.161±0.032	0.123±0.035	0.098±0.018

Table 22. Results (mg kg^{-1}) obtained for bottom sediments from Sepetiba Bay (Stations 140-141)

	140	141
^{139}La	7.85±0.24	6.12±0.35
^{140}Ce	16.3±0.6	11.7±0.5
^{141}Pr	1.69±0.04	1.23±0.09
^{143}Nd	5.55±0.46	4.31±0.44
^{147}Sm	0.722±0.107	0.562±0.086
^{151}Eu	0.045±0.006	0.058±0.015
^{157}Gd	0.708±0.052	0.539±0.113
^{159}Tb	0.063±0.015	0.042±0.013
^{163}Dy	0.348±0.058	0.267±0.025
^{165}Ho	0.044±0.012	0.043±0.012
^{166}Er	0.195±0.018	0.134±0.028
^{169}Tm	0.011±0.011	0.014±0.003
^{174}Yb	0.148±0.057	0.068±0.059
^{175}Lu	0.010±0.010	0.007±0.007

Table 23. Geographical coordinates of the surface sediment sampling stations.

Stations	Geographical coordinates		Stations	Geographical coordinates	
	Latitude	Longitude		Latitude	Longitude
SP-101	23°01'26.35"S	43°38'04.66"O	SP-120	22°56'52.63"S	43°50'58.33"O
SP-102	23°01'00.36"S	43°39'04.85"O	SP-121	22°58'47.54"S	43°50'57.57"O
SP-103	22°59'55.18"S	43°41'03.92"O	SP-122	23°00'52.03"S	43°51'00.62"O
SP-104	23°01'56.49"S	43°41'01.72"O	SP-123	22°54'49.45"S	43°51'55.99"O
SP-105	22°58'52.17"S	43°43'00.98"O	SP-124	22°55'48.52"S	43°51'58.48"O
SP-106	23°00'55.13"S	43°42'59.96"O	SP-125	22°57'49.11"S	43°51'59.07"O
SP-107	23°02'26.30"S	43°43'02.92"O	SP-126	22°59'50.55"S	43°51'59.66"O
SP-108	22°57'55.39"S	43°44'57.29"O	SP-130	22°58'47.33"S	43°53'58.61"O
SP-109	22°59'53.45"S	43°45'01.61"O	SP-131	23°00'50.23"S	43°53'56.66"O
SP-110	23°01'53.98"S	43°45'01.02"O	SP-132	23°02'51.17"S	43°53'58.63"O
SP-111	22°56'50.34"S	43°46'57.29"O	SP-133	22°56'46.24"S	43°55'57.41"O
SP-112	22°58'48.16"S	43°46'58.94"O	SP-134	22°58'46.62"S	43°55'57.91"O
SP-113	23°00'57.10"S	43°47'00.87"O	SP-135	23°01'50.83"S	43°55'58.71"O
SP-114	23°02'54.68"S	43°47'01.78"O	SP-136	22°56'44.96"S	43°57'58.13"O
SP-115	22°55'50.05"S	43°49'00.66"O	SP-137	22°58'46.23"S	43°57'56.12"O
SP-116	22°57'51.62"S	43°48'59.14"O	SP-138	23°00'47.33"S	43°57'56.74"O
SP-117	22°59'51.59"S	43°48'58.20"O	SP-139	22°57'47.46"S	43°59'55.33"O
SP-118	23°01'52.51"S	43°49'01.23"O	SP-140	22°59'46.05"S	43°59'55.82"O
SP-119	22°56'04.39"S	43°50'55.23"O	SP-141	23°01'49.99"S	43°59'53.36"O

Table 24. Geographical coordinates of the sediment cores sampling stations.

Stations sampling	Geographical coordinates	
	Latitude	Longitude
T-8	22°57'23.4"S	43°46'37.9"O
T-18	22°59'50.0"S	43°47'48.2"O
T-28	23°01'31.1"S	43°42'44.2"O

10
Attachment

A
Published papers

Microchemical Journal 149 (2019) 104026

Contents lists available at ScienceDirect

Microchemical Journal

journal homepage: www.elsevier.com/locate/microc

Determination of rare earth elements in environmental samples with high concentrations of barium by quadrupole inductively coupled plasma mass spectrometry

Wendy J. Sandoval Rojano[a], Tayná dos Anjos[b], Christiane B. Duyck[b,*], Tatiana D. Saint'Pierre[a]

[a] Departamento de Química, Pontifícia Universidade Católica do Rio de Janeiro, RJ, Brazil
[b] Departamento de Química Analítica, Instituto de Química, Universidade Federal Fluminense, Niteroi, RJ, Brazil

ARTICLE INFO

Keywords:
Rare earth elements
Barium interference
Asphalt
ICP-MS
ICP OES
Sample decomposition

ABSTRACT

This paper proposes a new method of sample preparation for the determination of rare earth elements (REE) by quadrupole inductively coupled plasma mass spectrometry (Q-ICP-MS) in challenging environmental samples with high Ba concentrations. The method consists in adding 10% (v/v) sulfuric acid to the wet sample digest, obtained after acid decomposition in an open system, in order to precipitate and separate $BaSO_4$. The removal of BaO interference in Eu isotopes was efficient for Ba concentrations in solution higher than 0.1 mg L^{-1}. The methodology was applied to asphalt pavement and the crushed stone used to produce it. Accuracy was assessed using two certified materials, NIST 688 Standard Reference Material of basalt rock and Geological Survey G2 granite, resulting in acceptable recoveries. Additionally, all samples were decomposed by fusion, and the concentrations of major elements and Eu were determined by inductively coupled plasma optical emission spectrometry (ICP OES). Eu results were in agreement with the proposed methodology, and limits of detection for REE varied from 0.003 mg L^{-1} (Lu) to 0.010 mg L^{-1} (Gd). The NASC normalized profiles of REE in the crushed stone showed a positive Eu anomaly, that was not observed in the asphalt sample. As well, the latter was enriched in heavy REE (Tb-Lu), suggesting a loss of carbonatite minerals, consequently to the weathering of the pavement.

Figure A.1. Published paper.

B
Participation in Congress

Oral presentation

Determinação de Elementos Terras Raras em Amostras Geológicas por Espectrometria de Massa com Plasma Indutivamente Acoplado (ICP-MS). **II Jornada de Pós-Graduação e Pesquisa-DQ/PUC-Rio**, Rio de Janeiro-RJ, Brasil, 2018.

Posters

Determination of REE in Leachates Simulating the Effect of Acid Rain in Fluorescent Lamp Powder by ICP-MS, **15th Rio Symposium on Atomic Spectrometry***, Mendoza, Argentina, 2019 (Congresso).*

Determination of Rare Earths Elements in Petroleum and Derivatives by ICP-MS. 2019. **15th Rio Symposium on Atomic Spectrometry***, Mendoza, Argentina, 2019 (Congresso).*

Direct Determination of REE in Oil and Derivatives by ICP-MS. **15th Rio Symposium on Atomic Spectrometry***, Mendoza, Argentina, 2019 (Congresso).*

Determination of Rare Earth Elements in Marine Sediment from Sepetiba Bay (RJ) Brazil by Inductively Coupled Plasma Spectrometries. **Colloquum Spectroscopicum Internationale XLI**, Ciudad de Mexico, Mexico, 2019 (Congresso).

Determination of Rare Earth Elements in Geological Samples by Inductively Coupled Plasma Spectrometries, **19º ENQA-Encontro Nacional de Química Analítica**, Caldas Novas-GO, Brasil, 2018 (Encontro).

Silica functionalized with 2,6-pyridinedicarboxylic acid for selective preconcentration of Rare Earth elements traces before ICP-MS analysis. **41ª Reunião Anual da Sociedade Brasileira de Química,** Foz do Iguaçu-PR, Brasil, 2018 (Congresso).

Multielemental Determination in Asphalt and Crushed Stone by Inductively Coupled Plasma Spectrometries after Lithium Metaborate Fusion or Acid Decomposition. **7th Conference on Mass Spectrometry,** Rio de Janeiro-RJ, Brasil, 2018 (Congresso).

Determination of Rare Earth Elements in Asphalt by Inductively Coupled Plasma Spectrometries. **14th Rio Symposium on Atomic Spectrometry,** Vitoria-ES, Brasil, 2017 (Congresso).

Determination of Rare Earth Elements in Leachates Simulating the Effect of Acid Rain in Asphalt by Inductively Coupled Plasma Spectrometries. **VI International Workshop on Pollutants in the Environment,** Rio de Janeiro, Brasil, 2017 (Workshop).

Determinação de terras raras em amostras de asfalto por espectrometria de massa com plasma indutivamente acoplado (ICP-MS), **XVI Encontro Regional da SBQ**, Rio de Janeiro-RJ, Brasil, 2017 (Encontro).

Determinação de Terras Raras em Amostras de Asfalto por Espectrometria De Massa com Plasma Indutivamente Acoplado (ICP-MS). **18° ENQA-Encontro Nacional de Química Analítica,** Florianópolis-SC, Brasil, 2016 (Encontro).